FINAL REPORT NASA GRANT NSG-1104

CRACK GROWTH IN BONDED ELASTIC HALF PLANES

December 31, 1975

Principal Investigator

James G. Goree

Department of Mechanical Engineering

College of Engineering

Clemson University

Clemson, South Carolina 29631

FINAL REPORT NASA GRANT NSG-1104

CRACK GROWTH IN BONDED ELASTIC HALF PLANES

Principal Investigator

James G. Goree
Associate Professor of Mechanics
and Mechanical Engineering
Clemson University
Clemson, South Carolina 29631

Graduate Assistants

William A. Venezia
Ph.D. Candidate in Engineering Mechanics

James O. Feemster, Jr.
M.S. Candidate in Mechanical Engineering

ABSTRACT

Two solutions are developed for the two dimensional problem of bonded linearly elastic half-planes. The first is for two bonded isotropic linearly elastic half-planes of different elastic properties having a crack along the interface as well as a perpendicular crack in one of the half-planes which may intersect the interface crack. The appropriate integral equations are developed through the use of displacement dislocations in conjunction with Mellin transforms. The resulting pair of singular integral equations is solved by obtaining the relationships between these solutions and the weight functions for Chebyshev and Jacobi polynomials. The second solution is for two bonded isotropic linearly elastic half-planes of different elastic properties having a crack along the interface, as well as a perpendicular crack in each of the half-planes, either or both of which may intersect the interface crack. The appropriate integral equations are again developed through the use of displacement dislocations in conjunction with Mellin transforms. The resulting three singular integral equations are solved by obtaining the relationships between these solutions and the weight functions for Chebyshev and Jacobi polynomials in a similar manner to the pair of equations in the first solution.

For each solution, numerical results are presented for

the stress intensity factors, strain energy release rate, stresses and displacements.

The behavior predicted by the above studies was investigated experimentally using polymers for the material pairs. Very close agreement was found for the critical stress intensity factor at fracture for the perpendicular crack near the interface. Fracture along the interface proved to be inconclusive due to difficulties in obtaining a brittle bond. Some interesting and predictable behavior regarding the potential for the crack to cross the interface was observed and is discussed.

ACKNOWLEDGMENT

The writer wishes to express his appreciation to the National Aeronautics and Space Administration for the support of this investigation.

TABLE OF CONTENTS

TABLE OF CONTENTS (Continued)

LIST OF TABLES

LIST OF FIGURES

LIST OF FIGURES (Continued)

LIST OF SYMBOLS

A_k , B_k	Mellin Transform integral functions.
a , a*	Distance of near crack tip from interface in materials 1 and 2 respectively.
a_o , a_o^*	$a_o = \frac{b - a}{2}$, $a_o^* = \frac{b^* - a^*}{2}$
b , b*	Distance of far crack tip from interface in materials 1 and 2 respectively.
b_o , b_o^*	$b_o = \frac{b + a}{2}$, $b_o^* = \frac{b^* + a^*}{2}$
C_i , C_i' , i = 1,8	Mellin transform integral functions.
c	Half length of interface crack.
C_n	Series coefficients for density function.
E_k	Young's modulus material k .
f(r), g(r)(ϕ(t))	Displacement dislocations on surface $\theta = \frac{\pi}{2}$ ($\phi(t) = g(ct) + if(ct)$).
h*(r), h(r)	Displacement dislocations on surface $\theta = 0$, $\theta = \pi$ respectively.
(ψ(t), ξ(t))	($\psi(t) = h(a_o t + b_o)$, $\xi(t) = h^*(a_o^* t + b_o^*)$).
Im[ ]	Imaginary part of function contained in brackets.
i	$\sqrt{-1}$
N	Numerical constant, upper limit in truncated infinite series, equation (63), (100), (101), (102), (103).
k(a),k(b), k(a*), k(b*)	Stress intensity factors at points a, b, a* , b* respectively, defined by equations (64), (65), (68), (104), (105), (106).
N(r)	Normal stress on interface.
N_o(r)	Normal stress on symmetry line.

LIST OF SYMBOLS (Continued)

M	Numerical constant, number of C_n computed from equation (63) or (96).
$M[\quad]$	Mellin transform of function in brackets.
m	Ratio of shear moduli $\frac{\mu_2}{\mu_1}$
$P_n^{(\alpha,\beta)}(y)$	Jacobi orthogonal polynomial.
$p(r)$, $q(r)$	Applied normal and shear stresses on the interface crack.
$p_o(s)$, $p_o^*(s)$	Applied normal stress on perpendicular cracks in materials 1 and 2 respectively.
$Re[\quad]$	Real part of function contained in brackets.
$T(r)$	Shear stress on interface.
$\frac{\partial U}{\partial c}$	Strain energy release rate given by equation (69).
$u_{kr}(r,\theta)$	Radial displacement in material k.
$u_{k\theta}(r,\theta)$	Tangential displacement in material k.
$V_k(s,\theta)$	Transform function defined by equation (1).
$v_k(r,\theta)$	Displacement function defined by equation (2).
α	Complex constant equal to $-\frac{1}{2} - i\omega$.
α_1	Real constant $= \mu_2(1 + m\kappa_1 + m + \kappa_2)/(1+m\kappa_1)/(m+\kappa_2)$.
β	Complex constant equal to $-\frac{1}{2} + i\omega$.
$\delta(r - r_o)$	Dirac delta function.
γ	Real constant $= [(m+\kappa_2) - (1+m\kappa_1)]/[(m+\kappa_2) + (1+m\kappa_1)]$.
κ_k	$3 - 4\nu_k$ for plane strain, $(3 - \nu_k)/(1 + \nu_k)$ for generalized plane stress.
μ_k	Shear modulus for material k.
ν_k	Poisson's ratio for material k.

LIST OF SYMBOLS (Continued)

$\sigma_o , \sigma_1 , \sigma_2$	Constant boundary stresses at infinity.
$\sigma_k(r, \theta)$	Complex function defined as $\tau_{kr\theta}(r , \theta) + i\tau_{k\theta\theta}(r , \theta)$.
$\Sigma_k(s , \theta)$	Mellin transform of $r^2\sigma_k(r, \theta)$.
$\tau_{kr\theta}(r , \theta)$	Shear stress in k^{th} region.
$\tau_{krr}(r , \theta)$	Radial stress in k^{th} region.
$\tau_{k\theta\theta}(r , \theta)$	Normal stress in theta direction for k^{th} region.
$\Phi(t)$	Complex function defined by equation (30).
$\triangleq$	Equal to and defined by.
$\overline{\phi(t)}$	$g(ct) - if(ct)$, complex conjugate of $\phi(t)$.

BONDED ELASTIC HALF-PLANES WITH AN INTERFACE CRACK AND A PERPENDICULAR INTERSECTING CRACK[1]

By

James G. Goree
Associate Professor of Mechanics and
Mechanical Engineering

William A. Venezia[2]
Graduate Assistant
Ph.D. Candidate in
Engineering Mechanics

The solution is given for two bonded isotropic linearly elastic half-planes of different elastic properties having a crack along the interface as well as a perpendicular crack in one of the half-planes which may intersect the interface crack. The appropriate integral equations are developed using displacement dislocations on the crack surfaces.

Numerical results are presented for the stress intensity factors, strain energy release rate, stresses and displacements.

---

[1] Presented at the 11th Annual Meeting of the Society of Engineering Science, Duke University, Durham, North Carolina, November 11, 1974. Published in the International Journal of Engineering Science, (In press).

[2] Currently at Johns Hopkins University, Applied Physics Laboratory, Laurel, Maryland 20810.

Introduction

In considering the fracture of composite materials due to the presence of imperfections, one finds a common mode of failure to be that of a crack originating in one material then extending until it reaches a bonded interface and spreading along the bond line. Other possible directions of crack growth are for the crack to cross the bond line or to be reflected by the interface into the original material.

An investigation of the effects of a crack in the near vicinity of a material interface is then essential in the fracture analysis of composite materials. In the analytical study of this problem a specific geometry that leads to tractable integral equations is the case of two elastic half-planes containing a finite length crack in one of the half-planes with the crack being perpendicular to the material interface. Of particular interest is the behavior of the stresses as one end of the crack approaches the interface and either terminates, crosses into the adjacent material, extends along the bond without crossing the interface, or upon reaching the interface, extends into the adjacent material and debonds along the interface. The instances of the crack terminating at the interface or crossing the interface have been investigated by Erdogan, Cook, and Biricikoglu in [1] and [2]. The present study considers the possibility of the crack spreading along the interface.

The appropriate integral equations are developed through the use of displacement dislocations in conjunction with Mellin transforms. The resulting singular integral equations are solved by obtaining the relationships between these solutions and the weight functions for Chebyshev and Jacobi polynomials.

Formulation

Assuming a coordinate system having the origin at the center of the interface crack, as shown in Figure 1, it is seen to be convenient to represent the solution in terms of the polar variables (r, θ), as the crack surfaces, the interface, and the horizontal plane of symmetry lie on constant θ surfaces.

An effective means of formulating linear elasticity problems having boundary conditions of this type is to make use of Mellin transforms on the radial variable. It is demonstrated in [1] and [2] that the use of displacement dislocations in conjunction with Mellin transforms gives a very simple and straightforward technique to develop the integral equations for a large class of problems of this general form.

The half-planes are assumed to be loaded with uniform stresses σ_o, σ_1 and σ_2 as shown in Figure 1, with the stresses being related in such a manner as to give constant strains in both the x and y directions at points remote from the cracks. The following relations must then hold,

$$\sigma_1 = \sigma_2 \frac{E_1}{E_2} - \sigma_o\left(\nu_2 \frac{E_1}{E_2} - \nu_1\right) \quad \text{for generalized plane stress}$$

and

$$\sigma_1 = \sigma_2 \frac{(1-\nu_2^2)E_1}{(1-\nu_1^2)E_2} - \sigma_o\left[\frac{\nu_2(1+\nu_2)E_1}{(1-\nu_1^2)E_2} - \frac{\nu_1}{1-\nu_1}\right] \quad \text{for plain strain.}$$

The complete solution may be represented as

$$\sigma \text{ total} = \sigma_I + \sigma_{II}$$

where σ_I = stresses in the half planes without cracks and loaded at infinity

and σ_{II} = stresses in the half planes having no applied loads at infinity and applied stresses on the crack surfaces equal to the negative of those given by σ_I. For the loads as stated above this would require normal stresses of $-\sigma_o$ and $-\sigma_1$ on the interface and perpendicular crack respectively.

The solution for σ_{II} is developed below in terms of a general system of applied tractions on the crack surfaces, although still requiring symmetry about the $y = 0$ plane, and will be restricted to the above constant normal stresses only for the numerical results.

As the present study is closely related to [1] and [2], an attempt to follow the form and notation of those investigations will be made, where possible, in order to eliminate unnecessary duplication.

Following [1], the Mellin transforms of the stresses and displacements are:

$$M[r^2\sigma_k(r,\theta)] = \Sigma_k(s,\theta) = 2i(s+1) \times \left[A_k s e^{is\theta} + B_k(s+1)e^{i(s+2)\theta} - \bar{B}_k e^{-i(s+2)\theta} \right],$$

$$M[r^2\tau_{krr}(r,\theta)] = -s(s+1)\left[A_k e^{is\theta} + \bar{A}_k e^{-is\theta} \right] - (s+1)(s+4)\left[B_k e^{i(s+2)\theta} + \bar{B}_k e^{-i(s+2)\theta} \right],$$

$$M[r^2 v_k(r,\theta)/2\mu_k] = V_k(s,\theta) \qquad (1)$$

$$= -\frac{s+1}{\mu_k}\left[A_k s e^{is\theta} + B_k(s+1)e^{i(s+2)\theta} + \kappa_k \bar{B}_k e^{-i(s+2)\theta} \right],$$

where

$$\kappa_k = \begin{cases} 3-4\nu_k & \text{for plane strain} \\ (3-\nu_k)/(1+\nu_k) & \text{for generalized plane stress} \end{cases}$$

and μ_k, ν_k are the shear modulus and Poisson's ratio respectively.

The transformed functions above are [1]

$$\sigma_k(r,\theta) = \tau_{kr\theta}(r,\theta) + i\tau_{k\theta\theta}(r,\theta),$$

$$\tau_{krr}(r,\theta) = \tau_{krr}(r,\theta) \qquad (2)$$

and

$$v_k(r,\theta) = 2\mu_k\left[\frac{\partial u_{kr}(r,\theta)}{\partial r} + i\,\frac{\partial u_{k\theta}(r,\theta)}{\partial r} \right] \text{with } k=1,2$$

for region 1 and 2 respectively.

Using displacement dislocations[1] on the surfaces $\theta = \frac{\pi}{2}$ and $\theta = \pi$, the boundary conditions are:

$$\tau_{2r\theta}(r,o) = u_{2\theta}(r,o) = 0 \text{ , on } \theta = 0 \text{ in material 2,} \tag{3}$$

$$\left.\begin{aligned} &\tau_{1r\theta}(r,\pi) = 0 \\ &\frac{\partial}{\partial r} u_{1\theta}(r,\pi) = -1/2h(r)\delta(r-r_o) \end{aligned}\right\} \text{, on } \theta = \pi \text{ in material 1} \tag{4}$$

and

$$\left.\begin{aligned} &\tau_{1r\theta}(r,\pi/2) = \tau_{2r\theta}(r,\pi/2) \\ &\tau_{1\theta\theta}(r,\pi/2) = \tau_{2\theta\theta}(r,\pi/2) \\ &\frac{\partial}{\partial r} u_{1r}(r,\pi/2) - \frac{\partial}{\partial r} u_{2r}(r,\pi/2) = -f(r)\delta(r-r_o) \\ &\frac{\partial}{\partial r} u_{1\theta}(r,\pi/2) - \frac{\partial}{\partial r} u_{2\theta}(r,\pi/2) = -g(r)\delta(r-r_o) \end{aligned}\right\} \text{, interface } \theta = \pi/2 \text{ .} \tag{5}$$

By defining the unknown functions A_k, B_k, $k = 1, 2$, as

$$A_1 = C_1 + iC_2 \text{ , } B_1 = C_3 + iC_4 \text{ , } A_2 = C_5 + iC_6 \text{ , } B_2 = C_7 + iC_8$$

and on transforming the above boundary conditions, the resulting eight equations specifying the unknowns C_i are as follows:

---

[1] Displacement dislocation as used in the present text implies a step discontinuity in the displacement slope at a particular point.

$$sC_6 + (s+1)C_8 + C_8 = 0 \quad , \tag{6}$$

$$sC_6 + (s+1)C_8 - \kappa_2 C_8 = 0 \quad , \tag{7}$$

$$sC_1 \sin(\pi s) + sC_2 \cos(\pi s) + (s+2)C_3 \sin(\pi s) + (s+2)C_4 \cos(\pi s) = 0 \tag{8}$$

$$sC_1 \sin(\pi s) + sC_2 \cos(\pi s) + (s+1-\kappa_1)C_3 \sin(\pi s) + (s+1-\kappa_1)C_4 \cos(\pi s) = \frac{h(r_o) r_o^{s+1} \mu_1}{2(s+1)} , \tag{9}$$

$$sC_1 \cos(\pi s/2) - sC_2 \sin(\pi s/2) - sC_3 \cos(\pi s/2) + sC_4 \sin(\pi s/2) - s(C_5 - C_7)\cos(\pi s/2) = 0 \quad , \tag{10}$$

$$sC_1 \sin(\pi s/2) + sC_2 \cos(\pi s/2) - (s+2)C_3 \sin(\pi s/2) - (s+2)C_4 \cos(\pi s/2) - [sC_5 - (s+2)C_7]\sin(\pi s/2) = 0 \quad , \tag{11}$$

$$-m[sC_1 \cos(\pi s/2) - sC_2 \sin(\pi s/2) - (s+1+\kappa_1)C_3 \cos(\pi s/2) + (s+1+\kappa_1)C_4 \sin(\pi s/2)] + [sC_5 - (s+1+\kappa_2)C_7]\cos(\pi s/2) = -\frac{\mu_2 f(r_o) r_o^{s+1}}{s+1} \quad , \tag{12}$$

and

$$-m[sC_1 \sin(\pi s/2) + sC_2 \cos(\pi s/2) - (s+1-\kappa_1)C_3 \sin(\pi s/2) - (s+1-\kappa_1)C_4 \cos(\pi s/2)] + [sC_5 - (s+1-\kappa_2)C_7]\sin(\pi s/2) = -\frac{\mu_2 g(r_o) r_o^{s+1}}{s+1} \quad , \tag{13}$$

where $m = \mu_2/\mu_1$ and in Equations (10) through (13) use has been made of Equations (6) and (7) which require that $C_6 = C_8 = 0$. The remaining functions are found to be

$$C_1 = -C_2 \frac{\cos(\pi s)}{\sin(\pi s)} + \frac{\mu_1 (s+2) h(r_o) r_o^{s+1}}{2s(s+1)(1+\kappa_1)\sin(\pi s)} , \qquad (14)$$

$$C_2 = \frac{\mu_2 r_o^{s+1}}{s(s+1)(1+m\kappa_1)(m+\kappa_2)} \Big[f(r_o)\sin(\pi s/2)[(s+1)(m+\kappa_2) - (1+m\kappa_1)] + g(r_o)\cos(\pi s/2)[(s+1)(m+\kappa_2)+(1+m\kappa_1)]\Big]$$

$$+ \frac{\mu_1 h(r_o) r_o^{s+1}}{2s(s+1)(1+\kappa_1)} \left[\frac{(1-m)(s+1)(2s+3)}{(1+m\kappa_1)} + \frac{(m\kappa_1-\kappa_2)}{(m+\kappa_2)} \right] , \qquad (15)$$

$$C_3 = -C_4 \frac{\cos(\pi s)}{\sin(\pi s)} - \frac{\mu_1 h(r_o) r_o^{s+1}}{2(s+1)(1+\kappa_1)\sin(\pi s)} , \qquad (16)$$

$$C_4 = \frac{\mu_2 r_o^{s+1}}{(s+1)(1+m\kappa_1)} [f(r_o)\sin(\pi s/2) + g(r_o)\cos(\pi s/2)] + \frac{\mu_1 (1-m)(2s+3) h(r_o) r_o^{s+1}}{2(s+1)(1+\kappa_1)(1+m\kappa_1)} , \qquad (17)$$

$$C_5 = \frac{\mu_2 r_o^{s+1}}{s(s+1)(1+m\kappa_1)(m+\kappa_2)\sin(\pi s)} \Big[f(r_o)\sin(\pi s/2) \times [(s+1)(1+m\kappa_1)-(m+\kappa_2)] - g(r_o)\cos(\pi s/2) \times [(s+1)(1+m\kappa_1)+(m+\kappa_2)]\Big] + \frac{\mu_2 h(r_o) r_o^{s+1}}{2s(s+1)\sin(\pi s)} \times \left[\frac{(2s+3)}{(1+m\kappa_1)} - \frac{(s+1)}{(m+\kappa_2)} \right] , \qquad (18)$$

and

$$C_7 = \frac{\mu_2 r_o^{s+1}}{(s+1)(m+\kappa_2)\sin(\pi s)}\left[f(r_o)\sin(\pi s/2) - g(r_o)\cos(\pi s/2)\right] - \frac{\mu_2 h(r_o) r_o^{s+1}}{2(s+1)(m+\kappa_2)\sin(\pi s)} \quad . \tag{19}$$

Substituting into the first of Equations (1), the transformed stresses on the surfaces $\theta = \pi/2$ and $\theta = \pi$ are

$$\Sigma_1(s,\pi/2) = \frac{\mu_2(1+m\kappa_1+m+\kappa_2) r_o^{s+1}}{(1+m\kappa_1)(m+\kappa_2)}\left[f(r_o)\tan(\pi s/2) - ig(r_o)\cot(\pi s/2) + \gamma\,[g(r_o) - if(r_o)]\right] + \frac{\mu_1 h(r_o) r_o^{s+1}}{2(1+\kappa_1)}\left[i\left[2(s+1) - \frac{(1-m)(2s+3)}{(1+m\kappa_1)} - \frac{(m\kappa_1-\kappa_2)}{(m+\kappa_2)}\right]\right.$$

$$\left. \times \frac{1}{\sin(\pi s/2)} - \left[2(s+2) - \frac{(1-m)(2s+3)}{(1+m\kappa_1)} + \frac{(m\kappa_1-\kappa_2)}{(m+\kappa_2)}\right]\frac{1}{\cos(\pi s/2)}\right], \tag{20}$$

and

$$\Sigma_1(s,\pi) = -\frac{i\mu_2 r_o^{s+1}}{(1+m\kappa_1)(m+\kappa_2)}\left[f(r_o) \times [2s(m+\kappa_2) - (1+m\kappa_1) + (m+\kappa_2)]\frac{1}{\cos(\pi s/2)} + g(r_o) \times [2s(m+\kappa_2) + (1+m\kappa_1) + (m+\kappa_2)]\frac{1}{\sin(\pi s/2)}\right] + \frac{2i\mu_1 h(r_o) r_o^{s+1}}{(1+\kappa_1)}$$

$$\left[\cot(\pi s) - \left[\frac{(m\kappa_1-\kappa_2)}{2(m+\kappa_2)} + \frac{(1-m)(2s+1)(2s+3)}{2(1+m\kappa_1)}\right]\frac{1}{\sin(\pi s)}\right], \tag{21}$$

where in Equation (20)

$$\gamma = \frac{(m+\kappa_2)-(1+m\kappa_1)}{(m+\kappa_2)+(1+m\kappa_1)}$$

and in Equation (21) $\Sigma_1(s,\pi) = M[ir^2\tau_{1\theta\theta}(r,r_o,\pi)]$, as $\tau_{1r\theta}(r,r_o,\pi) = 0$.

The integral equations in terms of the unknown density functions f(r), g(r), and h(r) are given by the conditions that

$$T(r)+iN(r) = \int_o^\infty [\tau_{1r\theta}(r,r_o,\pi/2)+i\tau_{1\theta\theta}(r,r_o,\pi/2)]dr_o \qquad (22)$$

and

$$N_o(r) = \int_o^\infty \tau_{1\theta\theta}(r,r_o,\pi)dr_o \qquad (23)$$

where N(r) and T(r) are the normal and shear stresses on the interface and $N_o(r)$ is the normal stress on the symmetry line.

On noting that

$$f(r_o) = g(r_o) = 0 \ , \ c < r_o < \infty$$

and

$$h(r_o) = 0 \ , \ 0 < r_o < a \ , \ b < r_o < \infty \ ,$$

then inverting Equations (20) and (21) and substituting into Equations (22) and (23) one has

$$N(r)-iT(r) = \frac{\mu_2[1+m\kappa_1+m+\kappa_2]}{(1+m\kappa_1)(m+\kappa_2)}\left[-\frac{1}{\pi i}\int_o^c [f(\xi)+ig(\xi)]\frac{d\xi}{\xi-r}\right.$$

$$\left. + \frac{1}{\pi i}\int_o^c [f(\xi)-ig(\xi)]\frac{d\xi}{\xi+r} - \gamma\,[f(r)+ig(r)]\right]$$

$$+\frac{\mu_1}{(1+\kappa_1)\pi}\int_a^b h(\eta)\left\{\eta\left[\left[2(\eta^2-r^2)-\frac{(1-m)(\eta^2-3r^2)}{1+m\kappa_1}\right]\times\right.\right.$$

$$\left.\frac{1}{\eta^2+r^2}+\frac{m\kappa_1-\kappa_2}{m+\kappa_2}\right]+ir\left[\left[2(\eta^2-r^2)-\frac{(1-m)(3\eta^2-r^2)}{(1+m\kappa_1)}\right]\times\right.$$

$$\left.\left.\frac{1}{\eta^2+r^2}-\frac{m\kappa_1-\kappa_2}{m+\kappa_2}\right]\right\}\frac{d\eta}{\eta^2+r^2} \qquad (24)$$

and

$$N_o(s)=\frac{2\mu_1}{(1+\kappa_1)\pi}\int_a^b h(\eta)\left[\frac{1}{\eta-s}-\frac{(1-m)}{2(1+m\kappa_1)}\times\right.$$

$$\left.\left[\frac{8s^2}{(\eta+s)^3}-\frac{12s}{(\eta+s)^2}\right]-\frac{1}{2}\left[\frac{m\kappa_1-\kappa_2}{m+\kappa_2}+\frac{3(1-m)}{1+m\kappa_1}\right]\frac{1}{\eta+s}\right]d\eta$$

$$+\frac{2\mu_2}{\pi(1+m\kappa_1)(m+\kappa_2)}\times$$

$$\int_o^c\left[-sf(\xi)\left[(1+m\kappa_1)+\frac{(m+\kappa_2)(5\xi^2+s^2)}{\xi^2+s^2}\right]\right.$$

$$\left.+\xi g(\xi)\left[(1+m\kappa_1)-\frac{(m+\kappa_2)(3\xi^2-s^2)}{\xi^2+s^2}\right]\right]\frac{d\xi}{\xi^2+s^2} \quad . \qquad (25)$$

Equations (24) and (25) are valid for all values of r and in particular

$$N(r)-iT(r)=p(r)-iq(r)\ ,\quad 0<r<c\ , \qquad (26)$$

and

$$N_o(s)=p_o(s)\ ,\quad a<s<b\ , \qquad (27)$$

where $p(r)$, $q(r)$ are the applied normal and shear stresses on the interface crack and $p_o(s)$ is the applied normal

stress on the perpendicular crack. Therefore, with the above restrictions on r and s in Equations (24) and (25), one has the integral equations necessary for the specification of the unknown density functions in terms of the known applied stresses. Note, if $h(t) = 0$, Equation (24) with $0 < r < c$ is the appropriate integral equation for an interface crack [3] and similarly if $f(t) = g(t) = 0$ with $a < s < b$, Equation (25) is the integral equation for a crack perpendicular to a bonded interface, [1, Equation (4.7)]. Equations (24) and (25) are similar to [2, Equations (7.a,b)]. However, in the present study no difficulty arises in letting $a = 0$ as was the case in [2]. That is, the second integrals in Equations (24) and (25) do not contribute to the singular behavior of the density functions as long as $c \neq 0$. This is seen by noting that if $a = 0$, following [4], then $h(t) = H^*(t)/(t-b)^{\beta}$, where $H^*(t)$ satisfies a Hölder condition on the closed interval $0 \leq t \leq b$. The nature of the singular stress field near the crack tips is then the same as in the individual problems and the effect of the two cracks is only to change the value of the stress intensity factors. The proof of this follows from [4, p. 75], as

$$f(t)+ig(t) = \Phi(t) = \frac{G(t)}{(t-c)^{\xi}} \tag{28}$$

and

$$h(t) = \begin{cases} \dfrac{H(t)}{(t-a)^{1-\beta}(t-b)^{\beta}} & \text{for } a > 0 \\ \dfrac{H^*(t)}{(t-b)^{\beta}} & \text{for } a = 0 \ , \end{cases} \tag{29}$$

with $G(t)$, $H(t)$ and $H^*(t)$ satisfying a Hölder condition on the appropriate limits. Then letting

$$\Phi(z) = \frac{1}{2\pi i}\int_o^c \frac{G(t)}{t-z}\,dt = \frac{1}{2\pi i}\int_o^c \frac{G(t)-G(c)}{(t-c)^{\xi}(t-z)}\,dt$$

$$+ \frac{G(c)}{2\pi i}\int_o^c \frac{dt}{(t-c)^{\xi}(t-z)} = \frac{G(c)e^{i\pi\xi}}{(r-c)^{\xi}\sin(\pi\xi)}$$

$$+ \text{Bounded function at } r = c \ , \tag{30}$$

and

near $z = c$, with $z = r$, one has

$$\Phi(r) = -\frac{G(c)\cot(\pi\xi)}{2i(r-c)^{\xi}} + \text{Bounded terms} \ . \tag{31}$$

Substituting into Equation (24), and multiplying by $(r-c)^{\xi}$ with $r \to c$, one finds the equation for ξ to be

$$\xi = \frac{1}{2} + \frac{1}{2\pi}\ln\left(\frac{1+\gamma}{1-\gamma}\right) \text{ as in [5]} \ . \tag{32}$$

Similarly, for $a > 0$, let

$$h(z) = \frac{1}{2\pi i}\int_a^b \frac{H(t)}{(t-a)^{\alpha}(t-b)^{\beta}(t-z)} \ , \tag{33}$$

from which

$$h(z) = \frac{H(a)e^{i\pi\alpha}}{2i(z-a)^{\alpha}(b-a)^{\beta}\sin(\pi\alpha)} - \frac{H(b)}{2i(b-a)^{\alpha}(z-b)^{\beta}\sin(\pi\beta)}$$

$$+ \text{bounded terms} \ . \tag{34}$$

Substituting into Equation (24) and multiplying successively

by $(z-a)^{\alpha}$, $z \to a$, then $(z-b)^{\beta}$, $z \to b$ the two equations are

$$\cot(\pi\alpha) = 0 \quad ,$$

and

$$\cot(\pi\beta) = 0$$

or, therefore,

$$\alpha = \beta = 1/2 \quad .$$

If $a = 0$, $h(t) = \dfrac{H^*(t)}{(t-b)^{\beta}}$ and $\beta = 1/2$, $\alpha = 0$ in Equation (34).

Making the following changes in Equations (24) and (25):

$$\xi = ct, \quad r = cy, \quad a_o = (b-a)/2, \quad b_o = (b+a)/2, \quad \eta = \begin{cases} a_o t + b_o, & a \neq 0 \\ bt, & a = 0 , \end{cases}$$

$$s = \begin{cases} a_o x + b_o , & a \neq 0 \\ bx , & a = 0 , \end{cases} \qquad P(y) = p(cy), \quad Q(y) = q(cy),$$

$\phi(t) = g(ct) + if(ct)$, $\psi(t) = h(\eta)$, $P_o(x) = p_o(s)$, and noting that

$$\int_0^c f(t)\,[\text{even function in } t]\,dt = -\frac{i}{2}\int_{-c}^{c} [g(t)+if(t)] \times [\text{even function in } t]dt$$

and

$$\int_0^c tg(t)\,[\text{even function in } t]\,dt = \frac{1}{2}\int_{-c}^{c} t[g(t)+if(t)] \times [\text{even function in } t]dt,$$

the pair of singular integral equations are normalized as

$$\frac{1}{\pi i}\int_{-1}^{1} \phi(t)\,\frac{dt}{t-y} - \gamma\phi(y) = -\frac{1}{\alpha_1}[Q(y)-iP(y)] + \int_{-1}^{1}\psi(t)G(t,y)dt, \quad -1 < y < 1 \qquad (35)$$

and

$$\frac{1}{\pi}\int_{-1}^{1}\psi(t)\,\frac{dt}{t-x} + \int_{-1}^{1}\psi(t)H(t,x)dt = -\int_{-1}^{1}\phi(t)I(t,x)dt + \frac{1+\kappa_1}{2\mu_1}P_o(x), \quad -1 < x < 1. \qquad (36)$$

The functions $G(t,y)$, $H(t,x)$ and $I(t,x)$ are

$$G(t,y)= -\frac{\mu_1 a^*}{\alpha_1 \pi(1+\kappa_1)} \times$$

$$\left\{ i\eta \left[\left[2(\eta^2 - c^2y^2) - \frac{(1-m)(\eta^2-3c^2y^2)}{(1+m\kappa_1)} \right] \frac{1}{\eta^2+c^2y^2} + \frac{m\kappa_1-\kappa_2}{m+\kappa_2} \right] \right.$$

$$\left. + cy \left[\left[2(\eta^2-c^2y^2) - \frac{(1-m)(3\eta^2-c^2y^2)}{(1+m\kappa_1)} \right] \frac{1}{\eta^2+c^2y^2} - \frac{m\kappa_1-\kappa_2}{m+\kappa_2} \right] \right\} \frac{1}{\eta^2+c^2y^2}, \tag{37}$$

$$H(t,x)=-\frac{a^*}{2\pi} \left[\frac{1-m}{1+m\kappa_1} \left[\frac{8s^2}{(\eta+s)^3} - \frac{12s}{(\eta+s)^2} \right] + \left[\frac{m\kappa_1-\kappa_2}{m+\kappa_2} + \frac{3(1-m)}{1+m\kappa_1} \right] \frac{1}{\eta+s} \right], \tag{38}$$

$$I(t,x)= \frac{cm(1+\kappa_1)}{2\pi(1+m\kappa_1)(m+\kappa_2)} \left[is \left[(1+m\kappa_1) + \frac{(m+\kappa_2)(5c^2t^2+s^2)}{c^2t^2+s^2} \right] \right.$$

$$\left. + ct \left[(1+m\kappa_1) - \frac{(m+\kappa_2)(3c^2t^2-s^2}{c^2t^2+s^2} \right] \right] \frac{1}{c^2t^2+s^2} \tag{39}$$

where $\alpha_1 = \mu_2 \dfrac{(1+m\kappa_1+m+\kappa_2)}{(1+m\kappa_1)(m+\kappa_2)}$ and $a^* = \begin{cases} a_o & \text{if } a \neq 0 \\ b & \text{if } a = 0 \end{cases}$.

It is of interest to note that the above equations may be written in terms of only two independent combinations of elastic constants as shown by Dundurs in [6]. The following definitions prove convenient in the present work. Let

$$k_1 = \frac{1+m\kappa_1}{1+\kappa_2} \quad \text{and} \quad k_2 = \frac{m+\kappa_2}{1+\kappa_2}$$

then,

$$\frac{\mu_1}{\alpha\ (1+\kappa_1)} = \frac{k_1 k_2}{(k_1+k_2)(k_1+k_2-1)} \quad ,$$

$$\frac{1-m}{1+m\kappa_1} = \frac{1-k_2}{k_1} \quad ,$$

$$\frac{m\kappa_1 - \kappa_2}{m+\kappa_2} = \frac{k_1 - 1}{k_2} \quad ,$$

$$\frac{m(1+\kappa_1)}{m+\kappa_2} = \frac{k_1 + k_2 - 1}{k_2} \quad ,$$

$$\frac{m(1+\kappa_1)}{1+m\kappa_1} = \frac{k_1 + k_2 - 1}{k_1} \quad ,$$

and

$$\gamma = \frac{k_1 - k_2}{k_1 + k_2} \quad .$$

The usefulness in making such a change is most evident if one is able to write an asymptotic expansion for the solution in the vicinity of the crack tip. For example see Ashbaugh [7] for an analysis of the problem considered in [1]. A similar investigation is being undertaken for the present problem.

Equation (35) is a singular integral equation of the second kind, and is similar to [8, Equation (14)], although somewhat simpler due to the manner in which the unknown function, $\phi(t)$, appears. Following the procedure of [8], [9], [10], and [11], it is possible to determine $\phi(t)$ in terms of the unknown function $\psi(t)$ and the loads. Substituting into Equation (36), for $\phi(t)$, one then has a singular integral equation of the first kind of the same form as [11, Equation (4.11)]. For $a = 0$ Equation (36) is

an equation of the second kind as the singularity at the origin vanishes. The solution will first be developed for $a > 0$ and then $a = 0$. It should be noted that the determination of $\phi(t)$ is the same in either case; that is, the first part of the following analysis is true for all values of a.

Referring to [8] one can write

$$\phi(y) = w(y)\Phi(y), \quad w(y) = (1-y)^{\alpha}(1+y)^{\beta}, \quad |y| < 1$$

and

$$\alpha = -\frac{1}{2} - i\omega, \quad \beta = -\frac{1}{2} + i\omega \quad \text{with} \quad \omega = \frac{1}{2\pi}\ln\left(\frac{1+\gamma}{1-\gamma}\right).$$

Noting, as in [8], that $w(y)$ is the weight function of the Jacobi polynomials $P_n^{(\alpha,\beta)}(y)$, the solution is then written as

$$\phi(y) = w(y)\sum_{n=0}^{\infty} C_n P_n^{(\alpha,\beta)}(y), \tag{40}$$

with the Jacobi polynomials satisfying the orthogonality relation [8],

$$\int_{-1}^{1} w(y) P_n^{(\alpha,\beta)}(y)\, P_m^{(\alpha,\beta)}(y)\, dy =$$

$$\begin{cases} = 0, & n \neq m, \\ = \dfrac{2^{(\alpha+\beta+1)}\,\Gamma(n+\alpha+1)\Gamma(n+\beta+1)}{(2n+\alpha+\beta+1)n!\,\Gamma(n+\alpha+\beta+1)} = L(n,\alpha,\beta), & n = m \neq 0, \\ = \dfrac{\pi}{\cosh(\pi\omega)}, & n = m = 0. \end{cases} \tag{41}$$

The displacements are then found by integrating Equations (4) and (5), from which the constant C_o and the continuity condition of the function $\psi(t)$ are specified.

Integration of Equation (4) gives the opening displacement on $\theta = \pi$ as follows: where if $a = 0$, a_o is replaced by b,

$$u_{1\theta}(x,\pi) = -\frac{a_o}{2}\int_{-1}^{x}\psi(t)dt + \frac{a_o}{2}\int_{-1}^{1}\psi(t)dt \quad . \tag{42}$$

Similarly, integrating Equation (5) and separating real and imaginary parts gives,

$$u_{1r}(y,\pi/2) - u_{2r}(y,\pi/2) = -\,cIm\int_{o}^{y}\phi(t)dt + Im\,[C^*] \quad ,$$

and (43)

$$u_{1\theta}(y,\pi/2) - u_{2\theta}(y,\pi/2) = -\,cRe\int_{o}^{y}\phi(t)dt + Re\,[C^*] \quad ,$$

where

$$C^* = c\int_{o}^{1}\phi(t)dt \quad . \tag{44}$$

It follows from the form of $\phi(t)$ that

$$Im\,[C^*] = -\frac{ic}{2}\int_{-1}^{1}\phi(t)dt \quad , \tag{45}$$

then as

$$u_{1r}(o,\pi/2) - u_{2r}(o,\pi/2) = u_{1r}(o,\pi/2) = -\,u_{1\theta}(-1,\pi) \quad , \tag{46}$$

or, therefore, from Equations (42), (43), and (46),

$$u_{1r}(o,\pi/2) = -\frac{ic}{2}\int_{-1}^{1}\phi(t)dt = -\frac{b}{2}\int_{-1}^{1}\psi(t)dt \quad . \tag{47}$$

Now using Equation (40) and (41) the constant C_o is

$$C_o = -\frac{ib\cosh(\pi\omega)}{\pi c}\int_{-1}^{1}\psi(t)dt \quad , \tag{48}$$

where Equation (42) requires that

$$\int_{-1}^{1}\psi(t)dt = 0 \quad \text{if} \quad a \neq 0 \quad . \tag{49}$$

The opening displacement, $u_{1r}(o,\pi/2) = -\,u_{1\theta}(-1,\pi)$, is then given in terms of C_o as

$$u_{1r}(o,\pi/2) = - \frac{i\pi c}{2\cosh(\pi\omega)} C_o \qquad (50)$$

where C_o is seen to be imaginary from Equations (42) and (48).

Now substitute Equation (40) into Equation (35), and using the relation [8, Equation (22)] and [10] with $n > 0$,

$$\frac{1}{\pi i}\int_{-1}^{1} w(t)P_n^{(\alpha,\beta)}(t)\frac{dt}{t-y} - \gamma w(y)P_n^{(\alpha,\beta)}(y) = \frac{\sqrt{1-\gamma^2}}{2i} P_{n-1}^{(-\alpha,-\beta)}(y), \quad |y| < 1 \qquad (51)$$

one has, for $n \geq 1$,

$$\frac{\sqrt{1-\gamma^2}}{2i}\sum_{n=1}^{\infty} C_n P_{n-1}^{(-\alpha,-\beta)}(y) = - \frac{1}{\alpha_1}[Q(y)-P(y)] + \int_{-1}^{1}\psi(t)G(t,y)dt. \qquad (52)$$

Multiplying Equation (52) by $(1-y)^{-\alpha}(1+y)^{-\beta}P_k^{(-\alpha,-\beta)}(y)$, then integrating the resulting expression with respect to y over $[-1,1]$ for $k = 0, 1, 2, \ldots$, and using the orthogonality relations, Equation (41), the complex constants C_n are then given explicitly in terms of integrals of the unknown function $\psi(t)$, with C_o given by Equation (48), as

$$C_n = \frac{2i}{\sqrt{1-\gamma^2}\,L(n-1,-\alpha,-\beta)}\int_{-1}^{1}\left[-\frac{1}{\alpha_1}[Q(y)-iP(y)] + \int_{-1}^{1}\psi(t)G(t,y)dt\right] \times (1-y)^{-\alpha}(1+y)^{-\beta}P_{n-1}^{(-\alpha,-\beta)}(y)\,dy, \quad n = 1,2,\ldots \qquad (53)$$

if $\psi(t) = 0$, which corresponds to an interface crack only, and letting $P(y) = -\sigma_o$, $Q(y) = 0$, Equations (49) and (53) give $C_o = 0$, $C_n = 0$, $n \geq 2$ and

$$C_1 = \frac{2\sigma_o}{\alpha_1\sqrt{1-\gamma^2}} . \qquad (54)$$

This is the same as [8, Equation (26)] except for the algebraic sign which is due to the difference in sign of $\phi(t)$, i.e., see Equation (5) above and [8, Equation (4)]. One similarly finds the stress intensity factor, as in [8], to be

$$k_1 + ik_2 = \lim_{y \to 1^+} \sqrt{c}\ (y-1)^{-\alpha}(y+1)^{-\beta}\ [\tau_{1\theta\theta} + i\tau_{1r\theta}] \ .$$

From Equation (35) for $y \to 1^+$ and noting that the integral on $\psi(t)$ is bounded and $\phi(y) = 0$, $|y| > 1$ then

$$Q(y) - iP(y) = \tau_{1r\theta} - i\tau_{1\theta\theta} = -\alpha_1 \frac{1}{\pi i} \int_{-1}^{1} \phi(t)\ \frac{dt}{t-y} \tag{55}$$

or as

$$\phi(t) = \sum_{n=0}^{\infty} C_n (1-t)^{\alpha}(1+t)^{\beta} P_n^{(\alpha,\beta)}(t) = \sum_{n=0}^{\infty} C_n e^{-i\pi\alpha} (t-1)^{\alpha}(t+1)^{\beta} P_n^{(\alpha,\beta)}(t) \tag{56}$$

then

$$\frac{1}{\pi i} \int_{-1}^{1} \phi(t)\ \frac{dt}{t-y} = e^{-i\pi\alpha} (1+\gamma)(y-1)^{\alpha}(y+1)^{\beta} \sum_{n=0}^{\infty} C_n P_n^{(\alpha,\beta)}(y) \ .$$

For $$C_1 = \frac{2\sigma_o}{\alpha_1 \sqrt{1-\gamma^2}} \ , \quad C_o = 0, \ C_n = 0 \ \ n \geq 2$$

$$\tau_{1\theta\theta} + i\tau_{1r\theta} = \alpha_1 \sqrt{1-\gamma^2}\ (y-1)^{\alpha}(y+1)^{\beta}\ C_1 P_1^{(\alpha,\beta)}(y)$$

and as $$P_1^{(\alpha,\beta)}(y) = \frac{1}{2}\ (y - 2i\omega) \ ,$$

then $$k_1 + ik_2 = \sqrt{c}\sigma_o(1 - 2i\omega) \ , \tag{57}$$

which is the same as [8, Equation (31)]. Note misprint in [8] for k_2. In general the stress intensity factors are

$$k_1 + ik_2 = \alpha_1 \sqrt{c}\ \sqrt{1-\gamma^2} \sum_{n=0}^{\infty} C_n P_n^{(\alpha,\beta)}(1) \tag{58}$$

Now substituting for $\phi(t)$, using Equations (40), (48), and (53), into Equation (36) one has[1]

$$\frac{1}{\pi}\int_{-1}^{1}\psi(t)\,\frac{dt}{t-x}+\int_{-1}^{1}\psi(t)\Bigg[H(t,x)-\frac{ib}{c\pi}\cosh(\pi\omega)\int_{-1}^{1}w(z)I(z,x)dz$$
$$+\frac{2i}{\sqrt{1-\gamma^2}}\sum_{n=1}^{\infty}\frac{1}{L(n-1,-\alpha,-\beta)}\int_{-1}^{1}w(z)I(z,x)P_n^{(\alpha,\beta)}(z)\,dz\;\times$$
$$\int_{-1}^{1}G(t,y)(1-y)^{-\alpha}(1+y)^{-\beta}\,P_{n-1}^{(-\alpha,-\beta)}(y)\,dy\Bigg]dt=\frac{1+\kappa_1}{2\mu_1}P_o(x)$$
$$+\frac{2i}{\alpha_1\sqrt{1-\gamma^2}}\sum_{n=1}^{\infty}\frac{1}{L(n-1,-\alpha,-\beta)}\int_{-1}^{1}w(z)I(z,x)P_n^{(\alpha,\beta)}(z)\,dz\;\times$$
$$\int_{-1}^{1}[Q(y)-iP(y)](1-y)^{-\alpha}(1+y)^{-\beta}\,P_{n-1}^{(-\alpha,-\beta)}(y)\,dy\,. \tag{59}$$

If $Q(y)=0$, $P(y)=-\sigma_o$, and as $P_o^{(-\alpha,-\beta)}(y)=1$ with

$$k(x,t)=H(t,x)-\frac{ib}{c\pi}\cosh(\pi\omega)\int_{-1}^{1}w(z)I(z,x)dz$$
$$+\frac{2i}{\sqrt{1-\gamma^2}}\sum_{n=1}^{\infty}\frac{1}{L(n-1,-\alpha,-\beta)}\int_{-1}^{1}w(z)I(z,x)P_n^{(\alpha,\beta)}(z)\,dz\;\times$$
$$\int_{-1}^{1}G(t,y)(1-y)^{-\alpha}(1+y)^{-\beta}\,P_{n-1}^{(-\alpha,-\beta)}(y)\,dy \tag{60}$$

then Equation (59) is

$$\frac{1}{\pi}\int_{-1}^{1}\psi(t)\,\frac{dt}{t-x}+\int_{-1}^{1}\psi(t)k(x,t)dt=\frac{1+\kappa_1}{2\mu_1}P_o(x)$$
$$-\frac{2\sigma_o}{\alpha_1\sqrt{1-\gamma^2}}\int_{-1}^{1}w(z)I(z,x)P_1^{(\alpha,\beta)}(z)\,dz \tag{61}$$

---

[1] The term $\frac{-ib}{c\pi}\cosh(\pi\omega)\int_{-1}^{1}w(z)I(z,x)dz$ is only present if $a=0$, if $a\neq 0$ this term is set equal to zero.

which is the same form as [11, Equation (4.1)] where the right hand side is denoted by $g(x)$.

For $a > 0$ this is an equation of the first kind and the solution follows exactly as in [11], in terms of the Chebyshev polynomials. Let

$$\psi(t) = \frac{1}{\sqrt{1-t^2}} F(t) \text{ with } \int_{-1}^{1} \psi(t)dt = 0 , \qquad (62)$$

and further assume $P_o(x) = -\sigma_1$.

Substituting into Equation (61) and referring to [11], the solution is

$$\sum_{k=1}^{N} \frac{1}{N} F(t_k)\left[\frac{1}{t_k - x_r} + \pi k(x_r, t_k)\right] = -\frac{1+\kappa_1}{2\mu_1}\sigma_1 - \frac{2\sigma_o}{\alpha_1\sqrt{1-\gamma^2}} \int_{-1}^{1} w(z) I(z,x_r) P_1^{(\alpha,\beta)}(z)\, dz, \qquad (63)$$

where $r = 1,2,\ldots,N-1$, $t_k = \cos\left[\frac{(2k-1)\pi}{2N}\right]$, $x_r = \cos\left(\frac{\pi r}{N}\right)$,

and $$\sum_{k=1}^{N} \frac{\pi}{N} F(t_k) = 0 \quad .$$

N is chosen large enough to give sufficient accuracy in the Gauss-Chebyshev integration formula, [12, p. 889]. The solution of Equation (63) then gives the value of the unknown function $F(t)$ at N points on $-1 < t < 1$, from which one can now determine approximate values for C_n from Equations (48) and (53) by numerically integrating the integrals containing $\psi(t)$. The stress intensity factors

for the ends a and b are then [1], for $a > 0$

$$k(a) = \frac{2\mu_1 \sqrt{a_o}}{1+\kappa_1} F(-1) \tag{64}$$

and

$$k(b) = -\frac{2\mu_1 \sqrt{a_o}}{1+\kappa_1} F(+1) \tag{65}$$

For $a = 0$, the appropriate change of variable for η and s in Equations (24) and (25) is shown in [13] to be

$$\eta = tb \ , \ s = xb \quad \text{and} \quad \psi(t) = h(tb).$$

It is further suggested in [13] that the range of definition of the function $\psi(t)$ be extended into the interval (-1,0) in order to use the Jacobian integration formula associated with $P_n^{(-1/2,-1/2)}(t)$.

Let, following [13],

$$\psi(t) = \frac{1}{\sqrt{1-t}} F(t) = \frac{1}{\sqrt{1-t^2}} \tilde{F}(t) \tag{66}$$

from which the solution is given by the set of equations

$$\sum_{k=1}^{N} \frac{1}{2N+1} \tilde{F}(t_k) \left[\frac{1}{t_k - x_r} + \pi k(x_r, t_k) \right]$$

$$= -\frac{1+\kappa_1}{2\mu_1} \sigma_1 - \frac{2\sigma_o}{\alpha_1 \sqrt{1-\gamma^2}} \int_{-1}^{1} w(z) I(z, x_r) P_1^{(\alpha,\beta)}(z) \, dz \tag{67}$$

where $r = 1,2,\ldots,N; X_r = \cos\left(\frac{\pi r}{2N+1}\right)$; $t_k = \cos\left[\frac{(2k-1)\pi}{4N+2}\right]$.

The stress intensity factor at the end, b, is

$$k(b) = -\frac{2\mu_1 \sqrt{b}}{1+\kappa_1} \tilde{F}(1) \ . \tag{68}$$

The strain energy release rate for the interface crack is given as [5, Equation 71], [14],

$$\frac{\partial U}{\partial c} = \frac{\pi(1+m\kappa_1)(m+\kappa_2)}{2\mu_2[(1+m\kappa_1)+(m+\kappa_2)]} (k_1^2 + k_2^2) \ . \tag{69}$$

Numerical Solution and Results

The numerical solution to Equations (62) and (63) for $a > 0$, and Equations (67) for $a = 0$, has been obtained for the particular case of aluminum-epoxy half-planes for ease in comparing with the results presented in [1] and [2]. The results presented are for constant pressure on the crack surfaces and no loads at infinity, or therefore the solution previously denoted by σ_{II}. The pressures are chosen by assuming solution σ_I to correspond to a unit vertical stress at infinity in the aluminum and a uniform horizontal stress giving zero horizontal strain in the aluminum. The stresses σ_o, σ_1 and σ_2 are then, for plane strain,

$$\sigma_o = \frac{\nu_1}{1-\nu_1} = 0.42857, \quad \sigma_1 = 1.0, \quad \sigma_2 = 0.26844, \quad \text{for aluminum-epoxy} \tag{70}$$

and

$$\sigma_o = \frac{\nu_2}{1-\nu_2} = 0.42857, \quad \sigma_1 = 0.26844, \quad \sigma_2 = 1.0, \quad \text{for epoxy-aluminum,}$$

where $E_{al.} = 1.0 \times 10^7$ psi, $E_{ep.} = 4.45 \times 10^5$ psi, $\nu_{al.} = 0.30$, $\nu_{ep.} = 0.35$.

With $F(t)$ known, the constants C_n are computed from Equation (49) and (53) and the solution is complete. The displacements are then given by Equation (42), (43), (44), (50), the stress intensity factors by Equations (58), (64), (65), and the strain energy release rate by Equation (69).

The number of points, N, taken in Equations (63) and (67) and the number of constants C_n, M, computed from Equation (53) were taken sufficiently large to give less

than one percent error in any of the above computed functions. The maximum error was determined by taking successively larger values for M and N and examining the change in the various computed functions mentioned above. Sufficient accuracy was assumed when the most slowly converging of these functions, which in all cases was the strain energy release rate, numerically converged to within the prescribed degree of accuracy. For example, if a = 0, b = 1, c = 1, values of M = N = 14 were found to be sufficient. If a = 0, b = 1, c = 0.1 it was necessary to take M = 30 and N = 20. Convergence was somewhat more rapid for the aluminum-epoxy pair than for epoxy-aluminum, apparently due to the increased distortion in the epoxy-aluminum.

Of particular importance in the investigation is the potential for further extension or arrest of a crack originating in one half-plane, as the crack either crosses the interface into the adjacent material or extends along the interface. By assuming each possibility for extension, computing the appropriate stress intensity factors as a function of continued growth, and comparing either stress intensity factors for the through crack or strain energy release rate for the interface crack with the critical values, one can determine if continued extension is possible or if the crack will arrest after a specified growth. It should be noted that for non-symmetrical loading or geometry, possible directions for crack extension are not as restricted.

As an illustration of this criterion, the case of a crack crossing the interface first will be presented using the results of [1] and [2]. The stress intensity factors for a crack originating in material one and growing toward and crossing the interface into material two are presented in Figures 2 and 3. Figure 2 is for an aluminum-epoxy pair and Figure 3 for an epoxy-aluminum pair. From Figure 2 it is seen that after crossing the interface into region 2 the stress intensity factor, $K(a)$ is initially a decreasing function of continued extension and then changes slope and approaches the full plane solution. It then appears possible to have some extension into the epoxy and subsequent arrest. For the epoxy-aluminum pair, Figure 3 indicates that the crack will extend to the left rather than toward the interface. However, if the crack does cross the interface, the stress intensity factor, $K(a)$ grows unbounded with continued extension and arrest is not possible.

Figure 4 represents the analogous cases as above, using the results developed in the present study, with the crack now assumed to extend along the interface rather than cross into the adjacent material. Until the crack tip, a, reaches the interface and begins to extend along the bond, the stress intensity factors, $K(a)$ and $K(b)$ depend only on σ_1 and have the same form as the left side of Figure 2 and Figure 3. Therefore, in Figure 4, only the strain energy release rate for the crack extending along the bond is

presented. Figure 4 is seen to represent the same general behaviour as K(a) in Figure 2 and again indicates the possibility of arrest. It is of considerable interest to note that for all material pairs investigated, $\frac{\partial U}{\partial c} \to 0$ as $c \to 0$ for $\frac{\mu_2}{\mu_1} = m < 1$ and $\frac{\partial U}{\partial c} \to \infty$ as $c \to 0$ for $m \geq 1$. This behaviour can be anticipated from the results of [1, Table 7] where the opening stress on the interface near the crack tip is shown to be compressive for $m < 1$ and tensile for $m \geq 1$.

The values of K(b) corresponding to the geometry and loads of Figure 4 are shown in Figure 5. The decrease in K(b) with increasing half length c as seen on the right hand side of Figure 5 is due to the closing affect of the interface crack on the $\theta = \pi$ surface. In fact, for the epoxy-aluminum pair with the loads given the crack on $\theta = \pi$ was found to partially close at $c = 2.75$. The closing stress is shown in Figures 6 and 7 for aluminum-epoxy and epoxy-aluminum respectively.

Some characteristic displacements for the crack surface on $\theta = \pi$ are depicted in Figure 8 and Figure 9 and numerical values for some of the significant computed functions given in Table 1 and Table 2. The effects of increased half-length, c on K(b) and the opening displacements are clearly seen in these two figures and the tables, with the epoxy-aluminum having the more noticeable change.

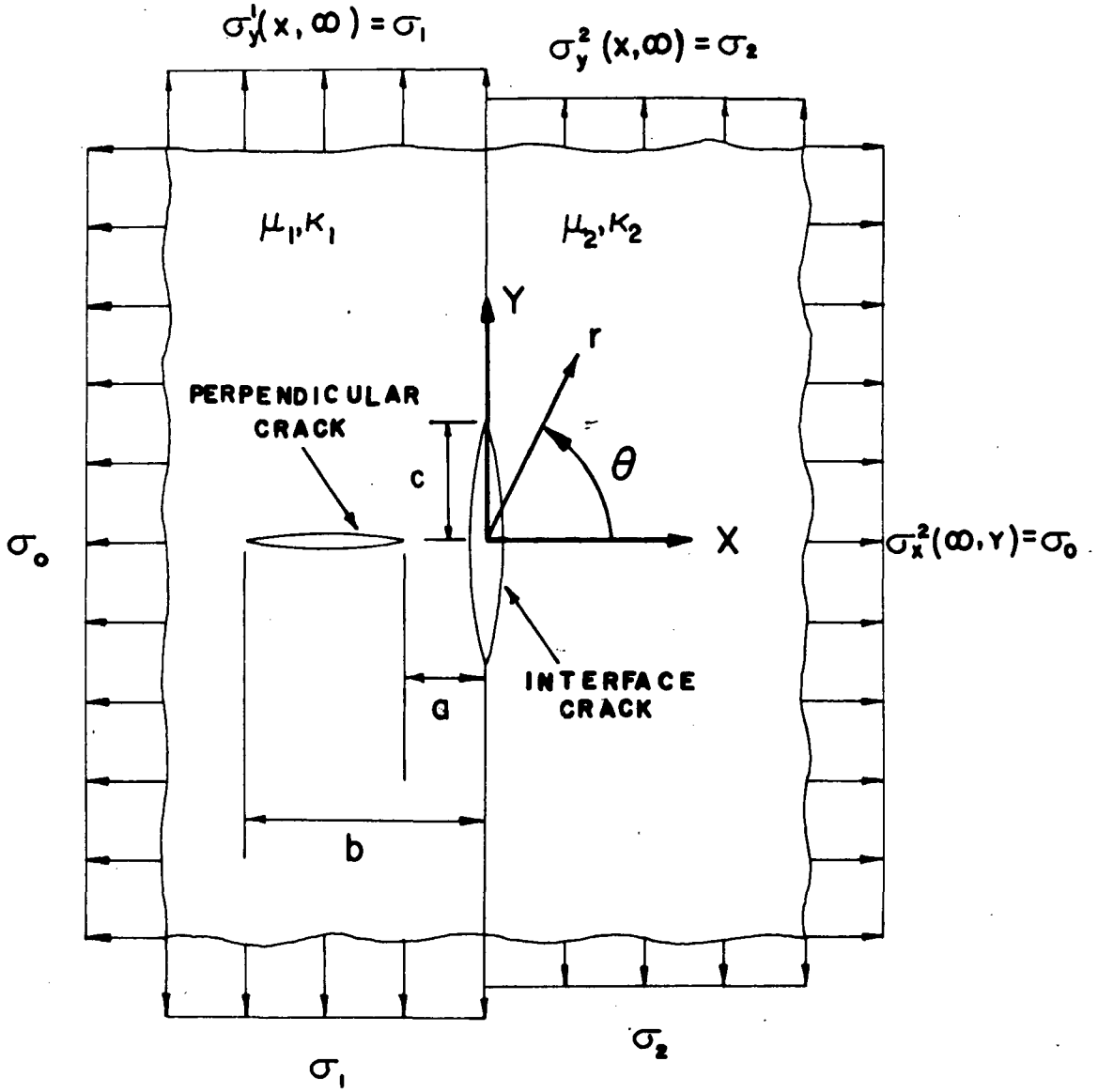

Figure 1. Bonded Elastic Half-Planes with Perpendicular Cracks.

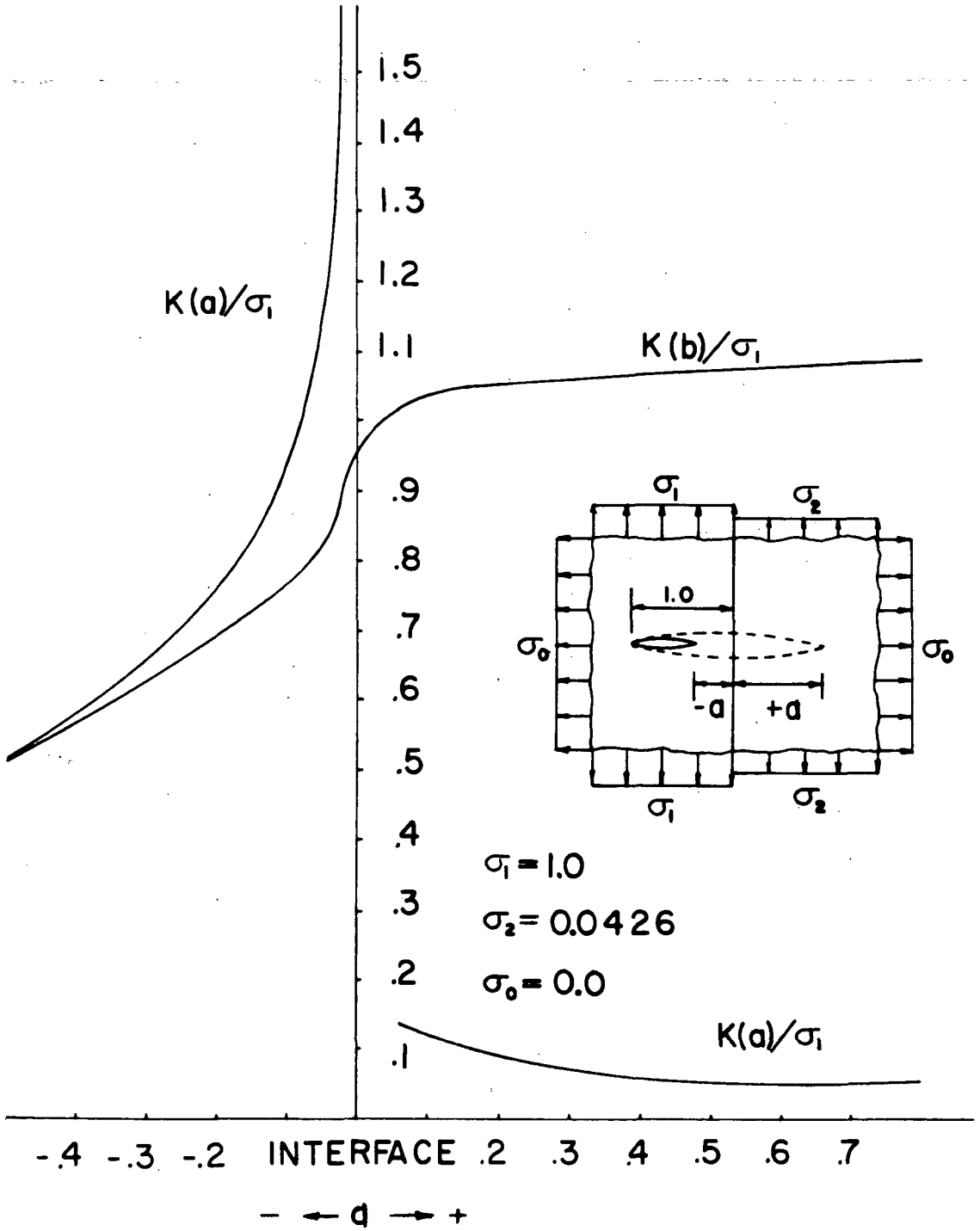

Figure 2. Stress Intensity Factors For a Crack Originating in an Aluminum Half-Plane and Growing into an Adjacent Epoxy Half-Plane (from [1] and [2]). Plane Strain.

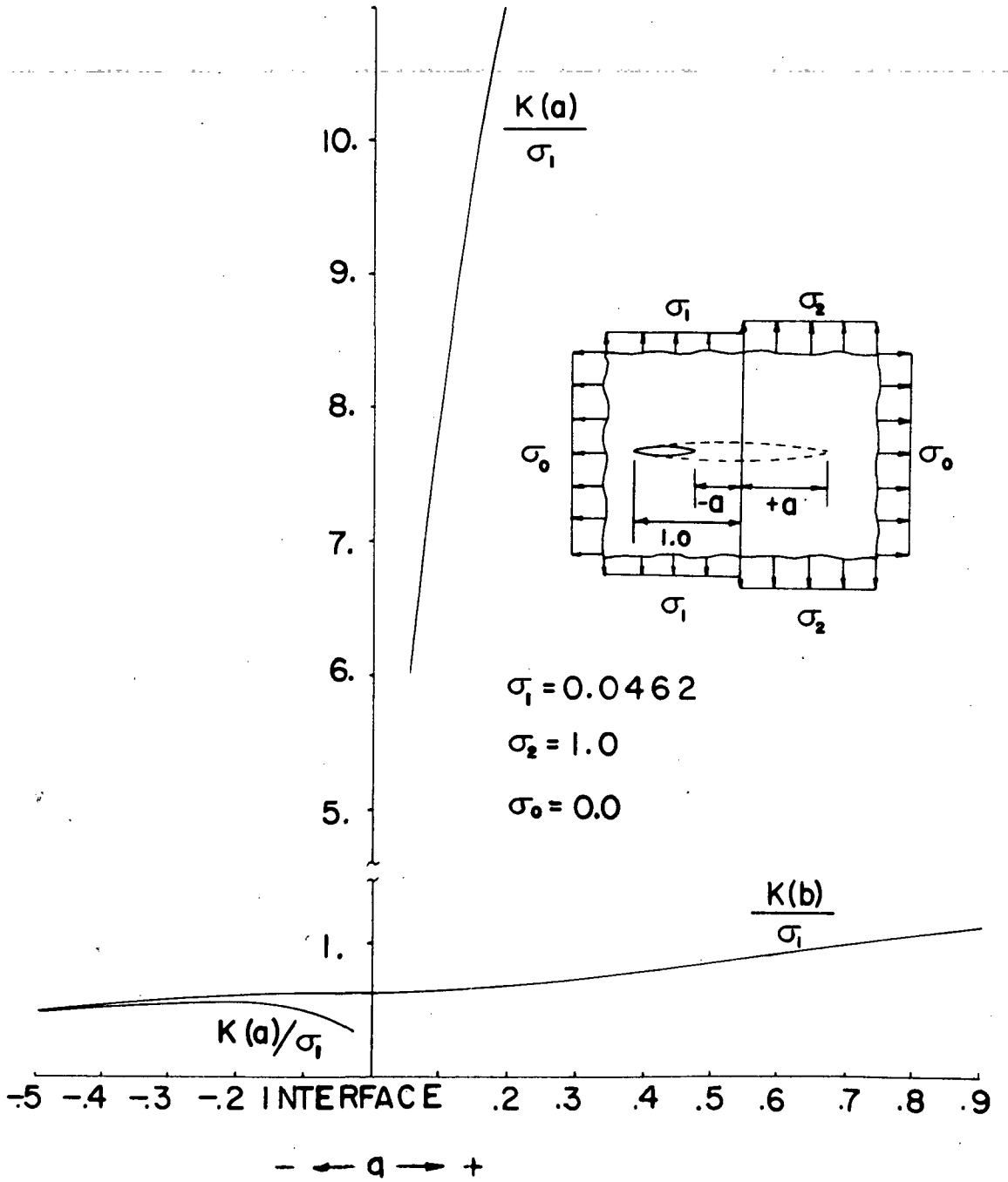

Figure 3. Stress Intensity Factors for a Crack Originating an Epoxy Half-Plane and Growing into an Adjacent Aluminum Half-Plane (from [1] and [2]). Plain Strain.

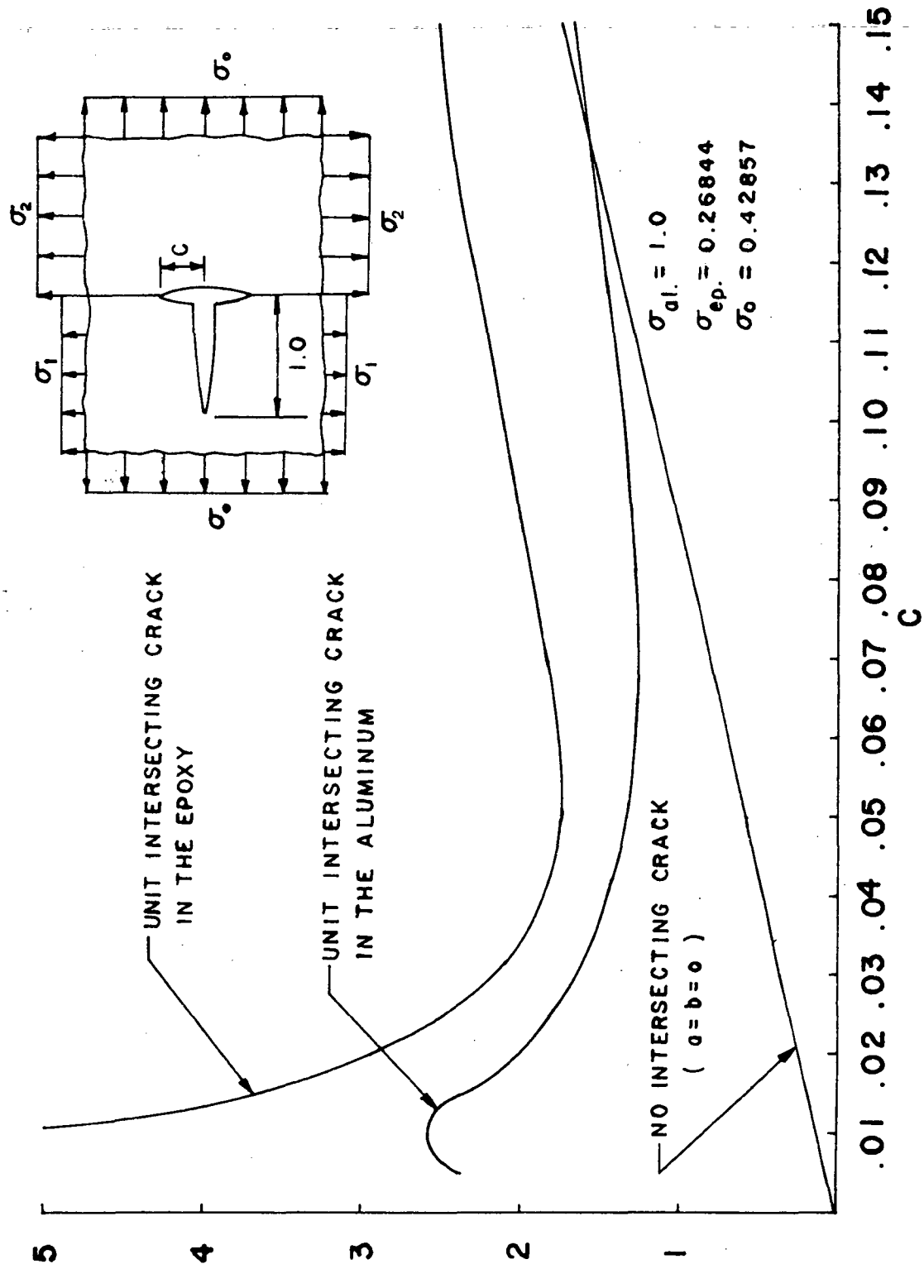

Figure 4. Strain Energy Release Rate for an Intersecting Crack with Extension Along the Interface. Plane Strain

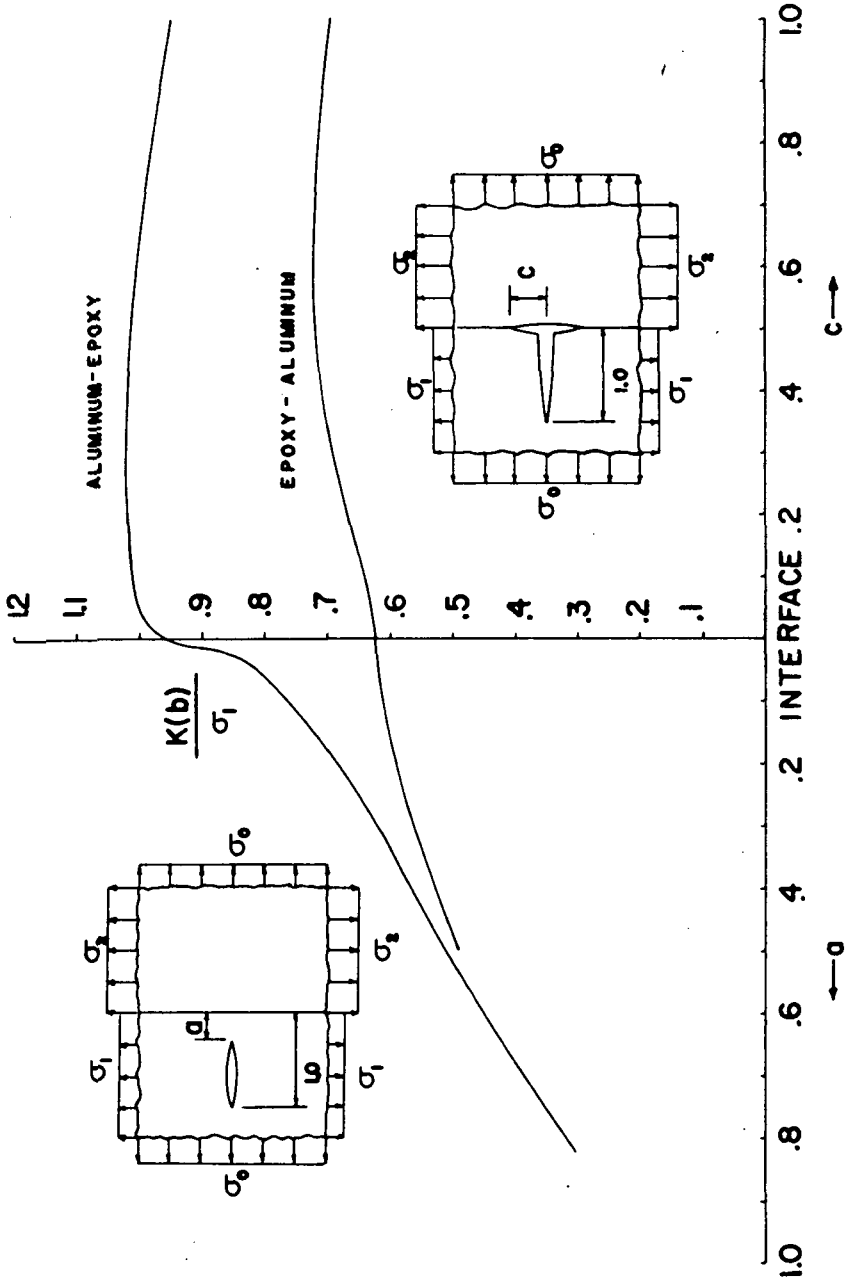

Figure 5. Stress Intensity Factor, k(b), for an Intersecting Crack with Extension along the Interface. Plane Strain.

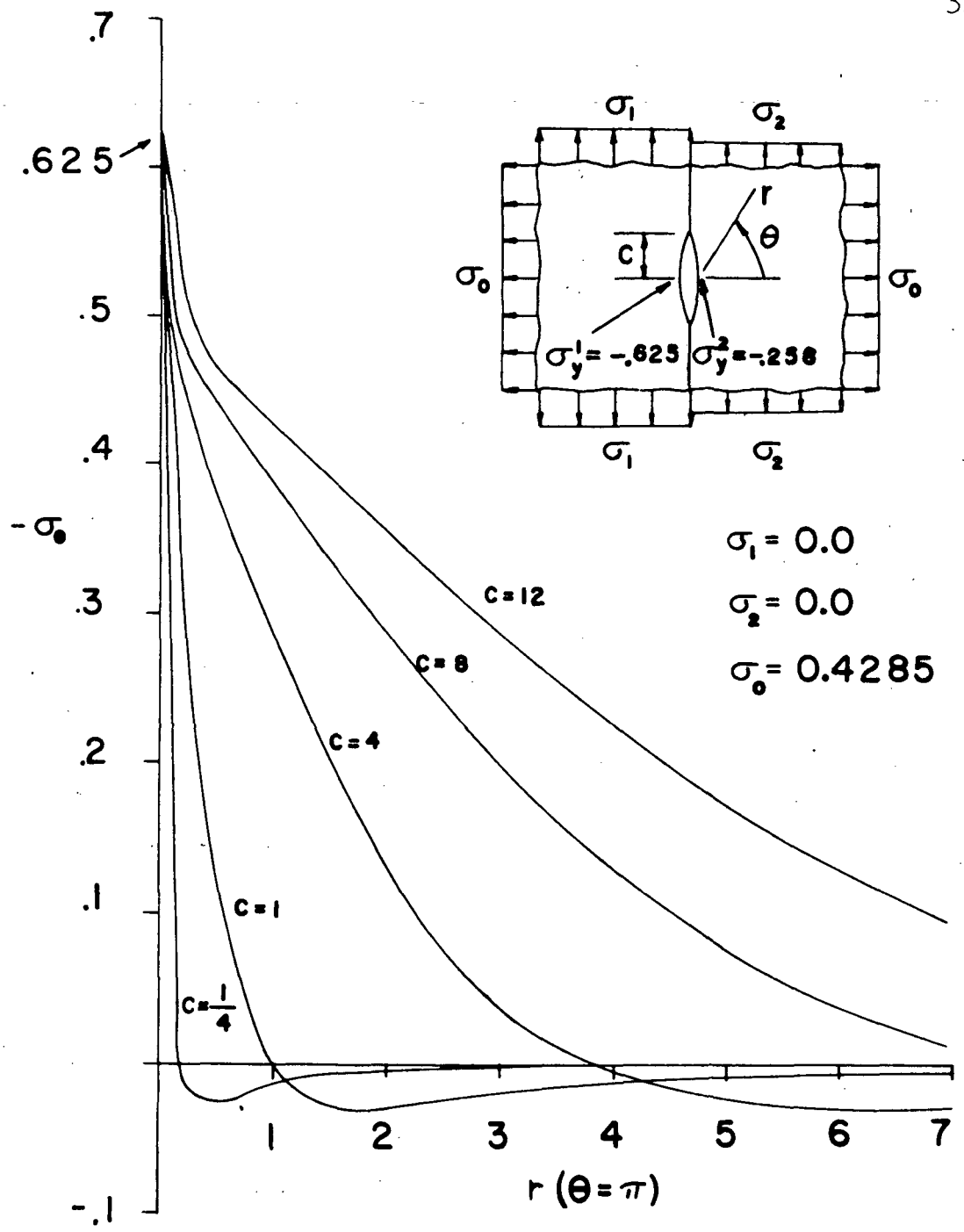

Figure 6. Normal Stress on $\theta = \pi$ due to a Crack on the Interface. Aluminum-Epoxy. Plane Strain.

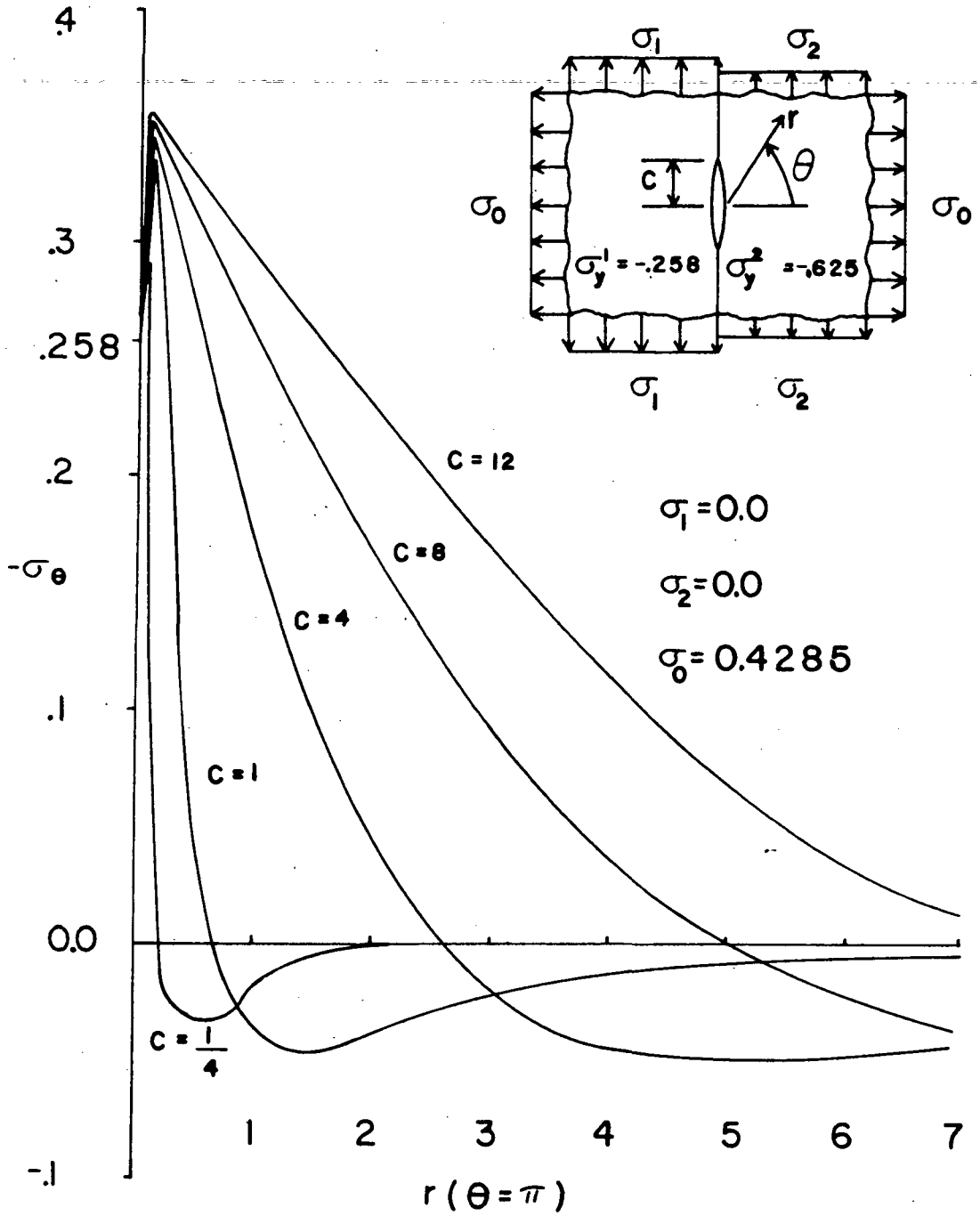

Figure 7. Normal Stress on $\theta = \pi$ due to a Crack on the Interface. Epoxy-Aluminum. Plane Strain.

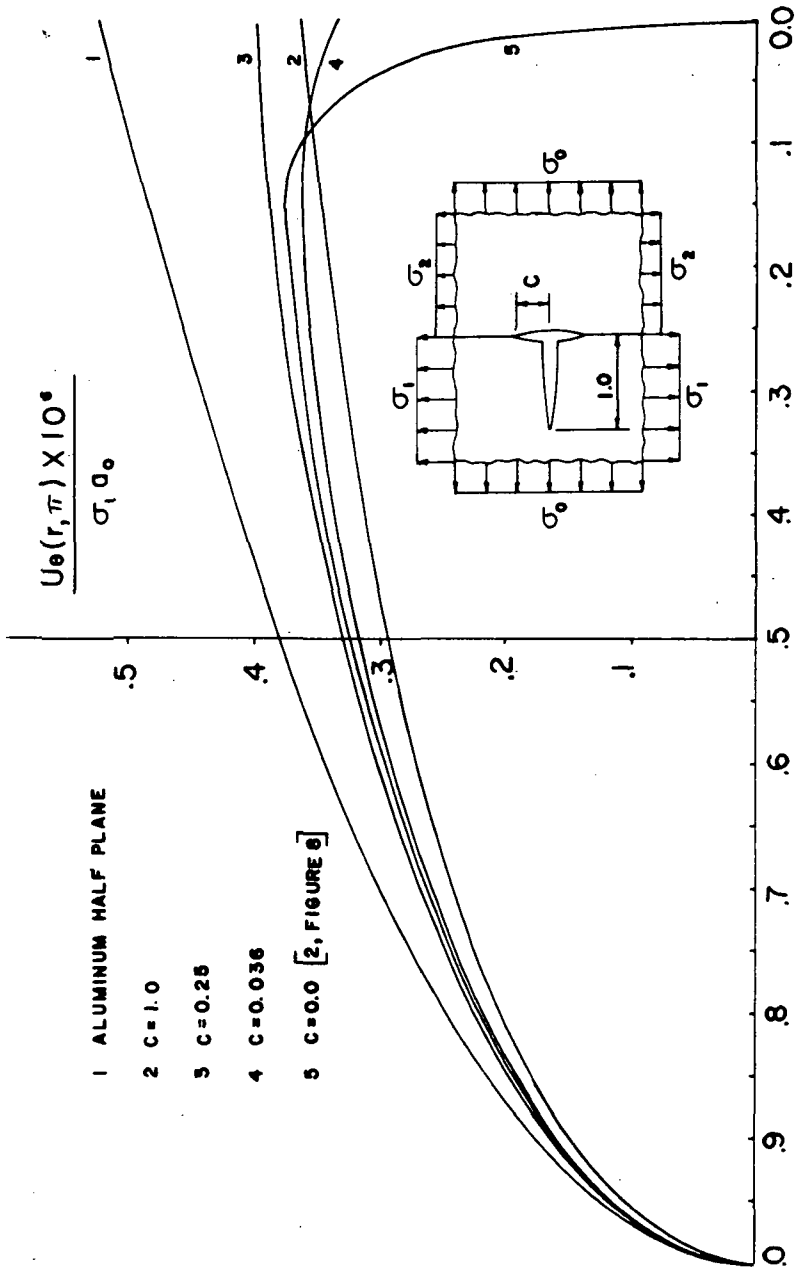

Figure 8. Crack Surface Opening Displacements on $\theta = \pi$ for Intersecting Cracks. Aluminum-Epoxy. Plane Strain. $\sigma_0 = 0.4285$, $\sigma_1 = 1.0$, $\sigma_2 = 0.2684$.

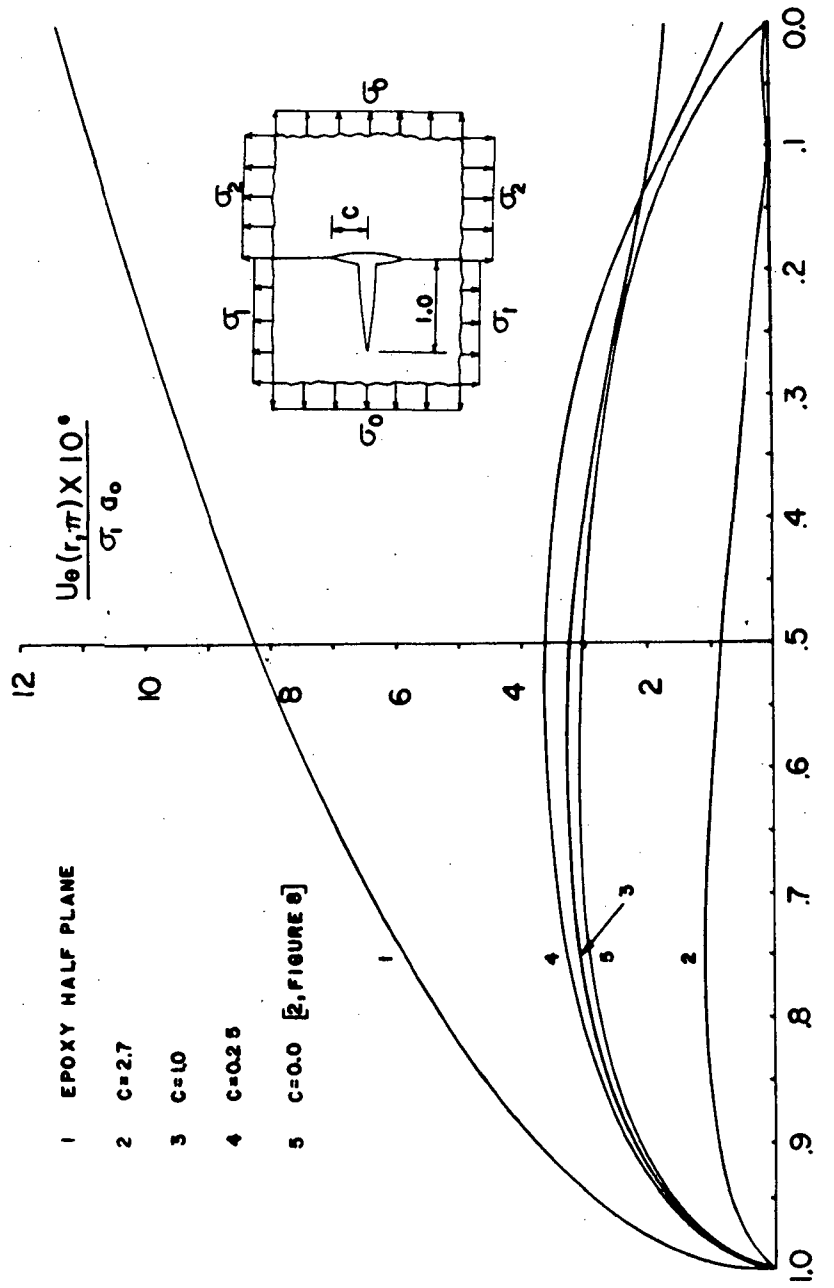

Figure 9. Crack Surface Opening Displacements on $\theta = \pi$ for intersecting Cracks. Epoxy-Aluminum. Plane Strain. $\sigma_0 = 0.4285$, $\sigma_1 = .2684$, $\sigma_2 = 1.0$.

a	c	$\frac{k(b)}{\sigma_1}$	$\frac{k(a)}{\sigma_1}$	k_1	k_2	STRAIN ENERGY RELEASE RATE X 10^7	STRAIN ENERGY RELEASE RATE X 10^7 (a=b=0)
0.3333	0.0	0.6050	0.6242	-	-	-	-
0.111	0.0	0.7522	0.8926	-	-	-	-
0.0697	0.0	0.7904	1.0210	-	-	-	-
0.0476	0.0	0.8154	1.1377	-	-	-	-
0.0	0.0	0.9582*	∞*	-	-	-	-
0.0	0.005	0.9746	0.0	0.0430	0.1916	2.3902	0.0580
0.0	0.010	0.9814	0.0	0.0483	0.1979	2.5726	0.1159
0.0	0.015	0.9861	0.0	0.0541	0.1820	2.2361	0.1739
0.0	0.050	1.0025	0.0	0.0873	0.1181	1.3379	0.5797
0.0	0.075	1.0090	0.0	0.1060	0.0971	1.2808	0.8696
0.0	0.100	1.0136	0.0	0.1224	0.0829	1.3558	1.1594
0.0	0.150	1.0197	0.0	0.1510	0.0640	1.6680	1.7391
0.0	4.0	0.7073	0.0	0.8575	-0.1111	46.3612	46.3770

*From [1].

Table 1. Numerical Value for Stress Intensity Factor and Strain Energy Release Rate for Intersecting Cracks. Aluminum-Epoxy. Plane Strain, b = 1.

a	c	$\frac{k(b)}{\sigma_1}$	$\frac{k(a)}{\sigma_1}$	k_1	k_2	STRAIN ENERGY RELEASE RATE X 10^7	STRAIN ENERGY RELEASE RATE X 10^7 (a=b=0)
0.3333	0.0	0.5551	0.5397	-	-	-	-
0.1111	0.0	0.6109	0.5224	-	-	-	-
0.0697	0.0	0.6172	0.4895	-	-	-	-
0.0476	0.0	0.6200	0.4605	-	-	-	-
0.0	0.0	0.6241*	0.0*	-	-	-	-
0.0	0.005	0.6245	0.0	0.1192	0.3747	9.5856	0.0580
0.0	0.010	0.6251	0.0	0.1262	0.2801	5.8517	0.1159
0.0	0.015	0.6258	0.0	0.1338	0.2035	3.6775	0.1739
0.0	0.050	0.6328	0.0	0.1571	0.0561	1.7252	0.5797
0.0	0.075	0.6387	0.0	0.1656	0.0559	1.8959	0.8696
0.0	0.100	0.6448	0.0	0.1725	0.0658	2.1136	1.1594
0.0	0.150	0.6577	0.0	0.1842	0.0804	2.5062	1.7391
0.0	2.7	0.3101	0.0	0.7023	0.1000	31.2066	31.3040

*From [1].

Table 2. Numerical Values for Stress Intensity Factors and Strain Energy Release Rate for Intersecting Cracks. Epoxy-Aluminum. Plane Strain, b= 1.

BIBLIOGRAPHY

1. T. S. Cook, and F. Erdogan, "Stresses in Bonded Materials with a Crack Perpendicular to the Interface," Int. J. Engr. Science, Vol. 10, (Nov. 1972), pp. 677-697.

2. F. Erdogan, and V. Biricikoglu, "Two Bonded Half-Planes with a Crack Going Through the Interface," Technical Report, NASA-TR-72-4, June, 1974.

3. F. Erdogan, "Simultaneous Dual Integral Equations with Trigonometric and Bessel Kernals," Z. Angew, Math. Mech., Vol. 48, (1968), pp. 217-225.

4. N. I. Muskhelishvili, Singular Integral Equations, P. Noordhoff, Groningen, The Netherlands, (1953).

5. F. Erdogan, and G. Gupta, "The Stress Analysis of Multi-layered Composites With a Flaw," Int. J. Solids Structures, Vol. 7, (1971), pp. 39-61.

6. J. Dundurs, "Effect of Elastic Constants on Stress in a Composite Under Plane Deformation," J. of Composite Materials, Vol. 1, No. 3, (July, 1967), pp. 310-322.

7. N. E. Ashbaugh, "On the Opening of a Finite Crack Normal to an Interface," J. Applied Mechanics, Vol. 40, No. 2, (June, 1973), pp. 533-540.

8. F. Erdogan, and G. D. Gupta, "Layered Composites with an Interface Flaw," Int. J. Solids Structures, Vol. 7, (1971), pp. 1089-1107.

9. L. N. Karpenko, "Approximate Solution of a Singular Integral Equation by Means of Jacobi Polynomials," PMM, Vol. 30, No. 3, (1960), pp. 564-569.

10. F. Erdogan, G. D. Gupta, and T. S. Cook, "Numerical Solution of Singular Integral Equations," Methods of Analysis and Solutions of Crack Problems, Edited by G. C. Sih, Noordhoff International Publishing, Leyden.

11. F. Erdogan, and G. D. Gupta, "On the Numerical Solution of Singular Integral Equations," Quarterly of Applied Mathematics, (January, 1972), pp. 525-534.

12. M. Abramowitz, and I. A. Stegun, "Handbook of Mathematical Functions," National Bureau of Standards, Appl. Math. Series 55, (1964).

13. G. D. Gupta and F. Erdogan, "The Problem of Edge Cracks in an Infinite Strip," J. Applied Mechanics, Vol. 41, No. 4, (December, 1974), pp. 1001-1006.

14. B. M. Malyshev, and R. L. Salganik, "The Strength of Adhesive Joints using the Theory of Fracture," Int. J. Fracture Mechanics, Vol. 1, (1965), pp. 114-128.

BONDED ELASTIC HALF-PLANES WITH AN INTERFACE CRACK AND A PERPENDICULAR INTERSECTING CRACK THAT EXTENDS INTO THE ADJACENT MATERIAL[1]

By

James G. Goree
Associate Professor of Mechanics and
Mechanical Engineering

William A. Venezia[2]
Graduate Assistant
Ph.D. Candidate in
Engineering Mechanics

The problem considered in this paper is a direct continuation of the preceeding study to include the case of the crack crossing the interface as well as debonding along the interface. The notation of the preceeding paper, refered to as Part I, will be used throughout and citations from Part I will be made directly by equation or reference number which are followed sequentially in the present study.

---

[1] Submitted to the 14th International Congress of Theoretical and Applied Mechanics.

[2] Currently at Johns Hopkins University, Applied Physics Laboratory, Laurel, Maryland 20810.

Formulation

Assuming a coordinate system having the origin at the center of the interface crack, as shown in Figure 10, it is seen to be convenient to represent the solution in terms of the polar variables (r,θ), as the crack surfaces, the interface, and the horizontal plane of symmetry lie on constant θ surfaces. The cases of intersecting cracks (a or a* equal to zero, separately or simultaneously) and non-intersecting cracks (a and a* not equal to zero) are considered.

Following Part I, the Mellin transforms of the stresses and displacement are:

$$M\left[r^2\sigma_k(r,\theta)\right] = \Sigma_k(s,\theta) = 2i(s+1) \quad X$$

$$\left[A_k s e^{is\theta} + B_k(s+1)e^{i(s+2)\theta} - \bar{B}_k e^{-i(s+2)\theta}\right],$$

$$M\left[r^2\tau_{krr}(r,\theta)\right] = -s(s+1)\left[A_k e^{is\theta} + \bar{A}_k e^{-is\theta}\right]$$

$$-(s+1)(s+4)\left[B_k e^{i(s+2)\theta} + \bar{B}_k e^{-i(s+2)\theta}\right],$$

$$M\left[r^2 v_k(r,\theta)/2\mu_k\right] = V_k(s,\theta)$$

$$= -(s+1)/\mu_k\left[A_k s e^{is\theta} + B_k(s+1)e^{i(s+2)\theta} + \kappa_k\bar{B}_k e^{-i(s+2)\theta}\right],$$

where $\kappa_k = \begin{cases} 3-4\nu_k & \text{for plane strain} \\ (3-\nu_k)/(1+\nu_k) & \text{for generalized plane stress} \end{cases}$

and μ_k , ν_k are the shear modulus and Poisson's ratio respectively. The transformed functions above are [1],

$$\sigma_k(r,\theta) = \tau_{kr\theta}(r,\theta) + i\tau_{k\theta\theta}(r,\theta) ,$$

$$\tau_{krr}(r,\theta) = \tau_{krr}(r,\theta)$$

and

$$v_k(r,\theta) = 2\mu_k \left[\frac{\partial u_{kr}(r,\theta)}{\partial r} + i \frac{\partial u_{k\theta}(r,\theta)}{\partial r} \right] \text{ with } k = 1,2$$

for region 1 and 2 respectively.

Using displacement dislocations on the surfaces $\theta = 0$, $\theta = \pi$, $\theta = \pi/2$, the boundary conditions are:

$$\left.\begin{aligned} &\tau_{2r\theta}(r,0) = 0 \\ &\frac{\partial}{\partial r}\mu_{2\theta}(r,0) = -\frac{1}{2} h^*(r)\delta(r-r_o) \end{aligned}\right\} \text{, on } \theta = 0 \text{ in material 2} \tag{71}$$

$$\left.\begin{aligned} &\tau_{1r\theta}(r,\pi) = 0 \\ &\frac{\partial}{\partial r} U_{1\theta}(r,\pi) = -\frac{1}{2} h(r)\delta(r-r_o) \end{aligned}\right\} \text{, on } \theta = \pi \text{ in material 1} \tag{72}$$

and

$$\left.\begin{aligned} &\tau_{1r\theta}(r,\pi/2) = \tau_{2r\theta}(r,\pi/2) \\ &\tau_{1\theta\theta}(r,\pi/2) = \tau_{2\theta\theta}(r,\pi/2) \\ &\frac{\partial}{\partial r} U_{1r}(r,\pi/2) - \frac{\partial}{\partial r} U_{2r}(r,\pi/2) = -f(r)\delta(r-r_o) \\ &\frac{\partial}{\partial r} U_{1\theta}(r,\pi/2) - \frac{\partial}{\partial r} U_{2\theta}(r,\pi/2) = -g(r)\delta(r-r_o) \end{aligned}\right\} \text{, interface } \theta = \pi/2 \tag{73}$$

where the second of Equations (71) is the only change from Part I. On transforming the above boundary conditions, the resulting eight equations specifying the unknowns C_i' are as follows:

$$sC_6' + (s+1)C_8' + C_8' = 0 , \tag{74}$$

$$sC_6' + (s+1)C_8' - \kappa_2 C_8' = -\frac{\mu_2 h^*(r_o) r_o^{s+1}}{2(s+1)} \tag{75}$$

$$sC_1'\sin(\pi s)+sC_2'\cos(\pi s)+(s+2)C_3'\sin(\pi s)+(s+2)C_4'\cos(\pi s)=0 , \tag{76}$$

$$sC_1'\sin(\pi s)+sC_2'\cos(\pi s)+(s+1-\kappa_1)C_3'\sin(\pi s)+(s+1-\kappa_1)C_4'\cos(\pi s) = \frac{\mu_1 h(r_o) r_o^{s+1}}{2(s+1)} , \tag{77}$$

$$sC_1'\cos(\pi s/2)-sC_2'\sin(\pi s/2)-sC_3'\cos(\pi s/2)+sC_4'\sin(\pi s/2) - s(C_5'-C_7')\cos(\pi s/2)+s(C_6'-C_8')\sin(\pi s/2)=0 , \tag{78}$$

$$sC_1'\sin(\pi s/2)+sC_2'\cos(\pi s/2)-(s+2)C_3'\sin(\pi s/2)-(s+2)C_4'\cos(\pi s/2) - [sC_5'-(s+2)C_7']\sin(\pi s/2)-[sC_6'-(s+2)C_8']\cos(\pi s/2)=0 , \tag{79}$$

$$-m[sC_1'\cos(\pi s/2)-sC_2'\sin(\pi s/2)-(s+1+\kappa_1)C_3'\cos(\pi s/2) + (s+1+\kappa_1)C_4'\sin(\pi s/2)]+[sC_5'-(s+1+\kappa_2)C_7']\cos(\pi s/2) -[sC_6'-(s+1+\kappa_2)C_8']\sin(\pi s/2)=-\frac{\mu_2 f(r_o) r_o^{s+1}}{s+1} , \tag{80}$$

$$-m[sC_1'\sin(\pi s/2)+sC_2'\cos(\pi s/2)-(s+1-\kappa_1)C_3'\sin(\pi s/2) - (s+1-\kappa_1)C_4'\cos(\pi s/2)]+[sC_5'-(s+1-\kappa_2)C_7']\sin(\pi s/2) +[sC_6-(s+1-\kappa_2)C_8]\cos(\pi s/2)=-\frac{\mu_2 g(r_o) r_o^{s+1}}{s+1} . \tag{81}$$

The functions C_i' are given by $C_i' = C_i + C_i^*$ where the C_i

are listed in (14) to (19) and C_i^* is the change in C_i due to the crack on $\theta = 0$. The C_i^* are given below as

$$C_1^* = - C_2^* \frac{\cos(\pi s)}{\sin(\pi s)} \tag{82}$$

$$C_2^* = \frac{\mu_2 h^*(r_o) r_o^{s+1}}{2(s+1)s} \left\{ \frac{s+1}{1+m\kappa_1} - \frac{2s+3}{m+\kappa_2} \right\} \tag{83}$$

$$C_3^* = - C_4^* \frac{\cos(\pi s)}{\sin(\pi s)} \tag{84}$$

$$C_4^* = \frac{\mu_2 h^*(r_o) r_o^{s+1}}{2(s+1)(1+m\kappa_1)} \tag{85}$$

$$C_5^* = - \frac{\mu_2 h^*(r_o) r_o^{s+1}}{2(s+1)\sin(\pi s)s(1+\kappa_2)} \times$$

$$\frac{\kappa_2 - m\kappa_1}{1+m\kappa_1} - \frac{(s+1)(2s+3)(1-m)}{m+\kappa_2} - (s+2)\cos(\pi s) \tag{86}$$

$$C_6^* = - \frac{\mu_2 h^*(r_o) r_o^{s+1}(s+2)}{2(s+1)(1+\kappa_2)(s)} \tag{87}$$

$$C_7^* = \frac{\mu_2 h^*(r_o) r_o^{s+1}}{2(s+1)\sin(\pi s)(m+\kappa_2)(1+\kappa_2)} \times$$

$$\left\{(2s+3)(1-m) - (m+\kappa_2)\cos(\pi s)\right\} \tag{88}$$

$$C_8^* = \frac{\mu_2 h^*(r_o) r_o^{s+1}}{2(s+1)(1+\kappa_2)} \tag{89}$$

The integral equations in terms of the unknown density functions $f(r)$, $g(r)$, $h(r)$, and $h^*(r)$ are given by the conditions that

$$T(r)+iN(r) = \int_0^\infty [\tau_{1r\theta}(r,r_o,\pi/2) + i\tau_{1\theta\theta}(r,r_o,\pi/2)]dr_o \ , \tag{90}$$

$$N_o(r)=\int_o^\infty \tau_{1\theta\theta}(r,r_o,\pi)dr_o \quad , \tag{91}$$

$$N_o^*(r)=\int_o^\infty \tau_{2\theta\theta}(r,r_o,0)dr_o \quad . \tag{92}$$

Equations (90) and (91) are exactly as (22) and (23), and (92) is due to the presence of the crack on $\theta = 0$. $N(r)$ and $T(r)$ are the normal and shear stresses on the interface, and $N_o(r)$, $N_o^*(r)$ are the normal stresses on the symmetry line in materials 1 and 2 respectively.

On noting as in Part I that

$$f(r_o) = g(r_o) = 0, \; c < r_o < \infty$$

$$h(r_o) = 0, \; 0 < r_o < a, \; b < r_o < \infty$$

$$h^*(r_o) = 0, \; 0 < r_o < a^*, \; b^* < r_o < \infty$$

and following the same procedure of Part I leads to the three integral equations

$$\frac{1}{\pi i}\int_{-1}^{1} \phi(t)\,\frac{dt}{t-y} - \gamma\phi(y) = -\frac{1}{\alpha_1}[Q(y)-iP(y)] + \int_{-1}^{1}\psi(t)G(t,y)dt + \int_{-1}^{1}\xi(t)G^*(t,y)dt, \; -1 < y < 1, \tag{93}$$

$$\frac{1}{\pi}\int_{-1}^{1} \psi(t)\,\frac{dt}{t-x} + \int_{-1}^{1}\psi(t)H(t,x)dt = \frac{1+\kappa_1}{2\mu_1}P_o(x) - \int_{-1}^{1}\xi(t)J^*(t,x)dt - \int_{-1}^{1}\phi(t)I(t,x)dt, \; -1 < x < 1, \tag{94}$$

$$\frac{1}{\pi}\int_{-1}^{1}\frac{\xi(t)}{t-x}\,dt + \int_{-1}^{1}\xi(t)H^*(t,x)dt = \frac{1+\kappa_2}{2\mu_2}P_o^*(x) - \int_{-1}^{1}\psi(t)J(t,x)dt - \int_{-1}^{1}\phi(t)I^*(t,x)dt, \; -1 < x < 1, \tag{95}$$

specifying $\phi(t)$, $\psi(t)$ and $\xi(t)$. In the following equations, if $a,a^* = 0$ then a_o, a_o^* is replaced by b,b^* respectively,

$$H^*(t,x) = -\frac{a_o^*}{2\pi}\left[\frac{1-\frac{1}{m}}{1+\frac{\kappa_2}{m}}\left[\frac{8\bar{s}^2}{(\bar{\eta}+\bar{s})^3} - \frac{12\bar{s}}{(\bar{\eta}+\bar{s})^2}\right] + \left[\frac{\frac{\kappa_2}{m}-\kappa_1}{\frac{1}{m}+\kappa_1} + \frac{3(1-\frac{1}{m})}{1+\frac{\kappa_2}{m}}\right]\frac{1}{\bar{\eta}+\bar{s}}\right],$$

$$I^*(t,x) = \frac{c(1+\kappa_2)}{2(1+m\kappa_1)(m+\kappa_2)\pi}\left[-i\bar{s}\left[(1+\frac{\kappa_2}{m}) + \frac{(\frac{1}{m}+\kappa_1)(5c^2t^2+\bar{s}^2)}{c^2t^2+\bar{s}^2}\right] + ct\left[(1+\frac{\kappa_2}{m}) - \frac{(\frac{1}{m}+\kappa_1)(3c^2t^2-\bar{s}^2)}{c^2t^2+\bar{s}^2}\right]\right]\frac{1}{c^2t^2+\bar{s}^2},$$

$$J(t,x) = \frac{a_o}{\pi}\left[\left[\frac{3(1+\kappa_2)}{2(m+\kappa_2)} - \frac{(1+\kappa_2)}{2(1+m\kappa_1)}\right]\frac{1}{\eta+\bar{s}} + \left[\frac{1+\kappa_2}{1+m\kappa_1} - \frac{1+\kappa_2}{m+\kappa_2}\right]\frac{\bar{s}}{(\eta+\bar{s})^2}\right],$$

$$J^*(t,x) = \frac{a_o^*}{\pi}\left\{\left[\frac{3(1+\kappa_1)}{2(\frac{1}{m}+\kappa_1)} - \frac{(1+\kappa_1)}{2(1+\frac{\kappa_2}{m})}\right]\frac{1}{\bar{\eta}+s} + \left[\frac{1+\kappa_1}{1+\frac{\kappa_2}{m}} - \frac{1+\kappa_1}{(\frac{1}{m}+\kappa_1)}\right]\frac{s}{(\bar{\eta}+s)^2}\right\},$$

$$G^*(t,y) = -\frac{\mu_2 a_o^*}{\alpha_1(1+\kappa_2)\pi}\left\{-i\bar{\eta}\left[\left[2(\bar{\eta}^2-c^2y^2) - \frac{(1-\frac{1}{m})(\bar{\eta}^2-3c^2y^2}{(1+\frac{\kappa_2}{m})}\right]X\right.\right.$$
$$\left.\frac{1}{\bar{\eta}^2+c^2y^2} + \frac{\frac{\kappa_2}{m}-\kappa_1}{\frac{1}{m}+\kappa_1}\right] + cy\left[\left[2(\bar{\eta}^2-c^2y^2) - \frac{(1-\frac{1}{m})(3\bar{\eta}^2-c^2y^2}{(1+\frac{\kappa_2}{m})}\right]X\right.$$
$$\left.\left.\frac{1}{\bar{\eta}^2+c^2y^2} - \frac{\frac{\kappa_2}{m}-\kappa_1}{\frac{1}{m}+\kappa_1}\right]\right\}\frac{1}{\bar{\eta}^2+c^2y^2},$$

with $\xi(t,x)$ and $H(t,x)$ given in Part I and $a_o^* = (b^*-a^*)/2$, $b_o^* = (b^*+a^*)/2$,

$$\bar{\eta} = \begin{cases} a_o^* t + b_o^* & \text{, if } a^* \neq 0 \\ b^* t & \text{, if } a^* = 0 \end{cases}, \qquad \bar{s} = \begin{cases} a_o^* x + b_o^* & \text{, if } a^* \neq 0 \\ b^* x & \text{, if } a^* = 0 \end{cases}.$$

Note that the above integral equations could be written down immediately by superposition, noting the solutions in [2] and Part I. That is, to obtain Equation (93) from (35) a term must be added to account for the normal and shear stress on $\theta = \frac{\pi}{2}$ due to a crack on $\theta = 0$. But whether or not the crack is on $\theta = 0$ or $\theta = \pi$ is a matter of nomenclature, and the terms corresponding to $\theta = 0$ may be obtained from the terms corresponding to $\theta = \pi$ by careful inspection. To obtain (94) from (36) the effect of the crack on $\theta = 0$ must be accounted for, and its effect is given in [2]. The third integral equation is given in [2] with the added term given by Part I to account for the effect of the interface crack on the symmetry line.

The solution for $\phi(t)$ from (93), follows directly from Part I, and the C_n are given by

$$C_n = \frac{2i}{\sqrt{1-\gamma^2}} \frac{1}{L(n-1,-\alpha,-\beta} \int_{-1}^{1} \left[\frac{-1}{\alpha_1}[Q(y)-iP(y)] + \int_{-1}^{1} \psi(t)G(t,y)dt + \int_{-1}^{1} \xi(t)G^*(t,y)dt \right] (1-y)^{-\alpha}(1+y)^{-\beta} P_{n-1}^{(-\alpha,-\beta)}(y)dy \qquad (96)$$

where the C_o term is determined as in Part I, and is given by the following:

if $a^* \neq 0$, $a \neq 0$ $\quad C_o = 0$

if $a^* \neq 0$, $a = 0$ $\quad C_o = -\frac{ib\cosh(\pi\omega)}{c\pi} \int_{-1}^{1} \psi(t)dt$

If $a^* = 0,\ a \neq 0 \quad C_o = \frac{ib^*\cosh(\pi\omega)}{c\pi} \int_{-1}^{1} \xi(t)dt$

If $a^* = 0,\ a = 0 \quad C_o = -\frac{ib\cosh(\pi\omega)}{c\pi} \int_{-1}^{1} \psi(t)dt + \frac{ib^*\cosh(\pi\omega)}{c\pi} \int_{-1}^{1} \xi(t)dt$.

The displacements are then found by integrating (71), (72), (73), from which the constant C_o has been found, and the continuity condition of the functions $\psi(t)$ and $\xi(t)$ are specified. Integration of (71) gives the opening displacement on $\theta = 0$, where if $a^* = 0$, a_o^*, is replaced by b^*,

$$u_{2\theta}(x,o) = \frac{a_o^*}{2} \int_{-1}^{x} \xi(t)dt - \frac{a_o^*}{2} \int_{-1}^{1} \xi(t)dt \qquad (97)$$

ϕ may now be substituted into (94) and (95), and letting $Q(y) = 0$, $P(y) = -\sigma_o$, one has

$$\frac{1}{\pi} \int_{-1}^{1} \psi(t) \frac{dt}{t-x} + \int_{-1}^{1} \psi(t)k(x,t)dt = \frac{1+\kappa_1}{2\mu_1} P_o(x) - \frac{2\sigma_o}{\alpha_1\sqrt{1-\gamma^2}} \int_{-1}^{1} w(z)I(z,x)P_1^{(\alpha,\beta)}(z)dz - \int_{-1}^{1} \xi(t)R^*(x,t)dt \ , \qquad (98)$$

and

$$\frac{1}{\pi} \int_{-1}^{1} \xi(t) \frac{dt}{t-x} + \int_{-1}^{1} \xi(t)k^*(x,t)dt = \frac{1+\kappa_2}{2\mu_2} P_o^*(x) - \frac{2\sigma_o}{\alpha_1\sqrt{1-\gamma^2}} \int_{-1}^{1} w(z)I^*(z,x)P_1^{(\alpha,\beta)}(z)dz - \int_{-1}^{1} \psi(t)R(x,t)dt \qquad (99)$$

where

$$R^*(x,t) = J^*(t,x) + \frac{ib^*\cosh(\pi\omega)}{c\pi} \int_{-1}^{1} w(z)I(z,x)dz + \frac{2i}{\sqrt{1-\gamma^2}} \sum_{n=1}^{\infty} \frac{1}{L(n-1,-\alpha,-\beta)} \int_{-1}^{1} w(z)I(z,x)P_n^{(\alpha,\beta)}(z)dz \times \int_{-1}^{1} G^*(t,y)(1-y)^{-\alpha}(1+y)^{-\beta}P_{n-1}^{(-\alpha,-\beta)}(y)dy \ ,$$

$$R(x,t) = J(t,x) - \frac{ib\cosh(\pi\omega)}{c\pi}\int_{-1}^{1} w(z)I^*(z,x)dz$$

$$+ \frac{2i}{\sqrt{1-\gamma^2}} \sum_{n=1}^{\infty} \frac{1}{L(n-1,-\alpha,-\beta)} \int_{-1}^{1} w(z)I^*(z,x)P_n^{(\alpha,\beta)}(z)\,dz \times$$

$$\int_{-1}^{1} G(t,y)(1-y)^{-\alpha}(1+y)^{-\beta}P_{n-1}^{(-\alpha,-\beta)}(y)\,dy \quad ,$$

$$k^*(t,x) = H^*(t,x) + \frac{ib^*\cosh(\pi\omega)}{c\pi}\int_{-1}^{1} w(z)I^*(z,x)dz$$

$$+ \frac{2i}{\sqrt{1-\gamma^2}} \sum_{n=1}^{\infty} \frac{1}{L(n-1,-\alpha,-\beta)} \int w(z)I^*(z,x)P_n^{(\alpha,\beta)}(z)\,dz \times$$

$$\int_{-1}^{1} G^*(t,y)(1-y)^{-\alpha}(1+y)^{-\beta}P_{n-1}^{(-\alpha,-\beta)}(y)dy \quad ,$$

and $k(t,x)$ is given in Part I.

Equations (98) and (99) may be solved in a similar fashon to (61) following Part I with the only change being rather than having one unknown function $F(t_k)$ to be solved for at k discrete points, two unknown functions may be assumed $F(t_k)$, $F^*(t_j)$, whose solutions are obtained from 2N simultaneous equations that are, in general, not separable.

For $a > 0$ let $\psi(t) = \frac{1}{\sqrt{1-t^2}} F(t)$ with $\int_{-1}^{1}\psi(t)dt = 0$.

For $a = 0$ let $\psi(t) = \frac{1}{\sqrt{1-t}} F(t) = \frac{1}{\sqrt{1-t^2}} \tilde{F}(t)$

For $a^* > 0$ let $\xi(t) = \frac{1}{\sqrt{1-t^2}} F^*(t)$ with $\int_{-1}^{1}\xi(t)dt = 0$

For $a^* = 0$ let $\xi(t) = \frac{1}{\sqrt{1-t}} F^*(t) = \frac{1}{\sqrt{1-t^2}} \tilde{F}^*(t)$.

Then for example when $a > 0$, $a^* > 0$ Equations (97) and (98) may be written as

$$\sum_{k=1}^{N} \frac{1}{N} F(t_k)\left[\frac{1}{t_k - x_r} + \pi k(x_r, t_k)\right] + \sum_{k=1}^{N} \frac{1}{N} F^*(t_k) R^*(x_r, t_k)$$

$$= -\frac{1+\kappa_1}{2\mu_1}\sigma_1 - \frac{2\sigma_o}{\alpha_1\sqrt{1-\gamma^2}} \int_{-1}^{1} w(z) I(z, x_r) P_1^{(\alpha,\beta)}(z)\, dz \quad ,$$

with

$$\sum_{k=1}^{N} \frac{\pi}{N} F(t_k) = 0 \quad , \tag{100}$$

and

$$\sum_{k=1}^{n} \frac{1}{N} F(t_k) R(x_r, t_k) + \sum_{k=1}^{N} \frac{1}{N} F^*(t_k)\left[\frac{1}{t_k - x_r} + \pi k^*(x_r, t_k)\right]$$

$$= -\frac{1+\kappa_2}{2\mu_2}\sigma_2 - \frac{2\sigma_o}{\alpha_1\sqrt{1-\gamma^2}} \int_{-1}^{1} w(t) I^*(z, x_r) P_1^{(\alpha,\beta)}(z)\, dz \quad ,$$

with

$$\sum_{k=1}^{N} \frac{\pi}{N} F^*(t_k) = 0 \tag{101}$$

where $r = 1, 2, \ldots, N-1$, $t_k = \cos\left[\frac{(2k-1)\pi}{2N}\right]$, $x_r = \cos\left(\frac{\pi r}{N}\right)$ and the upper limit in the first and second sum appearing in Equations (100) and (101) has been chosen to be identical for convenience.

Had a been equal to zero and a^* been chosen greater than zero, Equations (100) and (101) would appear as follows, [13]:

$$\sum_{k=1}^{N} \frac{1}{2N+1} \tilde{F}(t_k)\left[\frac{1}{t_k - x_r} + \pi k(x_r, t_k)\right] + \sum_{j=1}^{N} \frac{1}{N} F^*(t_j) R^*(x_r, t_j)$$

$$= \frac{1+\kappa_1}{2\mu_1}\sigma_1 - \frac{2\sigma_o}{\alpha_1\sqrt{1-\gamma^2}} \int_{-1}^{1} w(z) I(z, x_r) P_1^{(\alpha,\beta)}(z)\, dz \tag{102}$$

$$\sum_{k=1}^{N} \frac{1}{2N+1} F(t_k) R(\bar{x}_r, t_k) + \sum_{j=1}^{N} \frac{1}{N} F^*(t_j) \left[\frac{1}{t_j - \bar{x}_r} + \pi k^*(\bar{x}_r, t_j) \right]$$

$$= \frac{1+\kappa_2}{2\mu_2} \sigma_2 - \frac{2\sigma_o}{\alpha_1 \sqrt{1-\gamma^2}} \int_{-1}^{1} w(t) I^*(z, \bar{x}_r) P_1^{(\alpha,\beta)}(z)\, dz \quad ,$$

with $$\sum_{j=1}^{N} \frac{\pi}{N} F^*(t_j) = 0 \qquad (103)$$

where $r = 1,2,\ldots,N$, $x_r = \cos\left(\frac{\pi r}{2N+1}\right)$, $t_k = \cos\left[\frac{(2k-1)\pi}{4N+2}\right]$

$$r = 1,2,\ldots,N-1, \quad \bar{x}_r = \cos\left(\frac{\pi r}{N}\right) \quad , \quad t_j = \cos\left[\frac{(2j-1)\pi}{2N}\right]$$

and again the upper limit sums on t_k and t_j have been assumed equal for convenience.

The stress intensity factors for $a > 0$ are given by Equations (64) and (65), and for $a = 0$ by Equation (68).

For $a^* > 0$

$$k(a^*) = \frac{2\mu_2 \sqrt{a_o^*}}{1+\kappa_2} F^*(-1) \qquad (104)$$

$$k(b^*) = -\frac{2\mu_2 \sqrt{a_o^*}}{1+\kappa_2} F^*(+1) \qquad (105)$$

and for $a^* = 0$

$$k(b^*) = -\frac{2\mu_2 \sqrt{b^*}}{1+\kappa_2} \tilde{F}^*(+1) \quad . \qquad (106)$$

The strain energy release rate is given by Equation (69).

Numerical Solution and Results

The numerical solution to Equations (98) and (99) has been obtained for the particular case of aluminum-epoxy half-planes for ease in comparing with the results presented in Part I. As in Part I, the results presented are for plane strain and constant pressure on the crack surfaces with no loads at infinity.

Of particular importance in the investigation is the potential for further extension or arrest of a crack originating in one half-plane, as the crack reaches the interface. In Part I, the instances of a crack reaching the interface and either spreading along the bond or crossing (without spreading along the interface) was considered. It is seen in Figure 11, that extension of the crack into the adjacent epoxy half-plane decreases the tendency for interface crack growth compared with the results of Figure 4, and for larger values of half-length c, the strain energy release rate is less than for the no-interference interface crack.

Table 3 gives some numerical values of the stress intensity factors, strain energy release rate, and displacements for the problem of Figure 11. As the crack extends into the epoxy half-plane, k_1 initially decreases and k_2 changes sign as the direction of shear changes.

Figure 12 depicts the change in strain energy release rate for different locations of a unit length perpendicular crack, and, as suggested by Figure 4 of Part I, the geometry having the most potential for failure is for the crack to intersect the interface from the lower modulus side without crossing.

It seems reasonable to conclude from the results of Part I and the present study, that the most critical state for continued crack growth occurs when a perpendicular crack intersects the interface crack but does not cross. Further, for a crack approaching an undamaged interface from the higher modulus side, interface damage is much less likely than continued extension into the adjacent material. If the crack originates in the lower, or equal modulus half-plane, the potential for extension, either along the interface or crossing the interface, exists and depends on the relative bond strength and fracture properties of the half-planes. The combination of interface growth and extension into the higher modulus side appears unlikely.

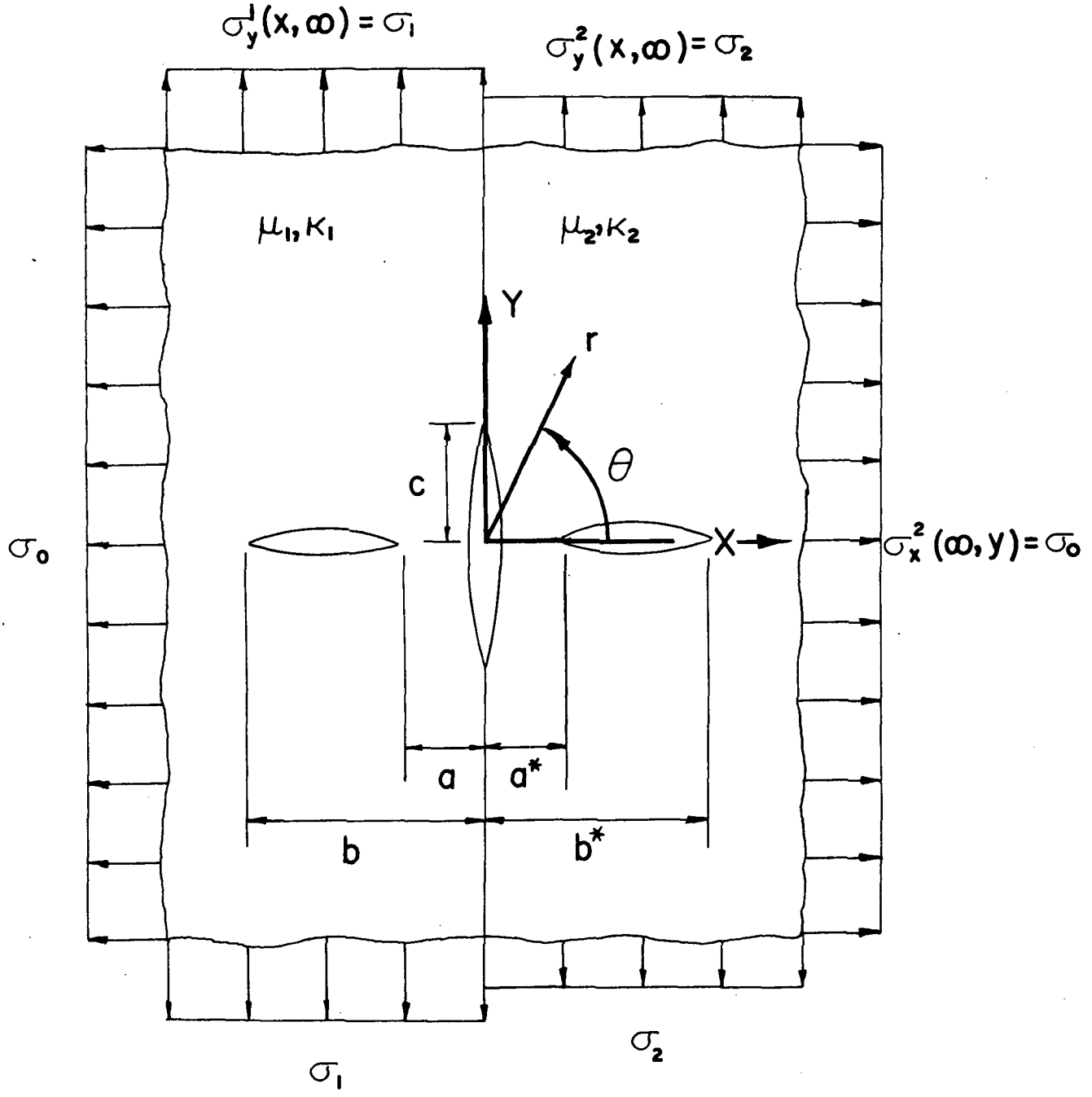

Figure 10. Bonded Elastic Half-Planes with an Interface Crack and Two Perpendicular Cracks.

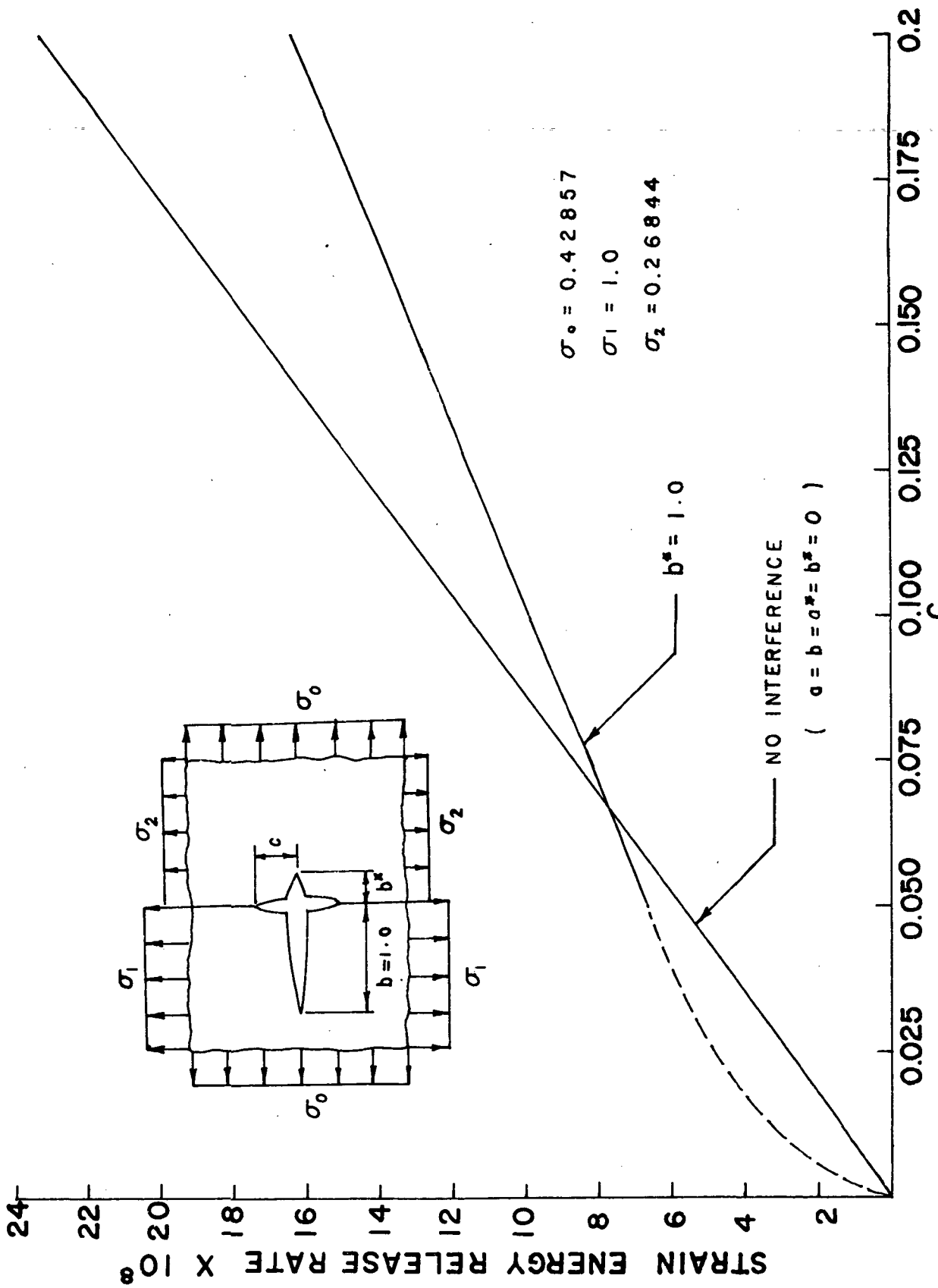

Figure 11. Strain Energy Release Rate for a Through Crack with Extension along the Interface. Aluminum-Epoxy. Plane Strain.

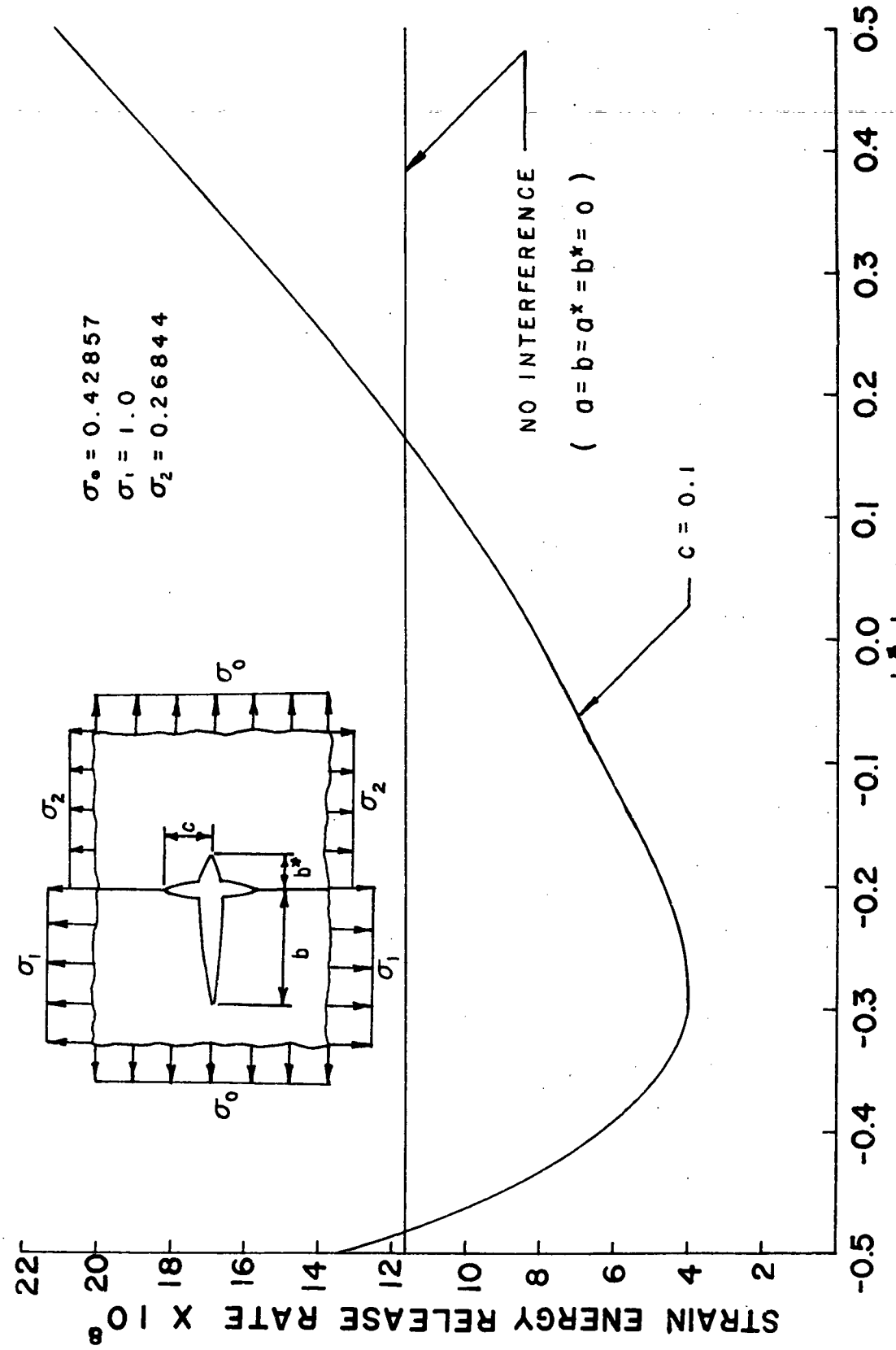

Figure 12. Strain Energy Release Rate for a Through Crack of Unit Length.

b^*	$k(b)$	$k(b^*)$	k_1	k_2	$\partial U/\partial c^* \times 10^8$	$[u_{1\theta}-u_{2\theta}] \times 10^7$ $(0,\pi/2)$	$[u_{1r}-u_{2r}] \times 10^7$ $(0,\pi/2)$	$[u_{1\theta}(b/2,\pi)-u_{2\theta}(b^*/2,0)] \times 10^7$
0	1.014	-	0.122	0.083	13.558	1.256	1.903	1.642
0.05	1.023	0.133	0.109	0.048	8.864	0.514	0.660	0.598
0.10	1.038	0.148	0.086	0.009	4.584	0.355	0.131	0.081
0.20	1.062	0.151	0.069	-0.020	3.150	0.625	-0.110	-0.490
0.40	1.099	0.161	0.078	-0.032	4.447	1.210	-0.170	-1.358
0.60	1.129	0.174	0.094	-0.035	6.279	1.630	-0.132	-2.147
0.80	1.157	0.187	0.109	-0.036	8.123	1.949	-0.070	-2.910
1.00	1.182	0.198	0.121	-0.031	9.811	2.198	0.017	-3.680
1.50	1.238	0.229	0.147	-0.027	13.840	2.702	0.347	-5.504
2.00	1.287	0.257	0.168	-0.016	17.532	3.064	0.787	-7.336
4.00	1.447	0.347	0.227	0.092	37.041	3.850	3.073	-14.661

* $\partial U/\partial c \times 10^8$ for no interference ($b = b^* = 0$) = 11.594

Table 3. Numerical Values for Aluminum-Epoxy Half-Planes with $a = a^* = 0$, $b = 1.0$, $c = 0.1$, $\sigma_o = 0.4285$, $\sigma_1 = 1.0$, $\sigma_2 = 0.26844$.

AN EXPERIMENTAL INVESTIGATION OF BONDED ELASTIC HALF-PLANES WITH AN INTERFACE CRACK AND A PERPENDICULAR INTERSECTING CRACK

By

James G. Goree
Associate Professor of Mechanics and
Mechanical Engineering

James O. Feemster, Jr.
Graduate Assistant M.S. Candidate in
Mechanical Engineering

In this study, the nature of crack growth near a bonded interface between two linearly elastic half-planes is investigated experimentally. The accuracy of some specific analytical solutions previously developed is demonstrated.

Material pairs of Plexiglas-Buterate and Plexiglas-Plexiglas were used with the interface bond formed by using ethylene dichloride. An initial perpendicular crack in the Plexiglas and/or an interface crack was developed by fatiguing the specimen until the desired configuration was reached. The static stress field necessary to initiate fracture was monitored with a network of strain gages in the vicinity of the crack or cracks and the behavior compared with the corresponding analytical solution.

The stress required to initiate fracture in the perpendicular crack as the near tip approaches the interface is shown to be in close agreement with the corresponding

analytical solution. The nature of the interface bond and the fracture toughness of the Buterate were both such that quantitative results could not be obtained as to the effect of the intersecting crack on the interface, the interface crack, or the perpendicular crack in the Buterate. However, some important observations can be made as to the behavior of these phenomena. When the perpendicular crack is formed in the higher modulus material, the crack tip has a tendency to extend into the adjacent half-plane and to leave the interface undamaged. In the Plexiglas-Plexiglas material pairs, the crack may either cross into the adjacent material or extend along the interface, depending upon the relative strength of the interface bond as compared to the fracture toughness of the two materials. In no instances did the crack extend along the interface and into the adjacent half-plane simultaneously.

INTRODUCTION

The purpose of this study was to investigate experimentally the nature of crack growth near a bonded interface between two linearly elastic half-planes and to demonstrate the accuracy of some specific analytical solutions developed for geometries amenable to experimental studies. It was assumed that crack propagation in the experimental work corresponded to brittle fracture, according to the classic Griffith crack criteria [1], [2].[1]

In the existing analytical solutions appropriate to the present work, the specific geometry considered was the case of two bonded elastic half-planes containing a finite length crack in one material, with the crack being perpendicular to the material interface as shown in Figure 13. The behavior of the stresses, stress intensity factors, and strain energy release rates were investigated, therefore indicating the potential for continued crack growth. Solutions for the crack terminating at the interface or crossing into the adjacent material have been presented by Erdogan, Cook, and Biricikoglu in [3], [4]. The instance of one end of the crack approaching the interface and debonding along the interface or debonding and crossing into the adjacent plane has been investigated by Goree and Venezia in [5], [6].

---

[1] References for this section of the report are listed seperately from those of Parts I and II. See page 89

SELECTION OF TEST MATERIALS

It was desirable to select materials with sufficiently low fracture toughness so as to allow fracture initiation at net stresses well below the elastic limits of the two materials. Polymers were chosen as test materials instead of metals, because the load levels needed to initiate fracture would be low, and polymers could be chemically bonded easily.

After investigating all of the commercially available polymers to use for experiments, a material pair of Plexiglas and Buterate was finally chosen. These materials have a common solvent, ethylene dichloride, thus allowing them to be edge-bonded to produce the desired type of interface. Plexiglas was found to be the most suitable of the materials available, as it behaves elastically at relatively low stesses, and brittle fracture can be initiated easily. It was desirable to find another polymer which was dissolved by the same solvent as Plexiglas, which had a different value of Young's modulus, and was not fracture tough. Buterate and Polycarbonate were the only readily available choices, even though they did not meet all of these requirements. Although they were the only other polymers available that use the same solvent as Plexiglas, both

materials were extremely fracture tough. Buterate was chosen instead of Polycarbonate, because a larger modulus ratio could be achieved with the Plexiglas-Buterate material pair. Because of the resistance of Buterate to fracture, it was used as the right half-plane in all of the experiments involving Plexiglas-Buterate material pairs. Providing that fracture was initiated in the Plexiglas, the fracture toughness of Buterate did not affect the outcome of the experimental work. However, fracture along the bonded interface was influenced by the toughness of the Buterate.

Another consideration in the choice of materials was the thickness of each test specimen. It was decided to use 1/8 in. (.3175 cm) thick sheets of Plexiglas and Buterate, as this thickness would be small enough to approximate the desired state of plane stress, while being thick enough to provide sufficient surface area to give a satisfactory interface bond between the two materials.

EXPERIMENTAL PROCEDURE

All experimental work was conducted on an Instron Model 109 dynamic testing machine as shown in Figure 14. With the aid of a network of strain gages placed on each test specimen, the stresses exerted by the machine could be monitored. Of considerable importance was the ability to obtain a stress field near the cracks which closely approximated the uniform stress field assumed in the analytical solution. Therefore, it was desirable to make each test specimen as large as possible within the limits imposed by the size of the testing machine, in order to minimize the effects due to the machine grips. Each material pair tested was 12 in. (30.48 cm) in height and 15 in. (38.10 cm) in width.

In order to calculate the stress in each test specimen, it was necessary to determine experimentally the value of Young's modulus E and Poisson's ratio ν for each material. The following values were found:

$$E_1 = E_{\text{Plexiglas}} = 5.07 \times 10^5 \text{ psi } \left(3.498 \times 10^6 \frac{kN}{m^2}\right)$$

$$\nu_1 = \nu_{\text{Plexiglas}} = 0.366 ,$$

$$\mu_{\text{Plexiglas}} = 1.856 \times 10^5 \text{ psi } \left(1.280 \times 10^6 \frac{kN}{m^2}\right)$$

$$E_2 = E_{\text{Buterate}} = 2.58 \times 10^5 \text{ psi } \left(1.780 \times 10^6 \frac{kN}{m^2}\right), \text{ and}$$

$$\nu_2 = \nu_{\text{Buterate}} = 0.37, \mu_{\text{Buterate}} = 9.416 \times 10^4 \text{ psi } \left(6.496 \times 10^5 \frac{kN}{m^2}\right).$$

In the analytical solutions [5], [6], the material half-planes were assumed to be loaded with uniform stresses σ_o, σ_1, and σ_2 as shown in Figure 13, with the strains being related in such a manner as to give constant strains in both the X and Y directions at points remote from the cracks. The following relations between the stresses must then hold:

$$\sigma_1 = \sigma_2 \frac{E_1}{E_2} - \sigma_o \left(\nu_2 \frac{E_1}{E_2} - \nu_1 \right) \tag{1}$$

for generalized plane stress, and

$$\sigma_1 = \sigma_2 \left(\frac{1 - \nu_2^2}{1 - \nu_1^2} \right) \frac{E_1}{E_2} - \sigma_o \left[\nu_2 \left(\frac{1 + \nu_2}{1 - \nu_1^2} \right) \frac{E_1}{E_2} - \frac{\nu_1}{1 - \nu_1} \right] \tag{2}$$

for plane strain.

In order to achieve uniform strain in the Y-direction across the specimen shown in Figure 13, the resultant load must act at a distance d from the material interface, as shown in Figure 15. This distance d for a specified material pair can be computed by first finding the relationship between the stresses σ_1 and σ_2, and then by summing moments about the material interface. By referring to Figure 15 for a specimen of thickness t, resultant loads are

$$R_1 = \sigma_1 \, t w_1 \text{ , and} \tag{3}$$

$$R_2 = \sigma_2 \, t w_2 \text{ .} \tag{4}$$

Summing moments about the interface of the specimen,

$$Rd = \frac{R_1 w_1}{2} - \frac{R_2 w_2}{2} \quad , \quad \text{where} \tag{5}$$

$$R = R_1 + R_2 \quad . \tag{6}$$

Substituting Equation (6) into Equation (5) gives the following relation for d:

$$d = \frac{\sigma_1 w_1^2 - \sigma_2 w_2^2}{2(\sigma_1 w_1 + \sigma_2 w_2)} \quad . \tag{7}$$

As an example, the distance d for a material pair of Plexiglas-Buterate in the state of plane stress with

$$w_1 = 6 \text{ in. } (15.24 \text{ cm}),$$

$$w_2 = 6 \text{ in. } (15.24 \text{ cm}),$$

$$\sigma_1 = 1.0, \quad \text{and}$$

$$\sigma_o = 0.5\ \sigma_1 \quad ,$$

will be calculated.

Using the experimentally determined values of E and ν for Plexiglas and Buterate, σ_2 is given by Equation (1) as

$$\sigma_2 = 0.6007\ \sigma_1 \quad ,$$

and Equation (7) then yields

$$d = \frac{\sigma_1 w_1^2 - \sigma_2 w_2^2}{2(\sigma_1 w_1 + \sigma_2 w_2)} = 0.748 \text{ in. } (1.899 \text{ cm}) \quad .$$

If the resultant R of the load is placed this distance from the interface in the higher modulus side of the material pair, uniform strain across the specimen in the Y-direction will result.

In the adaptation of the analytical problem to experimental work, it was found that this distance d could be approximated as zero, due to the manner in which each specimen was constrained during loading, and uniform strain parallel to the interface would still be obtained. Figure 16 shows the method of gripping each specimen for testing. The grips were fabricated from eight steel bars 3/8 in. (.952cm) × 1 in. (2.540 cm) × 12 in. (30.480 cm), which were bolted tightly on each test specimen, two on opposite sides of each of the four edges of the specimen. Underneath each steel grip was placed a strip of Plexiglas 1/8 in. (.317cm) × 1 1/2 in. (3.810 cm) × 12 in. (30.480 cm), in order to reinforce each test specimen and to distribute the load more evenly.

By considering the actual method of loading each specimen, the value of d, as shown in Figure 16, will again be calculated. Using the same Plexiglas-Buterate material pair in plane stress with

$$w_1 = 6 \text{ in. } (15.24 \text{ cm}),$$

$$w_2 = 6 \text{ in. } (15.24 \text{ cm}),$$

$$\sigma_1 = 1.0 \text{ , and}$$

$$\sigma_o = 0.5\ \sigma_1 \ ,$$

the value of d calculated will be shown to be negligible. For the purpose of computing this distance, the resultant R is shown in Figure 16 to be placed a distance d from the interface in the higher modulus material. It should be noted here that the stress field near the grips is not uniform. However, in order to obtain an approximate value for the distance d , which accounts for the presence of the lateral steel grips, the strains parallel to the interface will be taken as equal in all three materials and given by the average strain in either the Plexiglas or the Buterate, as computed from the uniform stress fields σ_o, σ_1, or σ_o, σ_2. Therefore,

$$\epsilon_{\text{Plexiglas}} = \epsilon_{\text{Buterate}} = \epsilon_{\text{Steel}} \ .$$

The relationship between the stresses σ_1 and σ_2 in the Plexiglas and Buterate was found previously to be

$$\sigma_2 = 0.6007\ \sigma_1 \ .$$

The value of the three strains can be found as follows:

$$\epsilon_{\text{Buterate}} = \frac{1}{E_2}\left(\sigma_2 - \nu_2 \sigma_o\right) = \epsilon_{\text{Plexiglas}} = \epsilon_{\text{Steel}}$$

where

$$E_2 = 2.58 \times 10^5 \text{ psi} \left(1.780 \times 10^6 \ \frac{\text{kN}}{\text{m}^2}\right) \ , \quad \text{and}$$

$$\nu_2 = 0.37 \ .$$

Then,

$$\epsilon_{Buterate} = 2.682 \times 10^{-6}\sigma_2 \text{ in/in} \left(2.682 \times 10^{-6}\sigma_2 \frac{cm}{cm}\right) .$$

The approximate tensile stress in each of the four lateral steel grips can now be found:

$$\sigma_s = \epsilon_{Steel} E_{Steel} = 80.46\, \sigma_2$$

where

$$\epsilon_{Steel} = 2.682 \times 10^{-6}\, \sigma_2 \text{ in/in} \left(2.682 \times 10^{-6}\sigma_2 \frac{cm}{cm}\right), \text{and}$$

$$E_{Steel} = 30 \times 10^6 \text{ psi } \left(2.070 \times 10^8 \frac{kN}{m^2}\right) .$$

The resultant R in Figure 16 is now found to be

$$R = 6\, \sigma_1 t + 6\, \sigma_2 t + 4\, \sigma_s\, (1)\, (3/8).$$

Summing moments about the interface of the specimen,

$$Rd = 6\, \sigma_1 t - 6\, \sigma_2 t .$$

Then,

$$d = \frac{6\sigma_1 t - 6\sigma_2 t}{6\sigma_1 t + 6\sigma_2 t + 1.5\sigma_s} = 0.004 \text{ in. } (0.010 \text{ cm}) .$$

Since this value of offset is then effectively zero within the accuracy of the tests, the resultant load under actual test conditions was placed along the centerline of each specimen. During testing, the condition of uniform strain across the specimen parallel to the interface was verified with the use of strain gages.

For each specimen tested, it was desired to establish

a specified ratio between the stress σ_1 and the lateral stress σ_o. This objective was achieved with the use of eight allen head screws threaded into the side grips as shown in Figure 16. By tightening these screws against the top and bottom grips, the side grips could be forced outward, thus creating a lateral stress on the specimen. It should be noted that high values of σ_o, such as $\sigma_o = 1.5\sigma_1$, could be easily achieved with this method. In order to establish the desired values of σ_1 and σ_o, the strain in the X and Y directions was carefully monitored by a network of strain gages, as is shown in Figure 16. Strain gages having 350 ohm resistance were used, because the problem of gage "drifting" associated with heating could be eliminated. Gages having 120 ohm resistance, and therefore larger current, had a tendency to store heat, because the polymers that were used as test materials were not good thermal conductors. In the initial tests, twenty strain gages were placed on each test specimen in order to investigate the stress state in the vicinity of the cracks. The information gathered in these initial tests suggested that the gage placement as shown in Figure 16 was both economical and practical, and that the stress state monitored in the vicinity of the cracks was uniform to within four percent.

In order to achieve satisfactory correlation between the analytical solutions and the experimental results, it

was necessary to form the cracks by fatigue to a desired length in each test specimen. With the use of the Instron Model 109 dynamic testing machine, the mean load, amplitude, and frequency of loading could be specified, thus enabling the operator to fatigue the test crack to any desired length.

Before the tests on the bonded material pairs were conducted, the critical stress intensity factor K_c for Plexiglas was determined. In order to find this value K_c, five test specimens were made and tested, as shown in Figure 17. In each case, a 5/32 in. (0.397 cm) hole was drilled in the specimen, and a notch was made with a surgical scalpel on each side of the hole perpendicular to the direction of loading. A crack was first fatigued to a desired length, and then loaded statically to determine the critical stress σ_1 at fracture. Strain gages were used to accurately monitor this stress. The value of K_c was then determined from the following relationship:

$$K_c = \sigma_1 \sqrt{\ell} \quad ,$$

where

σ_1 = stress at which the crack propagated, and

ℓ = half-length of the initial crack .

The value of K_c for the Plexiglas used in the experimental work was found to be

$$K_c = 530 \text{ psi} \sqrt{\text{in.}} \quad (5828 \frac{\text{kN}}{\text{m}^2} \sqrt{\text{cm}}) \quad .$$

After determining the value of K_c for Plexiglas, tests were then conducted on the Plexiglas-Buterate and Plexiglas-Plexiglas material pairs. First, the materials were edge-bonded to form an interface, and reinforced around the four edges with eight Plexiglas strips 1/8 in. (0.317 cm) × 1 1/2 in. (3.810 cm) × 12 in. (30.480 cm). In each case a hole 1/4 in. (0.635 cm) in diameter was drilled in the left half-plane a specified distance from the interface. A scalpel was again used to make a notch in one side of the hole nearest the bonded interface, as shown in Figure 16. The notch was made on one side only in order to keep the crack from propagating to the left under the fatigue load. If an interface crack in the test specimen was desired, a 1/32 in. (0.079 cm) wide slot was milled a desired distance along the interface, and a scalpel was used to put a notch at each end of the slot. At this time, the network of strain gages was placed on the specimen. The specimen was then secured in the testing machine, and turned perpendicular to the usual axis of loading, and an interface crack was fatiqued. In all of the tests performed, a fully satisfactory interface crack was never achieved, as the solvent used in bonding the materials changed the material properties slightly, thus making them more fracture tough. However, a more satisfactory interface crack was obtained in the Plexiglas-Plexiglas material pairs than in the Plexiglas-Buterate combination.

The test specimen was next placed in its normal loading position, as is shown in Figure 16, and was fatigued under a specified load and frequency until the end of the crack perpendicular to the interface had propagated to within a desired distance of the interface. It was then loaded statically under a specified ratio of σ_o/σ_1, which was monitored by the network of strain gages previously described, to determine the stress at which the end of the crack started to grow toward the interface. The effect of the crack upon reaching the interface or the interface crack was then observed. It should be noted that the presence of the drilled hole at the left end of the crack did affect the outcome of the experimental results for short cracks, as is shown in the following section.

EXPERIMENTAL RESULTS AND CONCLUSIONS

In Figure 18, a comparison of the analytical and experimental results in Plexiglas-Buterate material pairs is shown by curves 1 and 2 respectively. The critical stress, which is the stress required to initiate fracture, is plotted versus the distance of the crack tip from the interface. According to the results of [3] through [6], the critical stress approaches zero as the crack tip nears the interface, and approaches infinity as the crack length becomes zero. Curve 3 of Figure 18 gives the critical stress required for a comparable length crack in a full-plane of Plexiglas. The critical stress for the full-plane problem approaches infinity as ℓ approaches zero, as is shown from the following relationship:

$$\sigma_c = K_c / \sqrt{\ell}$$

where σ_c = critical stress

K_c = critical stress intensity factor, and

ℓ = half-length of the crack .

The experimental results agree closely with the analytical results in the region $a = 0.05$ in. (0.127 cm) to $a = 0.4$ in. (1.016 cm). However, in the region where the crack tip is in the vicinity of the drilled hole, the

stress concentration associated with the presence of the hole reduces the critical stress σ_1, as shown in curve 2 of Figure 18. The problem of determining the stresses and stress intensity factors for symmetric cracks emanating from a circular hole in a full plane was considered by Newman in [7]. The results given in TABLE 1 of [7] are reproduced in Table 4 of the present study. Note the column corresponding to F_o in TABLE I of [7] should read $\lambda = 0$ rather than $\lambda = 1$. Similarly, the column for F_1 should read $\lambda = 1$. These changes have been made in Table 4 of this investigation. The present one-sided crack seems to be influenced by the presence of the hole more strongly than the symmetric crack does. However, the trend is the same.

In Figure 18, curves 1 and 3 agree within 5 percent of each other until the crack tip is within approximately 0.2 in. (0.508 cm) of the material interface. The crack tip is then affected by the presence of the Buterate in the right half-plane, as is shown in curve 1, and reduces the critical stress required for fracture.

Because of the inability to produce a brittle interface, no quantitative results were obtained for the behavior of an interface crack or the effect of the perpendicular crack on initiating fracture along the bond. However, some important observations were made as to the influence of the modulus ratio of the materials in both

Plexiglas-Buterate and Plexiglas-Plexiglas material pairs.

In the Plexiglas-Buterate combination, an interface crack could not be formed as a result of a perpendicular crack intersecting the interface. According to the analytical solution [3], a material pair with the intersecting crack in the more rigid material actually has compressive stresses induced on the interface in the vicinity of the crack tip. When the perpendicular crack tip reached the interface, arrest occurred in all experiments, regardless of whether the test specimen was under a static load or a fatigue load at the time of intersection. By continued fatigue loading, the crack could always be forced to cross into the Buterate, as shown in Figures 19 and 20 , and after a crack growth of approximately 0.1 in. (0.2540 cm), brittle fracture would occur. As discussed in [3], the order of the stress singularity for the cleavage stress of the intersecting crack is larger than one-half, providing that the crack originates in the higher modulus material, and it is assumed that this large opening stress was sufficient to develop the fatigue crack in the Buterate. It is of considerable interest that a fatigue crack could be produced, and that brittle fracture would occur in the Buterate in this manner. In a full plane of Buterate with an initial configuration as shown in Figure 17, fatique loading in the identical load and frequency range would not generate a crack. After fatiguing for 200,000 cycles

at a load of 1400 ± 200 lbs. and a frequency of 15 hz., the crack tips in the full-plane of Buterate became highly distorted, and multiple irregular cracks were formed, as shown in Figure 21 , none of which lead to fracture. With a large lateral load, the interface in Plexiglas-Buterate material pairs could be made to fail in tension, as it was weaker than either of the two materials. In one experimental run, a crack originated on the interface due to a flaw in the bond approximately two inches from the intersecting crack tip. As the lateral load was increased, this crack behaved similarly to a brittle fracture, and it propagated along the interface until the intersecting crack tip was reached, at which time it stopped, leaving the bottom half of the interface still intact.

Unlike the Plexiglas-Buterate pair, a crack could be initiated along the interface in the vicinity of the intersecting crack tip in the Plexiglas-Plexiglas material combination, depending upon the lateral stress, σ_o and on the intersecting crack length. As in the Plexiglas-Buterate material pair, the interface always stopped the intersecting crack. Both the lateral stress, σ_o , and the intersecting crack length were significant in producing interface failure. However, the nature of the interface bond was such that consistent results could not be obtained. With large values of the lateral stress, such as $\sigma_o = 1.0\ \sigma_1$, the interface would first arrest

the intersecting crack tip, but under continued fatigue loading the interface would fail, providing that the intersecting crack length was 0.8 in. (2.0320 cm) or less. For intersecting cracks longer than this value, the crack tip would cross the interface, resulting in fracture of the test specimen.

In conclusion, for material pairs having $\mu_2/\mu_1 < 1$, compressive stresses exist on the interface in the vicinity of the intersecting crack. In this case, the strength of the interface bond is relatively unimportant, because failure is more likely to occur in the form of the intersecting crack crossing the interface into material 2. However, according to the analytical solution [3], [4], when $\mu_2/\mu_1 \geq 1$, the interface is subjected to tensile stresses, giving rise to both interface fracture or fracture through the interface into material 2 as possible modes of failure. The type of failure which occurs is then dependent on the strength of the interface bond as compared to the strengths of the two materials being used. In none of the experiments involving Plexiglas-Plexiglas half-planes did simultaneous crack extension occur along the interface and across the interface. This is in agreement with the analytical results discussed in [6].

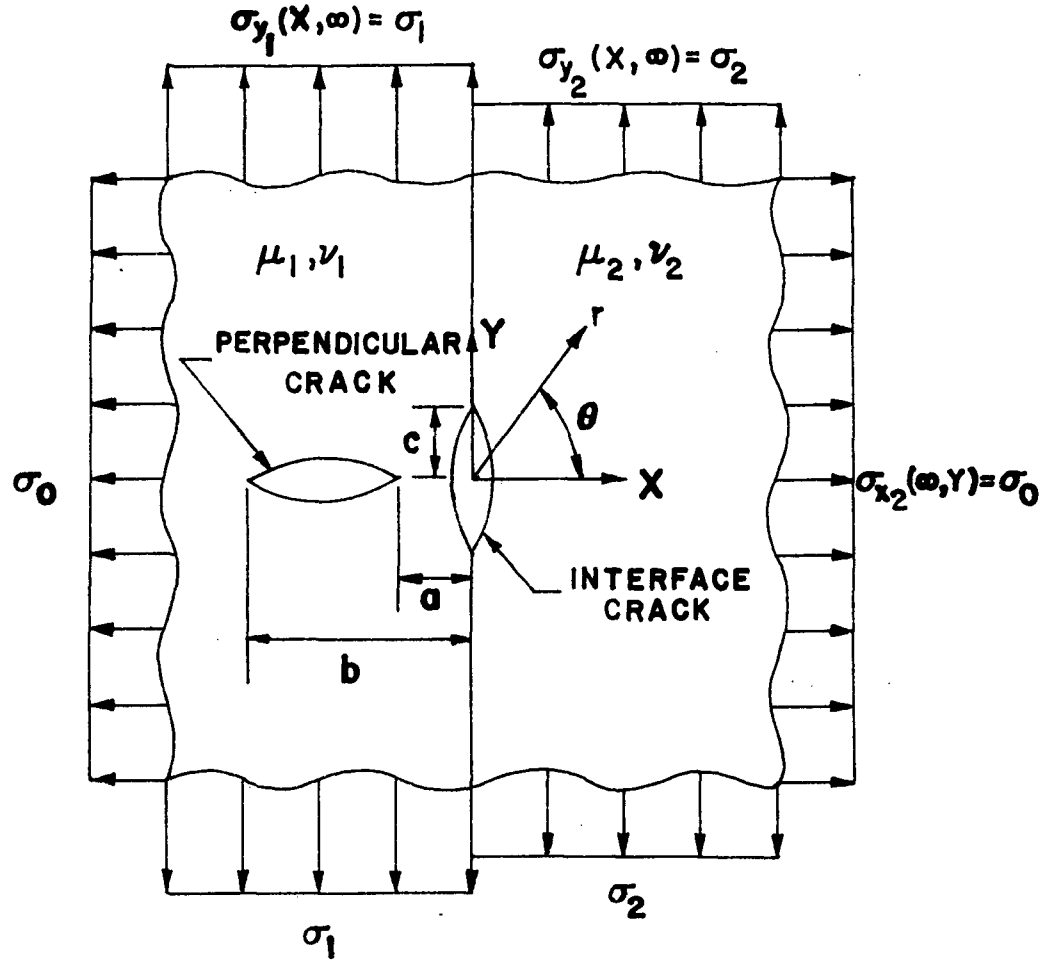

Figure 13. Bonded Elastic Half-Planes with Perpendicular Cracks.

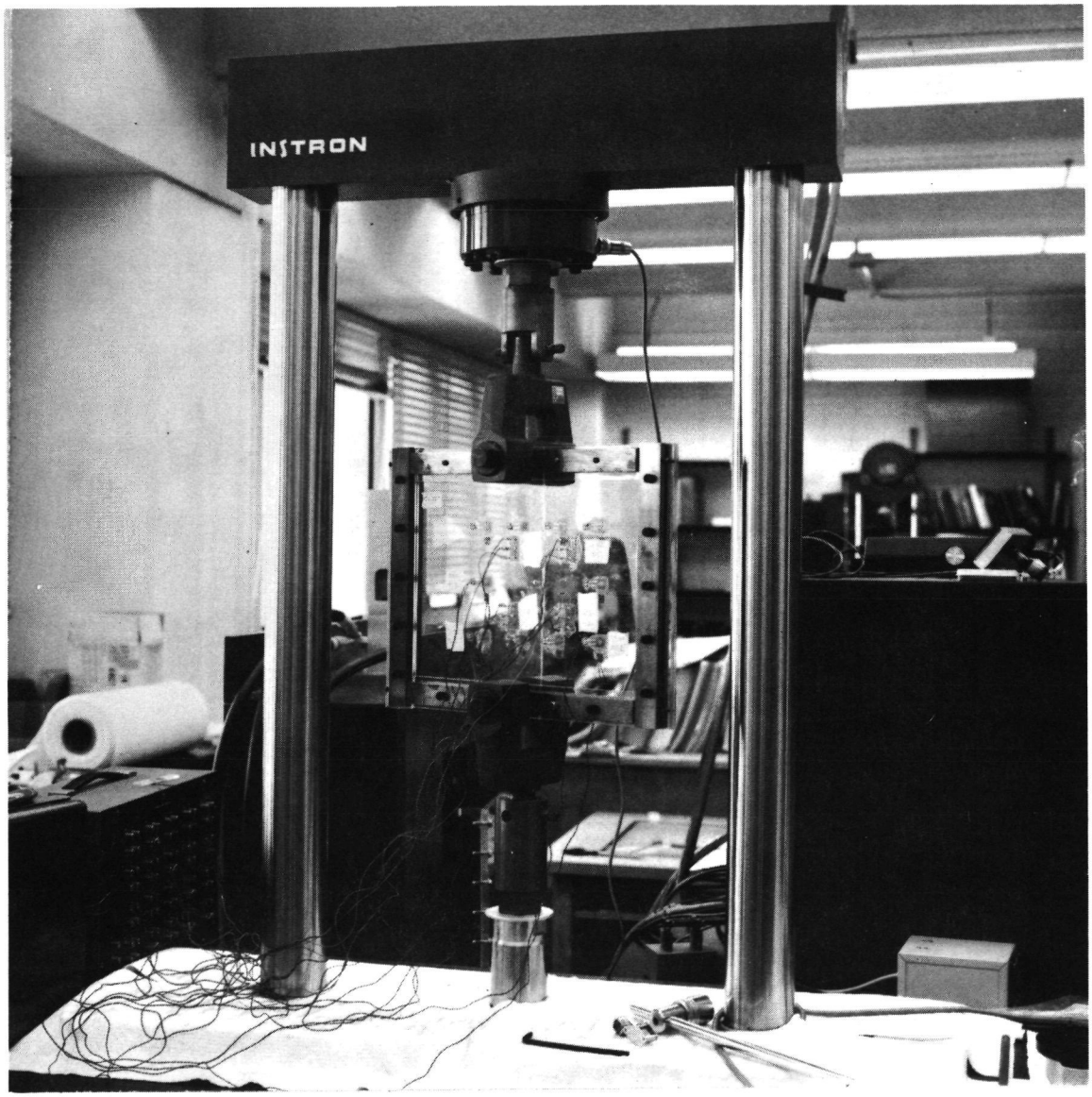

Figure 14. Instron Model 109 Dynamic Testing Machine.

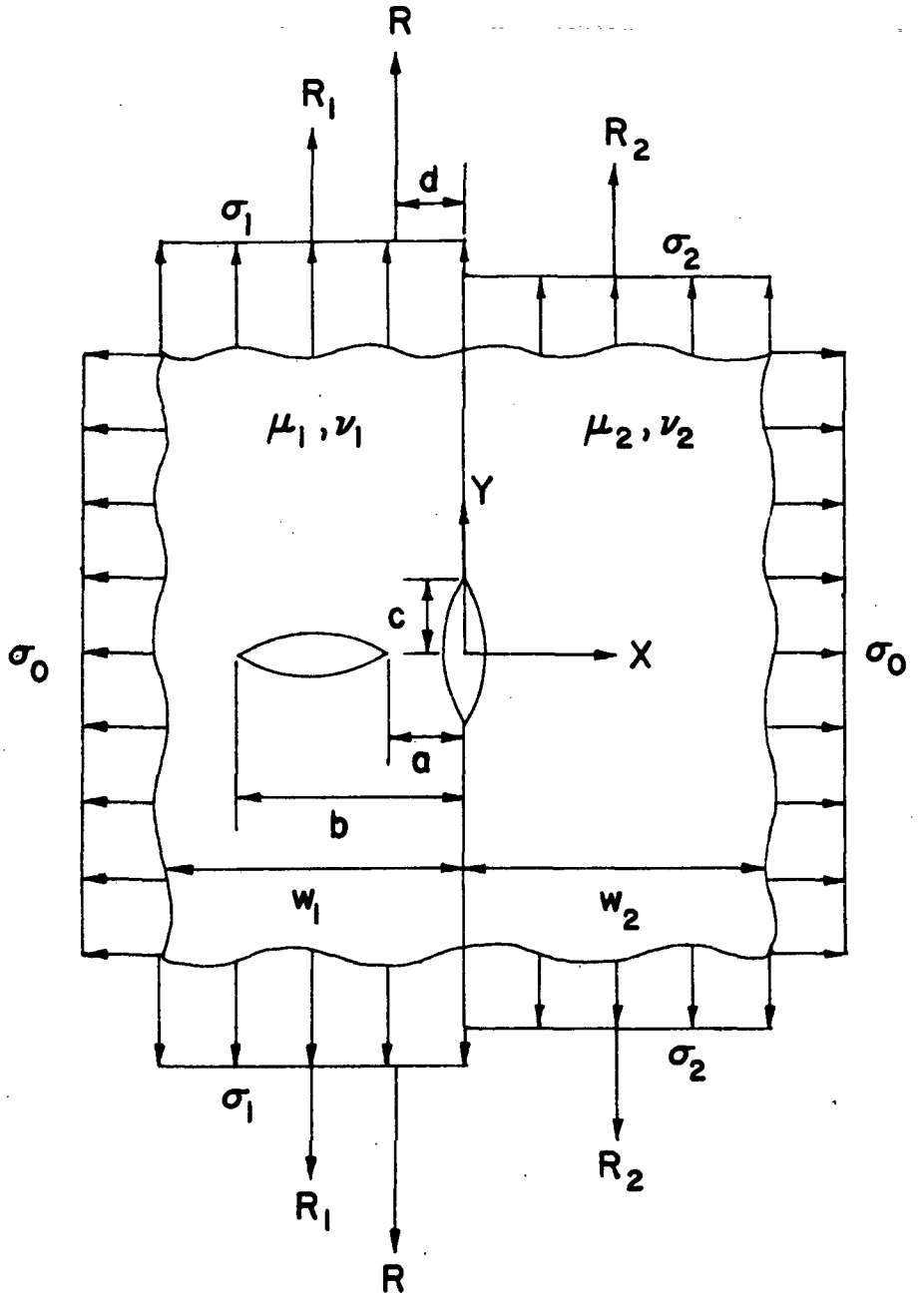

Figure 15. Theoretical Resultant Load Placement for a Plexiglas-Buterate Material Pair.

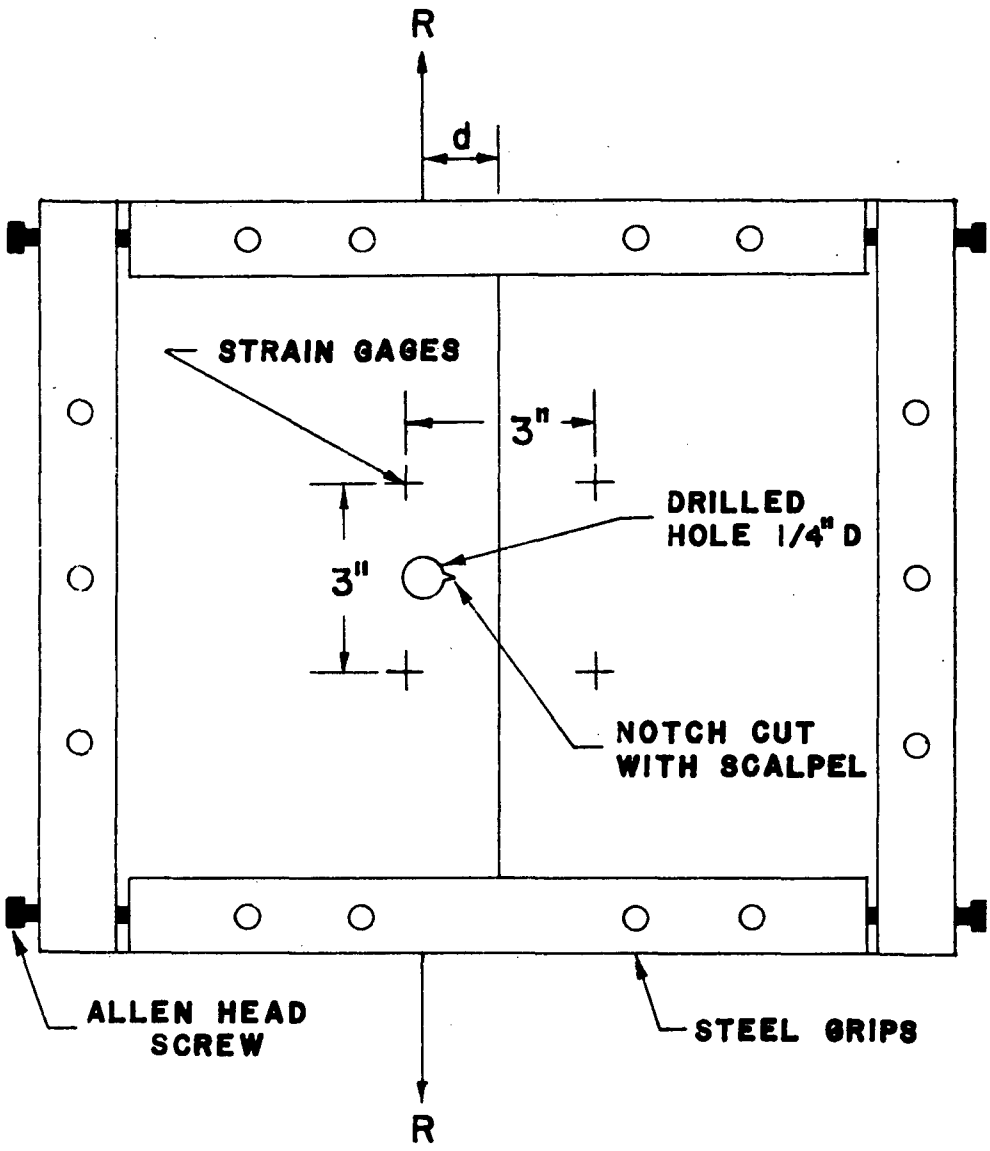

Figure 16. Configuration of Plexiglas-Buterate Material Pair with No Interface Crack Prior to Testing.

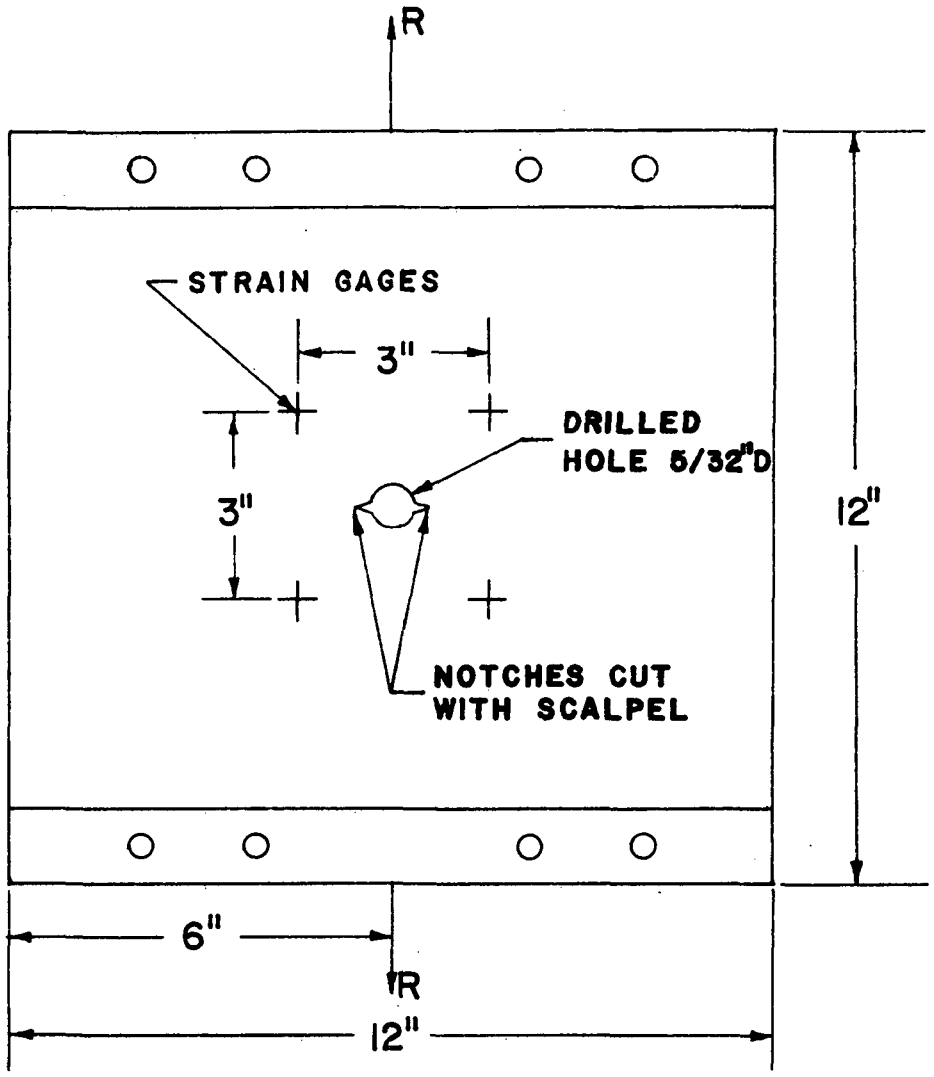

Figure 17. Configuration of Plexiglas or Buterate Full-Plane Prior to Fatigue Loading.

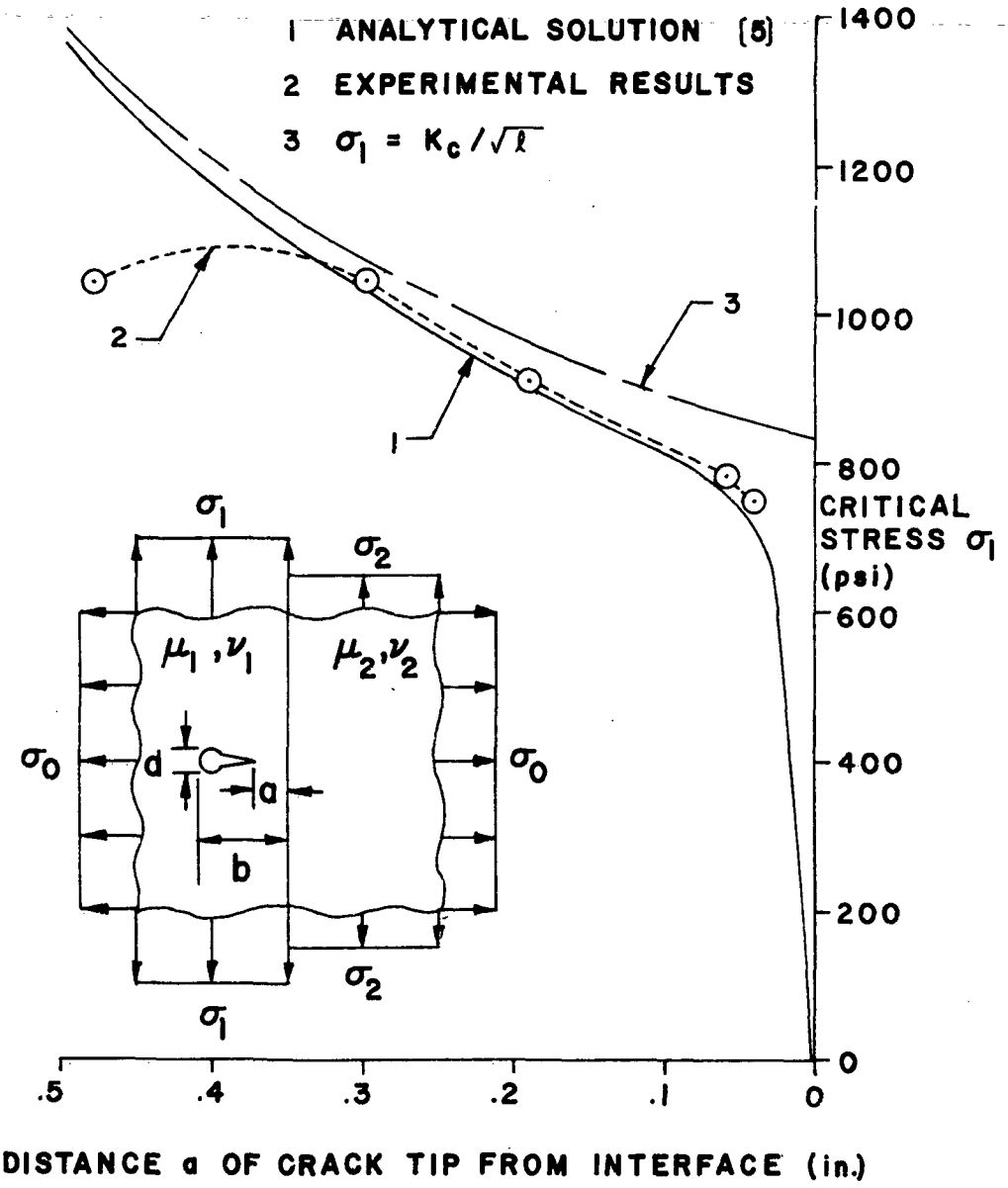

Figure 18. Comparison of Analytical and Experimental Values of Critical Stress for Plexiglas-Buterate Material Pairs, b = 0.8 in. (2.0320 cm), d = 0.25 in. (0.6350 cm), Plane Stress.

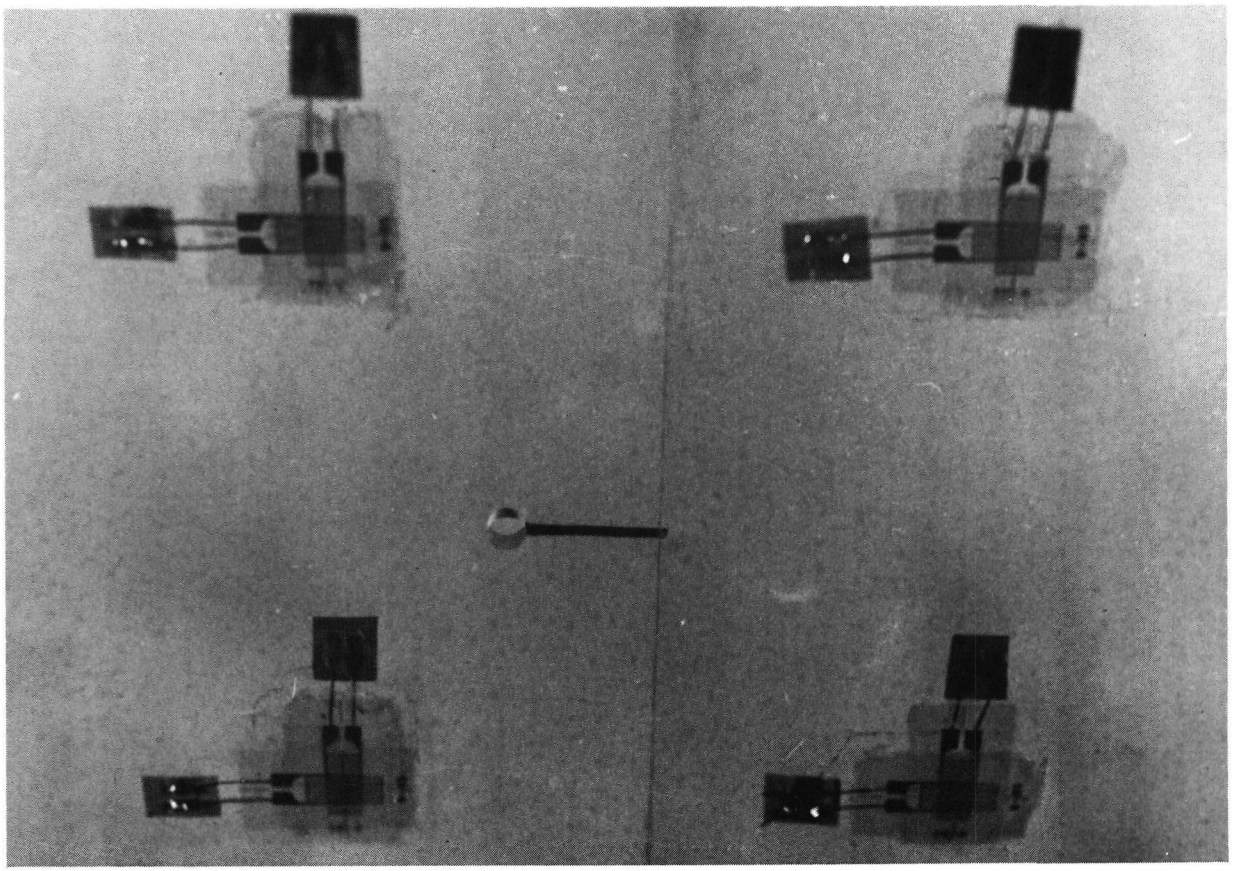

Figure 19. Perpendicular Intersecting Crack in a Plexiglas-Buterate Material Pair Crossing into the Buterate Half-Plane Following Continued Fatigue Loading.

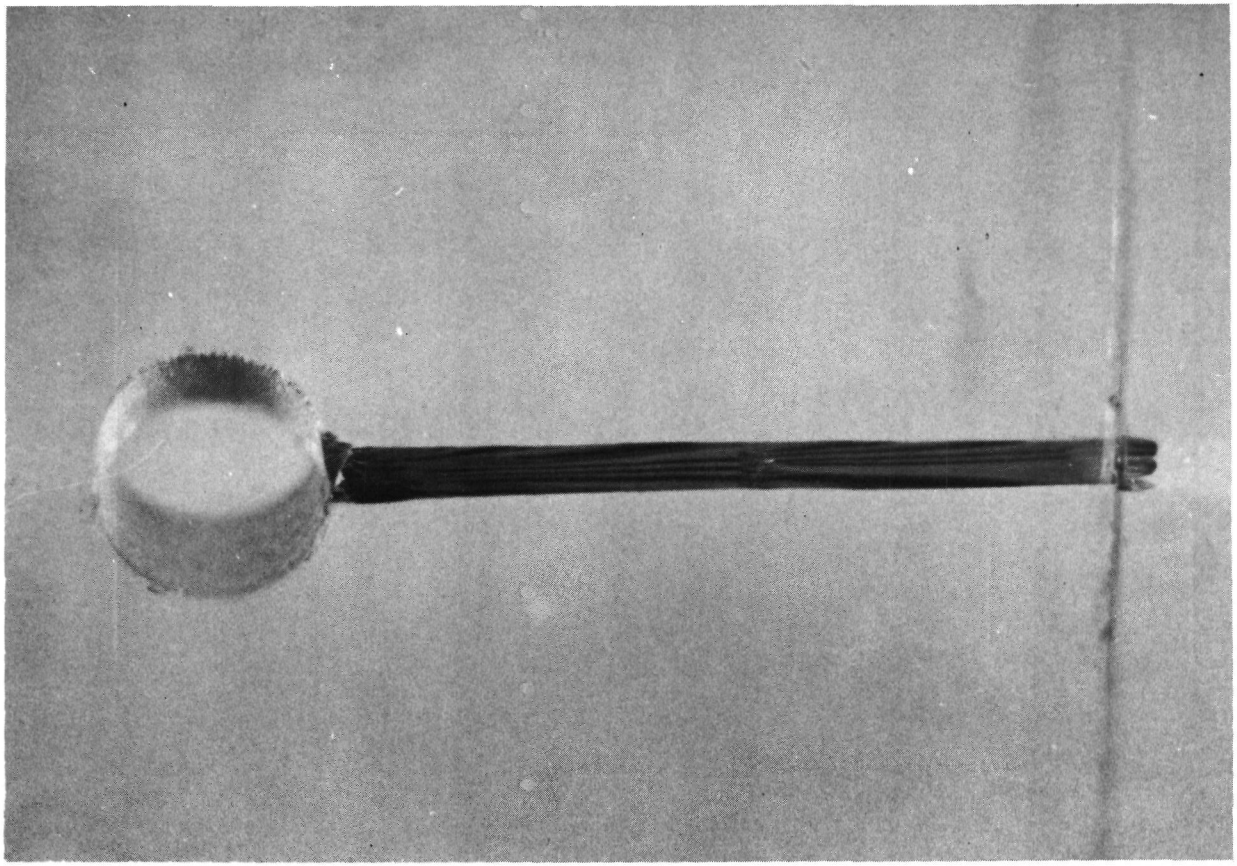

Figure 20. Magnified View of Crack Crossing into the Buterate Following Continued Fatigue Loading.

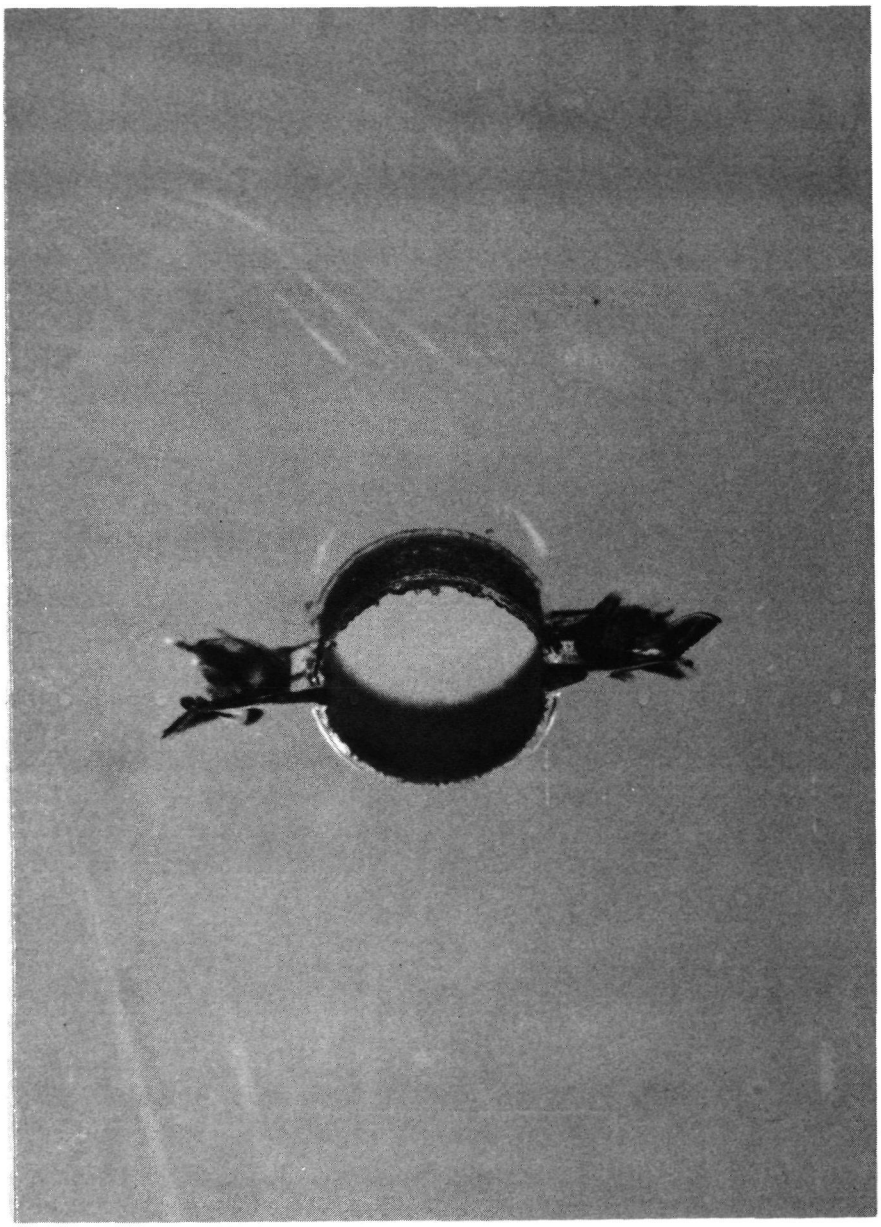

Figure 21. Irregular Crack Formation in a Full-Plane of Buterate Following Continued Fatigue Loading.

Table 4. Cracks Emanating from a Circular Hole in an Infinite Plate Subjected to Biaxial Stress from [7].

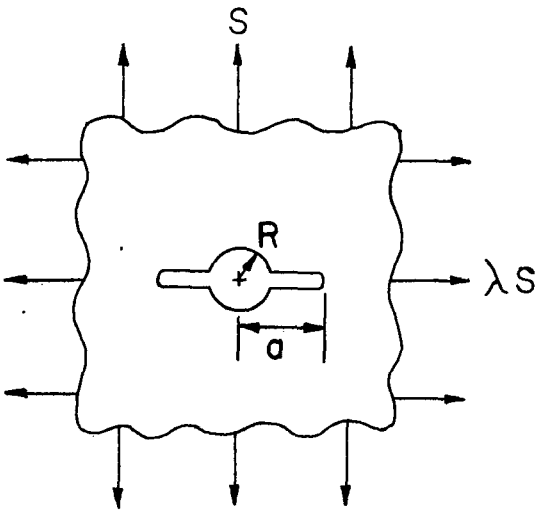

$$K = S\sqrt{\pi a}\ F$$

$$2N = 120$$

a/R	$F(\lambda = -1)$	$F_o(\lambda = 0)$	$F_1(\lambda = 1)$
1.01	0.4325	0.3256	0.2188
1.02	.5971	.4514	.3058
1.04	.7981	.6082	.4183
1.06	.9250	.7104	.4958
1.08	1.0135	.7843	.5551
1.10	1.0775	.8400	.6025
1.15	1.1746	.9322	.6898
1.20	1.2208	.9851	.7494
1.25	1.2405	1.0168	.7929
1.30	1.2457	1.0358	.8259
1.40	1.2350	1.0536	.8723
1.50	1.2134	1.0582	.9029
1.60	1.1899	1.0571	.9242
1.80	1.1476	1.0495	.9513
2.00	1.1149	1.0409	.9670
2.20	1.0904	1.0336	.9768
2.50	1.0649	1.0252	.9855
3.00	1.0395	1.0161	.9927
4.00	1.0178	1.0077	.9976

BIBLIOGRAPHY

1. A. A. Griffith, Phil. Trans. Roy. Soc. London, Ser. A., Vol. A221, (1921), p. 163.

2. A. A. Griffith, Proceedings of the 1st International Congress for Applied Mechanics, Delft (1924), p. 55.

3. T. S. Cook, and F. Erdogan, "Stresses in Bonded Materials with a Crack Perpendicular to the Interface," Int. J. Engr. Science, Vol. 10, (Nov. 1972), pp. 677-697.

4. F. Erdogan, and V. Biricikoglu, "Two Bonded Half-Planes with a Crack Going Through the Interface," Technical Report, NASA-TR-72-4, June, 1974.

5. J. G. Goree, and W. A. Venezia, "Bonded Elastic Half-Planes with an Interface Crack and a Perpendicular Intersecting Crack," Int. J. Engr. Science (In Press). Part I of this report.

6. J. G. Goree, and W. A. Venezia, "Bonded Elastic Half-Planes with an Interface Crack and a Perpendicular Intersecting Crack that Extends into the Adjacent Material," Int. J. Engr. Science (In Press). Part II of this report.

7. J. C. Newman, Jr., "An Improved Method of Collocation for the Stress Analysis of Cracked Plates with Various Shaped Boundaries," Technical Report, NASA TN D-6376, August, 1971.

APPENDIX A

ON THE TRANSFORM SOLUTION

1. The Mellin Transform and its use for the Plane Problem of Linear Elasticity

Following [1] and [14], the plane problem of linear elasticity may be formulated as follows:

$$\tau_{r\theta} + i\tau_{\theta\theta} = \sigma(r,\theta) = -\frac{\partial}{\partial r}\left(\frac{1}{r}\frac{\partial \chi}{\partial \theta}\right) + i\frac{\partial^2 \chi}{\partial r^2} \quad , \qquad \text{(A 1.1)}$$

$$\tau_{rr} = \frac{1}{r^2}\frac{\partial^2 \chi}{\partial \theta^2} + \frac{1}{r}\frac{\partial \chi}{\partial r} \quad , \qquad \text{(A 1.2)}$$

$$2\mu\left(\frac{\partial u_r}{\partial r} + i\frac{\partial u_\theta}{\partial r}\right) = \nu(r,\theta) = -\frac{\partial^2 \chi}{\partial r^2} + \frac{i}{r^2}\frac{\partial \chi}{\partial \theta} - \frac{i}{r}\frac{\partial^2 \chi}{\partial r \partial \theta}$$

$$+ (1-\nu)\left[\frac{\partial \psi}{\partial \theta} + 2ir\frac{\partial \psi}{\partial r} + r\frac{\partial^2 \psi}{\partial r \partial \theta} + ir^2\frac{\partial^2 \psi}{\partial r^2}\right], \qquad \text{(A 1.3)}$$

where μ is the shear modulus, ν is the Poisson's ratio, and

$$\nabla^4 \chi = 0, \quad \nabla^2 \psi = 0, \quad \frac{\partial}{\partial r}\left(r\frac{\partial \psi}{\partial \theta}\right) = \nabla^2 \chi = \frac{\partial^2 \chi}{\partial r^2} + \frac{1}{r}\frac{\partial \chi}{\partial r} + \frac{1}{r^2}\frac{\partial^2 \chi}{\partial \theta^2}. \qquad \text{(A 1.4)}$$

The Mellin transform of a function $f(r)$, defined and suitably regular on $(0, \infty)$, and its inverse are defined by

$$F(s) = M[f(r)] = \int_0^\infty f(r) r^{s-1} dr \quad , \qquad \text{(A 1.5)}$$

$$f(r) = \frac{1}{2\pi i}\int_{c-i\infty}^{c+i\infty} F(s) r^{-s}\, ds \quad , \qquad \text{(A 1.6)}$$

where c is such that $r^{c-1}f(r)$ is absolutely integrable

on $(0, \infty)$. The transform of derivatives is given by

$$\int_0^\infty \frac{d^n f(r)}{dr^n} r^{s-1+n}\, dr = (-1)^n \frac{\Gamma(s+n)}{\Gamma(s)} F(s), \quad \text{(A 1.7)}$$

provided

$$r^{s+m-1} \frac{d^{m-1} f}{dr^{m-1}} \to 0 \quad \text{as} \quad r \to (0, \infty), \; m = 1, \ldots, n \; . \quad \text{(A 1.8)}$$

The regularity conditions (A 1.8) provide the criterion for the choice of c .

Taking the Mellin transform and solving (A 1.4) from (A 1.1)-(A 1.3) we obtain

$$M[r^2\sigma(r,\theta)] = \Sigma(s,\theta) = 2i(s+1)\left[Ase^{is\theta} + B(s+1)e^{i(s+2)\theta} - \bar{B}e^{-i(s+2)\theta}\right], \quad \text{(A 1.9)}$$

$$M[r^2\tau_{rr}(r,\theta)] = -s(s+1)(Ae^{is\theta} + \bar{A}e^{-is\theta}) - (s+1)(s+4) \times \left[Be^{i(s+2)\theta} + \bar{B}e^{-i(s+2)\theta}\right], \quad \text{(A 1.10)}$$

$$M\left[\frac{r^2\nu(r,\theta)}{2\mu}\right] = V(s,\theta) = -\frac{s+1}{\mu}\left[Ase^{is\theta} + B(s+1)e^{i(s+2)\theta} + \kappa\bar{B}e^{-i(s+2)\theta}\right], \quad \text{(A 1.11)}$$

where $\kappa = 3 - 4\nu$ for plane strain $\kappa = (3-\nu)/(1+\nu)$ for generalized plane stress, and the "integration constants" A and B are complex and are determined from the boundary conditions specified along the wedge boundaries, θ = constant. After A and B have been determined, it is necessary to invert (A 1.9) through (A 1.11) to determine the stresses as a function of r and θ. The next section deals with the evaluation of particular integrals applicable to the problem in question.

2. Some Particular Inverse Mellin Transforms

Given below, for reference, is a listing of some of the Mellin inverses used in inverting (A 1.9) through (A 1.11). The details of a few of the integrals will be included for completeness.

$$\frac{1}{2\pi i}\int_{c-i\infty}^{c+i\infty}\left(\frac{r}{r_o}\right)^{-s-2} ds = r_o\,\delta(r-r_o) \qquad \text{(A 2.1)}$$

$$\frac{1}{2\pi i}\int_{c-i\infty}^{c+i\infty}\frac{1}{\sin(\pi s/2)}\left(\frac{r}{r_o}\right)^{-s-2} ds = -\frac{2}{\pi}\frac{r_o^2}{(r_o^2+r^2)} \qquad \text{(A 2.2)}$$

$$\frac{1}{2\pi i}\int_{c-i\infty}^{c+i\infty}\frac{1}{\cos(\pi s/2)}\left(\frac{r}{r_o}\right)^{-s-2} ds = -\frac{2r_o r}{\pi(r_o^2+r^2)} \qquad \text{(A 2.3)}$$

$$\frac{1}{2\pi i}\int_{c-i\infty}^{c+i\infty}\frac{s}{\sin(\pi s/2)}\left(\frac{r}{r_o}\right)^{-s-2} ds = \frac{4}{\pi}\frac{r_o^4}{(r_o^2+r^2)^2} \qquad \text{(A 2.4)}$$

$$\frac{1}{2\pi i}\int_{c-i\infty}^{c+i\infty}\frac{s}{\cos(\pi s/2)}\left(\frac{r}{r_o}\right)^{-s-2} ds = \frac{2}{\pi}\frac{r}{r_o}\left[\frac{3r_o^4+r_o^2r^2}{(r_o^2+r^2)^2}\right] \qquad \text{(A 2.5)}$$

$$\frac{1}{2\pi i}\int_{c-i\infty}^{c+i\infty}\frac{\sin(\pi s/2)}{\cos(\pi s/2)}\left(\frac{r}{r_o}\right)^{-s-2} ds = -\frac{2rr_o}{\pi}\frac{1}{(r_o^2-r^2)} \qquad \text{(A 2.6)}$$

$$\frac{1}{2\pi i}\int_{c-i\infty}^{c+i\infty}\frac{\cos(\pi s/2)}{\sin(\pi s/2)}\left(\frac{r}{r_o}\right)^{-s-2} ds = \frac{2r_o^2}{\pi(r_o^2-r^2)} \quad . \qquad \text{(A 2.7)}$$

Consider now the evaluation of (A 2.2) and (A 2.4)

Let $I = \frac{1}{2\pi i}\int_{c-i\infty}^{c+i\infty}\frac{1}{\sin(\pi s/2)}\left(\frac{r}{r_o}\right)^{-s-2} ds \;, \quad r < r_o$

applying the residue theorem and closing the contour to the left as shown, noting the zeros of sin $(\pi s/2)$ are at $s=\pm 2n$,

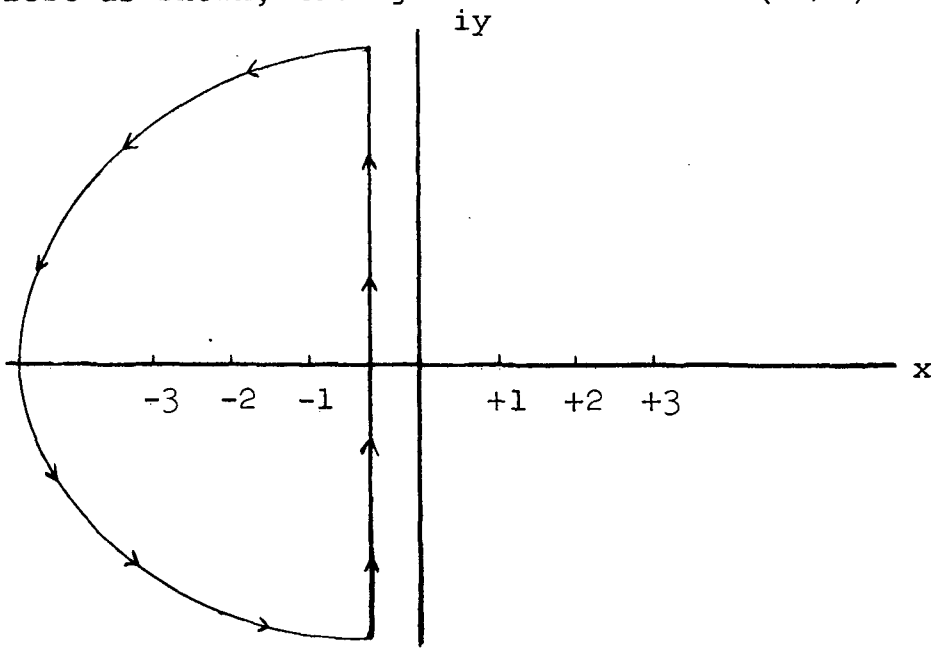

$$I = \frac{2}{\pi} \sum_{n=1}^{\infty} (-1)^n \left(\frac{r}{r_o}\right)^{2n-2} = \frac{2}{\pi} \sum_{m=0}^{\infty} (-1)^{m+1} \left(\frac{r}{r_o}\right)^{2m} = -\frac{2}{\pi} \sum_{n=0}^{\infty} (-1)^n \left(\frac{r}{r_o}\right)^{2n}$$

$$= -\frac{2}{\pi}\left[\frac{1}{1+\left(\frac{r}{r_o}\right)^2}\right] = -\frac{2r_o^2}{\pi(r_o^2+r^2)} \quad \text{as given by (A 2.2).}$$

For $r > r_o$, the contour is closed to the right and gives the same result.

For (A 2.4) let $I = \frac{1}{2\pi i} \int_{c-i\infty}^{c+i\infty} \frac{s}{\sin(\pi s/2)} \left(\frac{r}{r_o}\right)^{-s-2} ds$, $r < r_o$

again applying the residue theorem and closing the contour to the left.

$$I = \frac{2}{\pi}\sum_{n=1}^{\infty}(-2n)(-1)^n\left(\frac{r}{r_o}\right)^{2n-2} = -\frac{2}{\pi}\sum_{n=0}^{\infty}2(m+1)(-1)^{m+1}\left(\frac{r}{r_o}\right)^{2m}$$

$$= +\frac{4}{\pi}\sum_{m=0}^{\infty}(m+1)(-1)^m\left(\frac{r}{r_o}\right)^{2m}$$

noting that

$$\sum_{n=0}^{\infty}(-1)^n\left(\frac{r}{r_o}\right)^{2n} = \frac{1}{1+\left(\frac{r}{r_o}\right)^2} \quad ,$$

and differentiating both sides with respect to $\left(\frac{r}{r_o}\right)$ gives

$$\sum_{n=1}^{\infty}(-1)^n\,2n\left(\frac{r}{r_o}\right)^{2n-1} = -\frac{2\left(\frac{r}{r_o}\right)}{\left[1+\left(\frac{r}{r_o}\right)^2\right]^2}$$

$$\sum_{n=0}^{\infty}2(n+1)(-1)^{n+1}\left(\frac{r}{r_o}\right)^{2n+1} = -\frac{2\left(\frac{r}{r_o}\right)}{\left[1+\left(\frac{r}{r_o}\right)^2\right]^2}$$

$$-\frac{2r}{r_o}\sum_{n=0}^{\infty}(n+1)(-1)^n\left(\frac{r}{r_o}\right)^{2n} = -\frac{2\left(\frac{r}{r_o}\right)}{\left[1+\left(\frac{r}{r_o}\right)^2\right]^2}$$

$$\therefore \sum_{n=0}^{\infty}(n+1)(-1)^n\left(\frac{r}{r_o}\right)^{2n} = \frac{r_o^4}{\left[r_o^2+r^2\right]^2}$$

and $I = \frac{4}{\pi}\frac{r_o^4}{(r_o^2+r^2)^2}$ as given by (A 2.4) .

For $r > r_o$ the contour is closed to the right and again gives the same result.

A similar approach gives

$$\frac{1}{2\pi i}\int_{c-i\infty}^{c+i\infty}\frac{1}{\sin(\pi s)}\left(\frac{r}{r_o}\right)^{-s-2}ds = \frac{r_o}{\pi(r_o+r)} \qquad \text{(A2.8)}$$

$$\frac{1}{2\pi i}\int_{c-i\infty}^{c+i\infty}\frac{s}{\sin(\pi s)}\left(\frac{r}{r_o}\right)^{-s-2}ds = -\frac{2r_o^2+r_o r}{\pi(r_o+r)^2} \qquad \text{(A2.9)}$$

$$\frac{1}{2\pi i}\int_{c-i\infty}^{c+i\infty}\frac{\cos(\pi s)}{\sin(\pi s)}\left(\frac{r}{r_o}\right)^{-s-2}ds = \frac{r_o}{\pi(r_o-r)} \quad . \qquad \text{(A2.10)}$$

APPENDIX B

ON THE METHOD AND ACCURACY OF THE NUMERICAL SOLUTION

1. The Method of Numerical Integration

The numerical integration was performed using four basic integration Gaussian-type formula [12, p. 887-890]

$$\int_{-1}^{1} \frac{f(x)}{\sqrt{1-x^2}}\,dx \approx \sum_{i=1}^{n} w_i f(x_i), \quad x_i = \frac{\cos(2i-1)\pi}{2n}, \quad w_i = \frac{\pi}{n} \qquad \text{(B 1.1)}$$

$$\int_{-1}^{1} f(x)\sqrt{\frac{1+x}{1-x}}\,dx \approx 2\sum_{i=1}^{n} w_i f(x_i), \quad x_i = \cos\left(\frac{2i-1}{2n+1}\right)\pi, \quad w_i = \frac{2\pi(1+x_i)}{2n+1} \qquad \text{(B 1.2)}$$

$$\int_{-1}^{1} f(x)\sqrt{1-x^2} \approx \sum_{i=1}^{n} w_i f(x_i), \quad x_i = \cos\left(\frac{i\pi}{n+1}\right), \quad w_i = \frac{\pi}{n+1}\sin^2(x_i) \qquad \text{(B 1.3)}$$

$$\int_{a}^{b} f(x)dx \approx \frac{b-a}{2}\sum_{i=1}^{n} w_i f(x_i), x_i = \left(\frac{b-a}{2}\right)y_i + \left(\frac{b+a}{2}\right),$$

where

$$y_i = i^{th} \text{ zero of } P_n(x), \quad w_i = \frac{2}{(1-y_i^2)[P_n'(x_i)]^2}. \qquad \text{(B 1.4)}$$

and P_n is the n^{th} order Legendre Polynomial.

Wherever possible advantage was taken of the fact that the discrete values of $F(t_k)$, given by (63) of (67), were at the collocation points of (B 1.1) or (B 1.2) respectively if n was chosen equal to N. However, in the integrals specifying the displacements it was necessary to use integration formula whose limits were not, in general, -1 to 1.

For these integrals the discrete values of $F(t_k)$ were fitted by least squares analysis to a continuous function in the form of a K^{th} order polynomial and an integration formula of the form (B 1.4) was utilized.

2. The Accuracy of the Numerical Solution

The accuracy of the computer solution was determined in part by to what degree it could reproduce known solutions or how well it reduced to special cases whose solutions were known exactly. For instance, the special case of a unit crack in a full plane could be modeled one of three ways: either by taking $c = 0$, $\nu_1 = \nu_2$, $E_1 = E_2$, $a = 1$, $b = 2$; or $c = 1/2$, $a = 0$, $b = 0$, $\nu_1 = \nu_2$, $E_1 = E_2$; or lastly, it could be approximated by taking $c = 0$, a large, and $b = a + 1$. The numerical solution was correct to five significant figures for all special cases and was exact to the number of places carried, (usually four), for the known solutions of a crack approaching a bonded interface given by [2]. While these checks provide a measure of the accuracy, they are also necessary for the correctness of the computer solution.

The terms that necessarily go out in checking the special cases are the additive terms that provide for the new solution. To make sure that these terms were programed correctly, the computer solution of the integral equations was approached two ways, and the programs, independently written, were checked until agreement was reached.

The method that was not chosen for inclusion in the text was an iterative solution obtained as follows: As a first approximation it was assumed that C_1, given by Equation (54), was the only non zero C_n. Knowing the C_n, the right side of Equation (36) was completely defined and a set of $F(t_k)$ could be determined. Based on this set of F's, a new approximation to the C_n could be found from Equation (53). The right side of Equation (36) was again modified and a new set of F's determined. The procedure was continued until no significant change was determined in either the F's or the C_n. The accuracy of the complete solution was then determined by noting to what extent these two solutions agreed. For example, if $M = 14$, $N = 14$, $a = 0$, $b = 1$, $c = 1$, the iterative solution converged after four iterations, giving $k(b) = .9513$, $\frac{\partial U}{\partial c} = 1.117 \times 10^{-6}$, whereas, the computer program, discused in Appendix C, gives $k(b) = .9511$, $\frac{\partial U}{\partial c} = 1.116 \times 10^{-6}$.

APPENDIX C

COMPUTER PROGRAMS

1 Introduction to the Computer Programs

Two computer programs were written to obtain numerical results to the solutions presented in Chapters I and II. These will be referred to as PROGRAM 100 and PROGRAM 200 respectively. Adequate comments have been provided for the reader familiar with Chapters I and II to follow the logic of the programs. Wherever possible, these comments refer directly to equations in the text. Given below are two definitions that may prove helpful in the reading of the computer programs. The first is a fundamental integral containing $P_n^{(\alpha,\beta)}(t)$ which was indexed to limit the use of the recursion formula used to generate the Jacobi polynomials.

$$\text{PLSTAR}(N,KX) \triangleq \int_{-1}^{1} w(t) P_n^{(\alpha,\beta)}(t)\, I(t,x_k)\,dt \quad . \qquad \text{(C 1.2)}$$

The second integral contains $P_{n-1}^{(\alpha,\beta)}(y)$. It is related to the C_n and is given as part of Equation (53). Its definition follows from

$$\sum_{j=1}^{KQUAD} F(TJ)\,\text{PMSTAR}(N,J) \triangleq \int_{-1}^{1}\int_{-1}^{1} \frac{F(t)}{\sqrt{1-t^2}}\, G(t,y)\sqrt{1-y^2}\left(\frac{1-y}{1+y}\right)^{i\omega} X$$

$$P_{n-1}^{(-\alpha,-\beta)}(y)\,dy\,dt \qquad \text{(C 1.2)}$$

where $F(t)$ is given by Equation (63) and KQUAD is a

numerical constant the choice of which is discussed in the section that follows.

2. On the Choice of Constants Related to the Numerical Integration

Certain constants have been fixed in programs 100 and 200. The choice of these constants was governed by how a variation in the parameter effected the most sensitive output variable in trial runs using Aluminum-Epoxy material pairs. The constants along with their definitions are listed below for reference.

KQUAD - Upper limit in numerical integration formula used in integrating Equations (53) and (60). Fixed in program at value of 200.

NTERMS - Number of terms in polynomial curve fit used in numerical integration formula (B 1.4). in program at value of 10.

NODE - Number of nodal points used in evaluation of displacement integrals that were complete and could be evaluated using integration formula (B 1.1) or (B 1.2). Fixed in program at value of 100.

3 PROGRAM 100

Purpose

The solution is given for two bonded isotropic linearly elastic half-planes of different elastic properties having a crack along the interface as well as a perpendicular crack in one of the half-planes which may intersect the interface crack. A constant pressure is assumed on the crack surfaces, and no loads at infinity. For convenience, the inplane crack will be assumed to be in material one for all cases. The geometry is shown below.

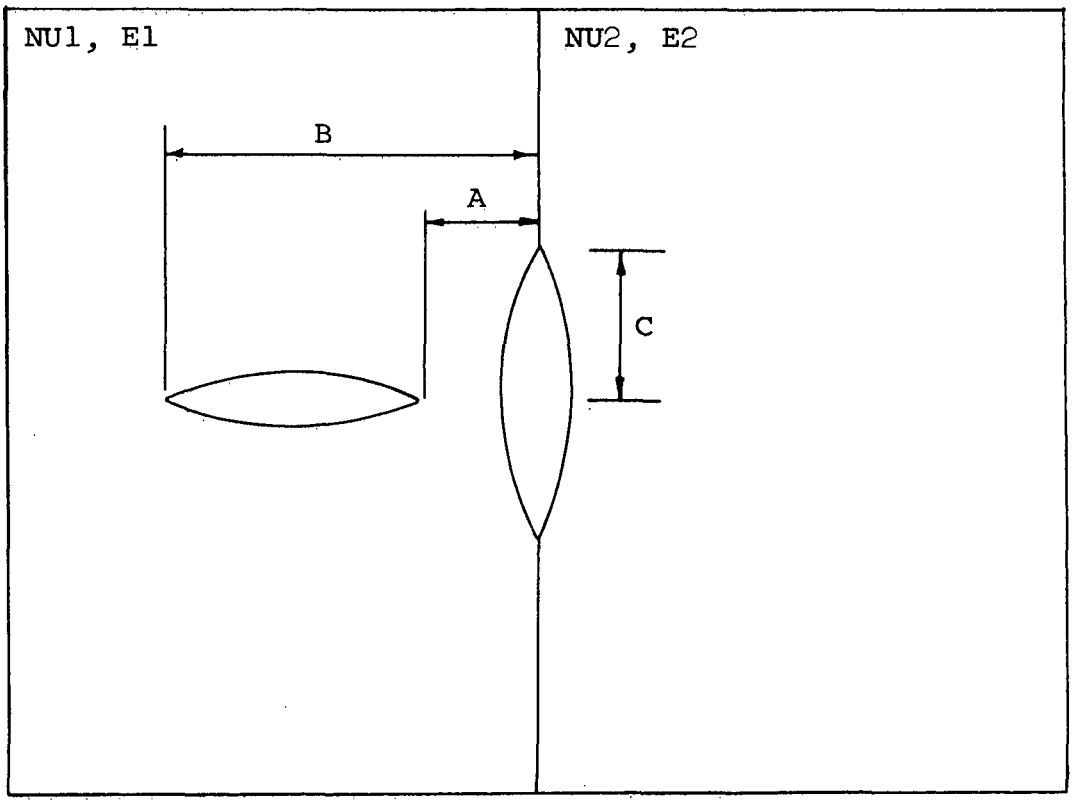

DESCRIPTION OF PARAMETERS

NSETS	Number of data sets to be read, a data set consists of cards No.2 to No.5, as described in INPUT.
A	Distance of near crack tip from interface.
B	Distance of far crack tip from interface.
C	Half length of interface crack
NU1	Poisson's ratio, material one.
E1	Young's modulus, material one.
NU2	Poisson's ratio, material two.
E2	Young's modulus, material two.
SIGMA0	Opening pressure on interface crack.
SIGMA1	Opening pressure on inplane crack.
NHALF	Number of half planes present.
N	Number of terms taken in Equation (63) and (67) ($11 \leq N \leq 28$).
M	Number of C_n generated by Equation (53) ($1 \leq M \leq 50$).
STRAIN	If strain set equal to 1, solution is for plane strain. If strain set equal to 2, solution is for generalized plane stress.

INPUT

DATA CARD	PARAMETERS	FORMAT
No.1	NSETS	I2
No.2	A, B, C	3(IPE14.7)
No.3	E1, NU1, E2, NU2	4(IPE14.7)
No.4	SIGMA0, SIGMA1	2(IPE14.7)
No.5	N, M, STRAIN, NHALF	4(I2)

OUTPUT

Numerical results are obtained for the stress intensity factors, strain energy release rate, stresses and displacements.

Comments

In test programs using Aluminum-Epoxy and Epoxy-Aluminum material pairs, the output was examined using successively larger values of M and N to determine when the numerical solution was sufficiently conditioned to give less than 1 percent variation in the most slowly converging output parameter.

It was found that the strain energy release rate converged most slowly in all cases and that K(b) converged most rapidly in all cases. Values that gave less than 1 percent variation in output at A = 0, B = 1, C = 1, were M = N = 14. If A = 0, B = 1, C = 0.1, it was necessary to take M = 30 and N = 20. The value of N = 26 was found to be large enough in all cases. If C is decreased below 0.1, it was necessary to take larger values of M to obtain accuracies of one percent in the strain energy release rate. PROGRAM 100 will solve the following problems illustrated below. Note A and C may not equal zero at the same time. Time required on the Clemson University IBM 370/158 computer was about two minuets for N=M=14 and fifteen minuets for N=26, M=48 .

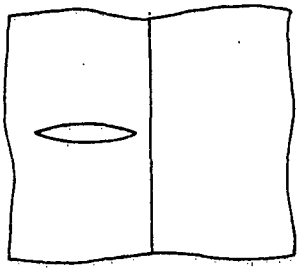

$A \neq 0$, $B \neq 0$, $C = 0$, NHALF=2

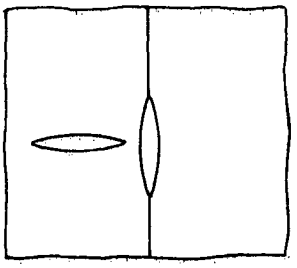

$A \neq 0$, $B \neq 0$, $C \neq 0$, NHALF=2

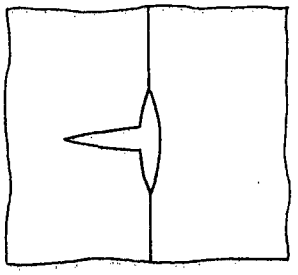

$A = 0$, $B \neq 0$, $C \neq 0$, NHALF=2

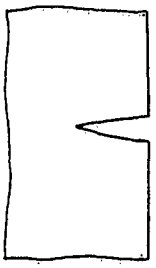

$A = 0$, $B \neq 0$, $C = 0$, NHALF=1, E2, NU2 any nonzero constant

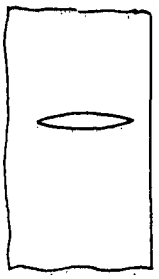

$A \neq 0$, $B \neq 0$, $C = 0$, NHALF=1, E2, NU2 any nonzero constant

4. PROGRAM 200

Purpose

The solution is given for two bonded isotropic elastic half-planes of different elastic properties having a crack along the interface as well as a perpendicular crack in both of the half-planes, either of which may intersect the interface crack. A constant pressure is assumed on the crack surfaces and no loads at infinity. The geometry of the problem is shown below.

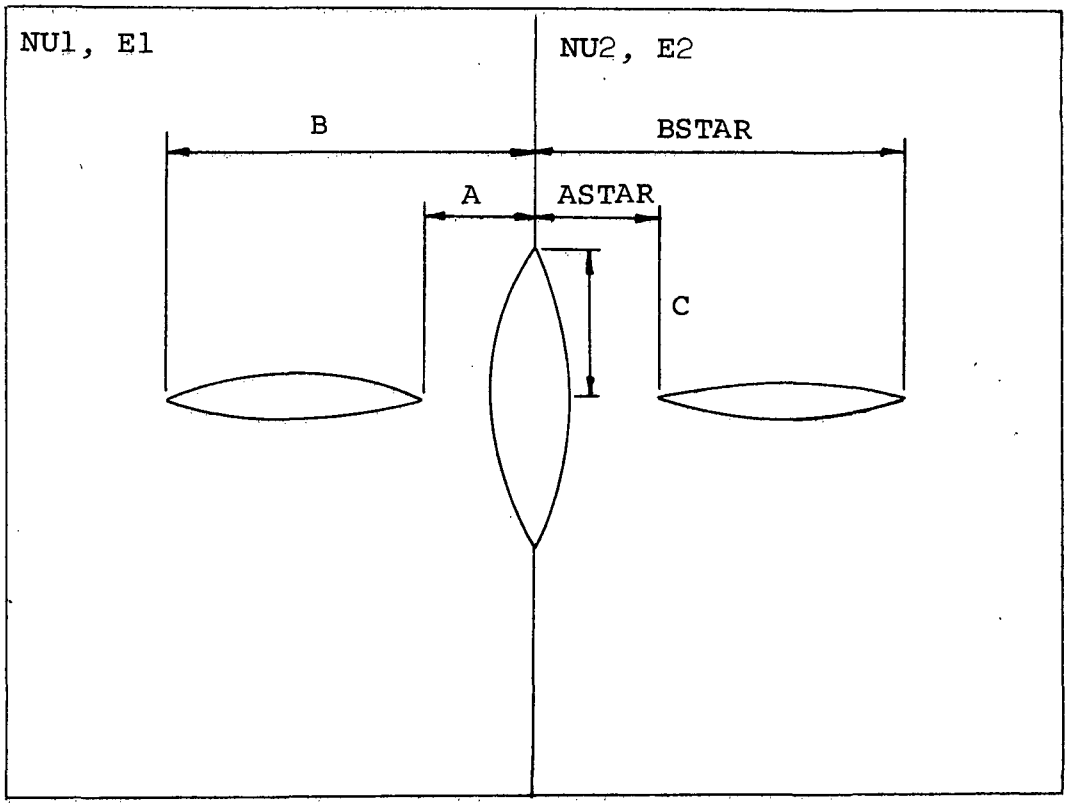

DESCRIPTION OF PARAMETERS

NSETS	Number of data sets to be read. A data set consists of cards No.2 to No.5, as described in INPUT.
A	Distance of near crack tip from interface in material one.
B	Distance of far crack tip from the interface in material one.
C	Half length of interface crack.
ASTAR	Distance of near crack tip from interface in material two.
BSTAR	Distance of far crack tip from interface in material two.
NU1	Poisson's ratio, material one.
E1	Young's modulus, material one.
NU2	Poisson's ratio, material two.
E2	Young's modulus, material two.
SIGMA0	Opening pressure on interface crack.
SIGMA1	Opening pressure on inplane crack in material one.
SIGMA2	Opening pressure on inplane crack in material two.
N	Number of terms taken in Equations (100) to (103) ($11 \leq N \leq 28$).
M	Number of C_n generated by Equation (96) ($1 \leq M \leq 50$).
STRAIN	STRAIN = 1 implies plane strain, STRAIN = 2 implies generalized plane stress.

INPUT

DATA CARD	PARAMETERS	FORMAT
No.1	NSETS	I2
No.2	A, B, C, ASTAR, BSTAR	5(1PE14.7)
No.3	E1, NU1, E2, NU2	4(1PE14.7)
No.4	SIGMA0, SIGMAI	3(1PE14.7)
No.5	N, M, STRAIN	3(I2)

OUTPUT

Numerical results are obtained for the stress intensity factors, strain energy rate, stresses and displacements.

Comments

In test programs using Aluminum-Epoxy and Epoxy-Aluminum material pairs, the output was examined using successively larger values of M and N to determine when the numerical solution was sufficiently conditioned to give less than 1 percent variation in the most slowly converging output parameter. It was found that the strain energy release rate converged most slowly in all cases. K(B) and K(BSTAR) were the most rapidly convergent output parameters in all cases. Values that gave less than one percent variation in output at A = 0, B = 1, C = 1, ASTAR=0, BSTAR=1, were M = 14, N = 14. For N=M=14 the computer time was about four minuets and N=26, M=48 required twenty five minuets, (necessary for $C \leq 0.1$).

PROGRAM 200 will solve the following problems illustrated below. Note, if C = 0, A or ASTAR may not equal zero.

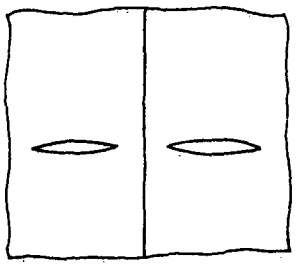

$C = 0$, $A \neq 0$, $B \neq 0$, ASTAR $\neq 0$, BSTAR $\neq 0$, SIGMA0 $= 0$

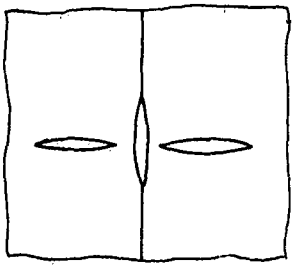

$A \neq 0$, $B \neq 0$, $C \neq 0$, ASTAR $\neq 0$, BSTAR $\neq 0$

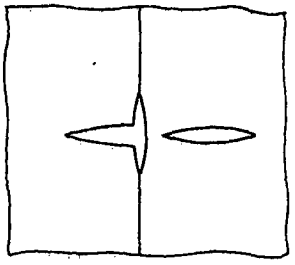

$A = 0$, $B \neq 0$, $C \neq 0$, ASTAR $\neq 0$, BSTAR $\neq 0$

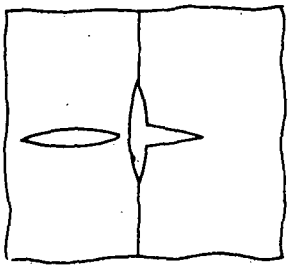

$A \neq 0$, $B \neq 0$, $C \neq 0$, ASTAR $= 0$, BSTAR $\neq 0$

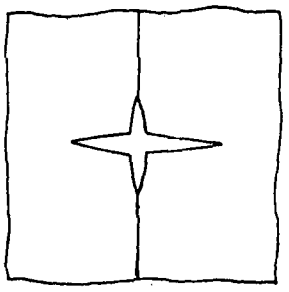

$A = 0$, $B \neq 0$, $C \neq 0$, ASTAR $= 0$, BSTAR $\neq 0$